Coordination Chemistry Reviews, 104 (1990) 39–112
Elsevier Science Publishers B.V., Amsterdam

SPECTROSCOPY, PHOTOPHYSICS AND PHOTOCHEMISTRY OF ZEROVALENT TRANSITION METAL α-DIIMINE COMPLEXES

DERK J. STUFKENS

Anorganisch Chemisch Laboratorium, Universiteit van Amsterdam, J.H. van't Hoff Instituut, Nieuwe Achtergracht 166, 1018 WV Amsterdam (The Netherlands)

(Received 20 July 1989)

CONTENTS

A. Introduction 41
B. $M(CO)_4$(α-diimine) (M=Cr, Mo, W) 43
(i) Formation of the complexes 43
(ii) Electronic transitions 45
(iii) Photophysical properties 52
(iv) Photochemical behaviour 56
(v) Concluding remarks 61
C. $(CO)_5M'M(CO)_3$(α-diimine) (M, M'=Mn, Re) 61
(i) Formation of the complexes 61
(ii) Electronic transitions 62
(iii) Photophysical properties 65
(iv) Photochemical behaviour 66
D. $Ph_3SnM(CO)_3$(α-diimine) (M=Mn, Re) 76
E. $(CO)_4CoM(CO)_3$(α-diimine) (M=Mn, Re) 80
F. Photochemical mechanism 83
G. $M(CO)_3$(α-diimine) (M=Fe, Ru) 86
(i) Formation of the complexes 86
(ii) Bonding properties and electronic transitions 88
(iii) Photochemical behaviour 92
(iv) Photochemical mechanism 96
H. $Ni(CO)_2$(α-diimine) 98
(i) Formation of the complexes 98
(ii) Bonding properties and electronic transitions 99
(iii) Photochemical behaviour 103
(iv) Photochemical mechanism 107
Acknowledgements 107
References 107

ABBREVIATIONS

bpy	2,2′-bipyridine
bpy′	4,4′-Me_2-bpy

0010-8545/90/$25.90

cHex	cyclohexyl
COD	cyclooctadiene
cPr	cyclopropyl
EP	excitation profile
EPA	ethanol, isopentane, ether (2:5:5)
Et	ethyl
ETC	electron transfer chain
HE	high energy
hfs	hyperfine splitting
HOMO	highest occupied molecular orbital
IAE	bis-(1-alkylimino)-2-(alkylimino)-ethane-*N*,*N*′
IP	ionization potential
iPr	isopropyl
iPr_2-Ph	2,6-diisopropylphenyl
LE	low energy
LF	ligand field
LUMO	lowest unoccupied molecular orbital
LXe	liquid xenon
MCD	magnetic circular dichroism
Me	methyl
Me_2-Ph	2,6-dimethylphenyl
Mes	mesityl
2-MeTHF	2-methyltetrahydrofuran
ML	metal–ligand
MLCT	metal-to-ligand charge transfer
MO	molecular orbital
*n*Bu	*n*-butyl
N-N	α-diimine
OMe	methoxy
OPh	phenoxy
OTF	orthotrifluoromethanesulphonate
PE	photoelectron
Ph	phenyl
phen	1,10-phenanthroline
*p*Tol	*p*-tolyl
py	pyridine
pyz	pyrazine
R-DAB	1,4-diaza-1,3-butadiene (RN=CH−C=NR)
R-DAB(R′,R′)	RN=CR′−CR′=NR
R-PyCa	pyridine-2-carbaldehyde imine (C_5H_4N−CH=NR)
R-PyCa(R′)	C_5H_4N−CR′=NR
RR	resonance Raman

RT	room temperature
*t*Bu	*t*-butyl
THF	tetrahydrofuran
tmen	*N*,*N*,*N*′,*N*′-tetramethylethylenediamine

A. INTRODUCTION

The development of ligand field (LF) theory about 30 years ago has strongly stimulated research in the fields of photophysics and photochemistry of transition metal complexes. General rules concerning the LF photochemistry of chromium(III) complexes were already published in 1967 [1].

In later years many scientists changed their research interest from LF photochemistry to the photophysics and photochemistry of complexes with a metal-to-ligand charge transfer (MLCT) state as the lowest excited state. Usually such MLCT states are not reactive and are rather long lived, which makes them very well suited for energy and electron transfer. In this respect most attention has been paid to the cation $Ru(bpy)_3^{2+}$ which has favourable oxidation and reduction potentials and a long lifetime of its lowest MLCT state. Moreover, this complex ion is photostable and absorbs in the region of sunlight. The spectroscopy, photochemistry and especially the photoelectron transfer processes of this complex ion have been described in many reviews [2–8].

Although light has always played an important role in preparative organometallic chemistry, most fundamental research activities in this field started in the course of the 1970s. The first review on the primary photoprocesses of transition metal carbonyls appeared in 1976 [9] and a broad survey of this research area was presented by Geoffroy and Wrighton in 1979 in their book *Organometallic Photochemistry* [10]. During the last ten years mechanistic studies in this field have received more attention owing to the development of new spectroscopic techniques for the identification of reactive intermediates. Photochemical reactions can now be understood more easily by following them under normal conditions with flash photolysis (in some cases with IR detection) or by stabilizing reactive intermediates in low temperature solutions or rigid media. In the field of organometallic photochemistry these new techniques have mainly been applied to photochemical studies of transition metal carbonyls for which the ground and excited state properties are best known. Most mononuclear transition metal carbonyls are photolabile since their lowest excited state normally has LF character. Binuclear and polynuclear metal–metal-bonded complexes photodecompose because they possess a repulsive $^3\sigma\sigma^*$ state of the

metal–metal bond as lowest excited state. The photochemistry of these complexes has been described in several reviews [10–15].

Recently, the first review on the luminescence properties of organometallic complexes has appeared [16].

In contrast with studies on $Ru(bpy)_3^{2+}$, there has been much less attention paid to the spectroscopy, photophysics and photochemistry of transition metal carbonyls possessing a lowest MLCT state. Only the complexes $XRe(CO)_3(bpy)$ (X=halide) have received wide interest because of their ability to act as efficient photosensitizers for electron transfer processes. In most carbonyl complexes with a lowest MLCT state, L represents one of the four most widely used and simplest representatives of the group of α-diimine ligands shown in Fig. 1.

Bpy and phen differ in two respects from the other two α-diimines. First, their lowest π^* orbital is at higher energy and it has a smaller contribution from the N-atomic orbitals. As a result, π backbonding to bpy and phen is much weaker than for R-PyCa and R-DAB. This effect will, however, only show up in low valent, preferably zerovalent, transition metal complexes $M(CO)_nL$. It has also a dramatic influence on the spectroscopic, photophysical and photochemical properties of these complexes, whereas no such effect has been observed for higher valent complexes. Secondly, bpy and phen can only bind to a metal via one or two N atoms, since the other bonds form part of an aromatic ring system. The R-DAB and R-PyCa ligands, however, cannot only coordinate via N but can also coordinate in various ways via one or two CN bonds. Again, this difference in coordinating behaviour only shows up when the metal is zerovalent. In several reviews Vrieze and van Koten [17–20] have shown that this versatile coordination of R-DAB and R-PyCa gives rise to a much richer chemistry with respect to zerovalent metals than observed for bpy and phen.

This review describes the effect of the metal and the α-diimine ligand on

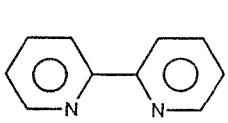

2,2'-Bipyridine (bpy)

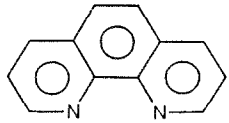

1,10-Phenanthroline (phen)

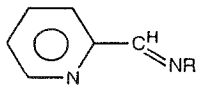

Pyridine-2-carbaldehyde imine (R-PyCa)

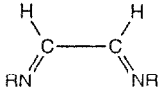

1,4-Diaza-1,3-butadiene (R-DAB)

Fig. 1. Structures of the α-diimine ligands bpy, phen, R-PyCa and R-DAB in their chelating conformation.

the spectroscopy, photophysics and photochemistry of the zerovalent complexes d^6-$M(CO)_4L$ (M=Cr, Mo, W), d^7-$L'_nM'M(CO)_3L$ (L'_nM'=$(CO)_5Mn$, $(CO)_5Re$, $(CO)_4Co$, Ph_3Sn; M=Mn, Re), d^8-$M(CO)_3L$ (M=Fe, Ru), d^{10}-$Ni(CO)_2L$ (L-α-diimine=N-N), as it is these which have been studied in detail. It does not present a general survey of the literature but rather discusses in depth those data which are crucial for a better understanding of the ground and excited state properties of these complexes.

B. $M(CO)_4$(α-DIIMINE) (M=Cr, Mo, W)

(i) Formation of the complexes

These complexes have a long history since one of them, $Mo(CO)_4$(phen), was prepared by Hieber and Mühlbauer as long ago as 1935 [21]. Abel et al. [22] synthesized the corresponding bpy complex in 1959. The syntheses and bonding properties of several $Mo(CO)_4$(R-DAB) and $Mo(CO)_4$(R-PyCa) complexes were described for the first time by Bock and tom Dieck [23] and Brunner and Herrmann [24] respectively. The corresponding chromium and tungsten complexes were all prepared in later years.

The synthetic methods mainly consisted of a direct reaction, thermal or photochemical, between the hexacarbonyl and the α-diimine ligand. Alternatively, the complexes have been prepared by substituting one or two loosely bonded ligands L in $M(CO)_5L$ or $M(CO)_4L_2$ by the appropriate α-diimine.

Irradiation of $M(CO)_6$ in THF produces $M(CO)_5$(THF) which readily loses THF and converts to $M(CO)_4$(N-N) (N-N=α-diimine) in the presence of excess α-diimine. Staal et al. [25] first observed that this reaction proceeds via formation of the transient $M(CO)_5$(N-N), in which the α-diimine ligand coordinates to the metal in a monodentate fashion. At room temperature, this pentacarbonyl is readily converted to $M(CO)_4$(N-N). When the substitution of THF by α-diimine is, however, performed at lower

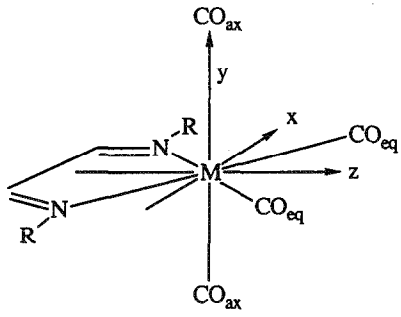

Fig. 2. Structure of $M(CO)_4$(R-DAB) (M=Cr, Mo, W).

temperatures ($T < -20°C$), $M(CO)_5$(N-N) is formed as a thermally stable complex in the case of the R-DAB and R-PyCa ligands. Lees and coworkers [26–33] confirmed the formation of these intermediates at room temperature by studying the UV–visible spectral changes directly after irradiation of a solution of $M(CO)_6$ and excess α-diimine. For this purpose they used a rapid-recording microprocessor-controlled diode-array absorption spectrophotometer. Spectra were recorded within 2 s after irradiation and at short time intervals after that. In this way, intermediates $M(CO)_5$(N-N) could be detected for R-DAB and R-PyCa ligands and even in the case of bpy. No discernible $M(CO)_5$(phen) intermediates could, however, be observed. The conversion of $M(CO)_5$(N-N) into $M(CO)_4$(N-N) appeared to proceed via a first-order kinetic process. The reaction rates decreased in the sequence molybdenum > chromium > tungsten, analogous to the order of CO release in $M(CO)_6$. This bond breaking process is, however, not purely dissociative but it has a substantial associative component since the activation enthalpies of the chelation reactions are low and strongly dependent on the α-diimine ligand [30–32].

In the $M(CO)_5$(R-PyCa) complexes, the R-PyCa ligand can in principle coordinate via the pyridine or the imine N atom. Lees and coworkers [31,33] demonstrated that these ligands preferentially coordinate via the pyridine ring unless this ring has a substituent close to its N atom. Two of these reactive intermediates, $W(CO)_5$(4,4′-(*n*-$C_{19}H_{39})_2$-bpy) [34] and $W(CO)_5$(*t*Bu-PyCa) [33] have been characterized by rapid scan IR spectroscopy. In principle all these $M(CO)_5$(N-N) intermediates can be detected with these rapid scan techniques with the exception of those of phen and its derivatives. For these ligands, chelation to give $M(CO)_4$(phen) is apparently too fast to be observed on this time scale. Quite recently, Oishi [35] and Kalyanasundaram [36] independently reported the kinetics of the photochemical reactions of the hexacarbonyls with phen and with other α-diimines by using laser flash photolysis. Their results agree with the following reaction scheme:

$$M(CO)_6 \xrightarrow{h\nu} M(CO)_5 + CO \quad (1)$$

$$M(CO)_5 + \text{Solv.} \rightarrow M(CO)_5(\text{Solv.}) \quad (2)$$

$$M(CO)_5(\text{Solv.}) + \text{N-N} \rightarrow M(CO)_5(\text{N-N}) + \text{Solv.} \quad (3)$$

$$M(CO)_5(\text{N-N}) \rightarrow M(CO)_4(\text{N-N}) + CO \quad (4)$$

The products of reactions (2)–(4) are formed on very different time scales. This is clearly demonstrated in Fig. 3, which presents the evolution of the absorption spectrum after irradiation of a solution of $Mo(CO)_6$ and phen with a 10 ns 353 nm Nd: YAG laser pulse [36]. The first spectrum, recorded directly after the flash (t=0) belongs to $Mo(CO)_5$(Solv.) since the naked $Mo(CO)_5$ transient is too short-lived to be detected on a nanosecond

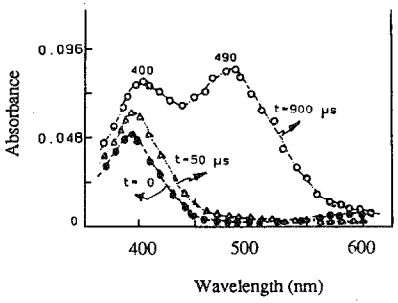

Fig. 3. Electronic absorption spectra of transient intermediates formed after 353 nm laser photolysis of an $Mo(CO)_6$-phen solution in C_6H_6. (Reproduced with permission from ref. 36.)

timescale. The LF band of $Mo(CO)_5$(phen), observed in the t=50 μs spectrum, is only slightly shifted with respect to $Mo(CO)_5$(Solv.) (Solv.=benzene). The spectrum, recorded 900 μs after the flash, has an extra MLCT band at 500 nm characteristic for a complex with a chelating α-diimine ligand. In the case of $Cr(CO)_5$(phen) the LF band was found at lower energy than for the closely analogous $Cr(CO)_5$(py) and $Cr(CO)_5$(bpy) complexes (440 nm compared with 410 nm) [35]. This effect was attributed to an electronic interaction between the non-coordinated N atom of phen and Cr, giving rise to a distortion from octahedral coordination.

Chelation of phen according to reaction (4) is faster by at least a factor of 10^4 than that of bpy and other α-diimines. This is due to the fact that the N atoms of phen are held coplanar, which facilitates chelation, whereas the other α-diimines normally exist in an S trans conformation.

(ii) Electronic transitions

Much attention has been paid to the characteristic spectral features of these $M(CO)_4$(N-N) complexes which are nicely reflected in the absorption spectrum shown in Fig. 4 [37]. The complexes have C_{2v} or C_s symmetry depending on the symmetry of the α-diimine ligand. A qualitative MO diagram for C_{2v} symmetry is presented in Fig. 5 and the molecular structure of the complexes is shown in Fig. 2.

Transitions are allowed from all three filled metal d-orbitals to the lowest $\pi^*(b_2)$ orbital of the α-diimine ligand. They cause the appearance of a structured low energy absorption band in apolar solvents (Fig. 4). The z-polarized $b_2 \rightarrow b_2^*$ transition is the strongest since it takes place between orbitals which strongly interact in the ground and excited states [38–43]. Two transitions are allowed to the second π^* orbital of the α-diimine (a_2^*). They are close in energy to the first LF transitions but can be distinguished from them by means of their characteristic solvatochromism (vide infra).

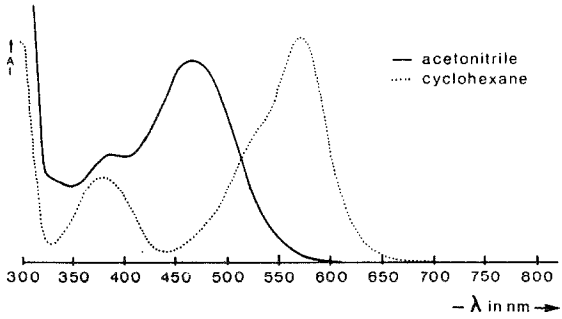

Fig. 4. Electronic absorption spectra of $Mo(CO)_4$(iPr-PyCa) in acetonitrile and cyclohexane. (Reproduced with permission from ref. 37.)

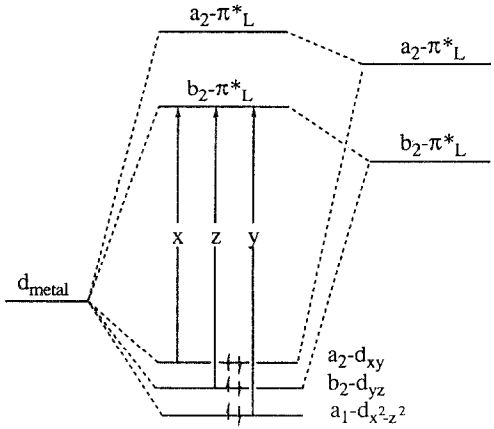

Fig. 5. Molecular orbitals of $M(CO)_4$(N-N) (M=Cr, Mo, W) involved in the lowest energy MLCT transitions.

An important property of the $b_2 \rightarrow b_2^*$ transition is that its MLCT character, and as a result its solvatochromism, can vary strongly from one complex to another. This is because the b_2 and b_2^* orbitals have varying degrees of metal (d) and ligand (π^*) character. In the ground state this metal–ligand interaction is called π backbonding. The strength of this π backbonding depends on the overlap between the orbitals and their relative energies. The π^* orbital decreases in energy on going from bpy and phen to R-PyCa and R-DAB. The overlap with the metal (d) orbital increases in the same order owing to a higher atomic coefficient for the coordinating N atoms in this π^* orbital. A similar increase in π backbonding to the α-diimine occurs when the d orbitals are raised in energy by substituting a CO ligand by PR_3 or by replacing rhenium(I) by tungsten(0).

It goes without saying that a change of interaction between these metal

and ligand orbitals strongly influences the MLCT character of this $b_2 \rightarrow b_2^*$ transition. For complexes of, for example, bpy and phen, having a weak metal to α-diimine π backbonding, this transition has much MLCT character. In the case of the R-DAB complexes, the π backbonding is much stronger. As a result the $b_2 \rightarrow b_2^*$ transition has nearly lost its MLCT character and become metal–ligand bonding to antibonding $(d + \pi^* \rightarrow \pi^* - d)$.

These differences in MLCT character, which are schematically illustrated in Fig. 6, can be nicely demonstrated with resonance Raman (RR) spectroscopy. RR spectroscopy is a valuable technique for the detection and characterization of different allowed electronic transitions within one absorption band. The RR spectra of several of these complexes have been studied in detail and for some of them excitation profiles (EPs) have been derived [43]. Figure 7 presents the EPs of three representative $W(CO)_4$(N-N) complexes (N-N=4,7-Ph_2-phen, iPr-PyCa, iPr-DAB), which will now be discussed in some detail.

The RR spectra were measured with exciting laser lines varying from about 600 to 458 nm and the intensities of the most strongly resonance-enhanced Raman bands were reproduced as a function of the exciting wavelength. The EPs obtained in this way reflect the coupling of the vibration in question to the different electronic transitions within the MLCT band. For all three complexes two maxima are observed which correspond to different electronic transitions. The EPs of the iPr-PyCa and iPr-DAB complexes indicate the presence of a third maximum at the long-wavelength side of the absorption band.

These EPs clearly demonstrate the influence of the α-diimine ligand on the difference in character between the main MLCT transitions. In the case of $W(CO)_4$(4,7-Ph_2-phen) both transitions show strong RR effects for the symmetrical ligand stretching modes and especially for ν(phen II). This

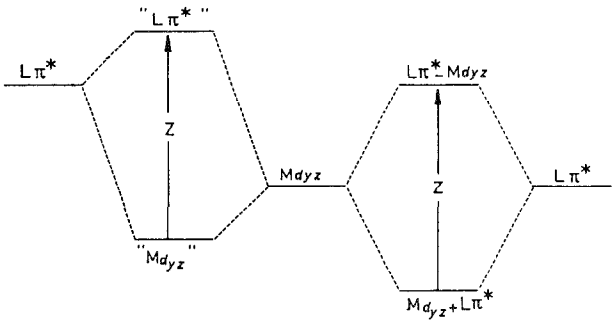

Fig. 6. Influence of the metal to α-diimine π backbonding on the MLCT character of the z-polarized $b_2 \rightarrow b_2^*$ transition.

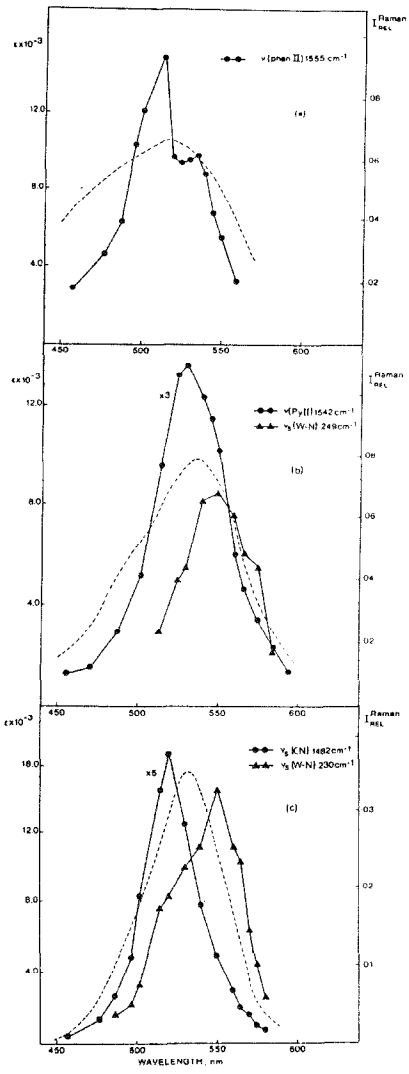

Fig. 7. Resonance Raman excitation profiles (–·–·) and MLCT bands (– – –) of (a) $W(CO)_4$(4,7-Ph_2-phen), (b) $W(CO)_4$(iPr-PyCa) and (c) $W(CO)_4$(iPr-DAB) in C_6H_6. Raman intensities are relative to the 992 cm^{-1} solvent band. (Reproduced with permission from ref. 43.)

means that both transitions are accompanied by drastic changes in the normal coordinates of these vibrations. This will be the case when the transitions have a strong MLCT character since the ligand is then reduced in the excited state. It is noteworthy that the symmetrical metal–N stretching mode does not show an RR effect. It could hardly be detected even in the Raman spectra. Apparently, the loss of π backbonding during these

transitions is compensated by an increase of ionic interaction in the excited state.

Remarkable changes occur in the EPs upon going from the 4,7-Ph_2-phen to the iPr-PyCa and iPr-DAB complexes. The high energy transition is still accompanied by a strong RR effect for the symmetrical ligand stretching modes, illustrating the strong MLCT character of this transition for all three complexes. In contrast with this, drastic changes are observed at the low energy side of the EPs. The RR effects for the symmetrical ligand stretching modes, which are weak but still noticeable for the iPr-PyCa complex, have completely disappeared for the iPr-DAB complex. This means that for this low energy transition the MLCT character decreases from top to bottom. The concomitant increase in the RR effect for ν_s(W–N) shows that this decrease in MLCT character is accompanied by an increase in metal–ligand bonding to antibonding character.

Apparently, this low energy maximum in the EPs corresponds to the $b_2 \rightarrow b_2^*$ transition and the observed RR data are clear proof for the changing character of this transition, illustrated in Fig. 6. The maximum at higher energy and the long-wavelength shoulder which appeared in the EPs of two of the complexes will correspond to the other two MLCT transitions ($a_1 \rightarrow b_2^*$ and $a_2 \rightarrow b_2^*$ respectively) for which no such ligand dependence of the MLCT character is expected. In one respect the above results have to be treated with some caution. The maxima of the EPs do not necessarily coincide with the maxima of the electronic transitions since interference between resonance effects induced by different close lying transitions may influence the positions of these EP maxima [44]. This becomes evident, for example, from a comparison of the RR and MCD spectra of $W(CO)_4$(4,7-Ph_2-phen). The $b_2 \rightarrow b_2^*$ transition of this complex corresponds to a *B* term in the MCD spectrum at 550 nm, whereas the EP has a maximum at 535 nm. The results of these EPs have also been used in combination with luminescence excitation spectra to interpret the emission spectra of these complexes (vide infra).

One important property of these $M(CO)_4$(N-N) complexes, also derived from their RR spectra but not included in the EPs of Fig. 7, is the involvement of the axial carbonyl groups (see Fig. 2) in the MLCT transitions [37,40,41]. Since this effect is closely related to the photochemistry of these complexes, it will be discussed hereafter in relation to these photochemical data.

A characteristic property of these $M(CO)_4$(N-N) complexes, which has received much attention during the last 20 years, is the solvatochromic behaviour of their MLCT bands [45–62]. Normally these bands shift to higher energy upon going to more polar solvents (negative solvatochromism, see Fig. 4). Most studies have been concerned with the correlation

between this solvatochromism and empirical solvent polarity parameters such as Reichardt's E_T parameter [63], Kosower's Z parameter [64] and Kamlet and Taft's π^* solvent scale [65,66]. In general, good agreement was obtained between the energies of the MLCT bands (E_{MLCT}) and these solvent parameters, provided that the solvents were grouped according to different classes (aliphatic, aromatic, chlorinated, alcohols). This grouping was necessary in order to take into account specific (e.g. H bridging) solute–solvent interactions. On the basis of an extensive study of the solvent dependences of the MLCT bands of a series of $W(CO)_4$(N-N) complexes, Manuta and Lees [58] derived a new solvent parameter E^*_{MLCT} defined as

$$E^*_{MLCT}=\frac{E_{MLCT}-E^0_{MLCT}}{E^1_{MLCT}-E^0_{MLCT}} \tag{5}$$

In this equation, which uses the MLCT energies in solvent (E_{MLCT}), isooctane (E^0_{MLCT}) and dimethyl sulphoxide (E^1_{MLCT}), E^*_{MLCT} takes on values from 0 to 1 with increasing polarity of the solvent. Excellent fits were obtained with this solvent scale for other transition metal complexes having low lying MLCT states.

Unfortunately, as noted by Manuta and Lees [59], these empirical data offer little to an understanding of solvent phenomena on the molecular level. It was generally accepted that the solvent dependence was due to the fact that these complexes are highly polar and that the transition moment of the main MLCT transition lies antiparallel to the ground state dipole moment [38,53,54]. Lees and coworkers [59,67] and Kaim and Kohlmann [60] showed, however, that similar strong solvatochromic effects occur for complexes such as $(CO)_5W(pyz)W(CO)_5$ (pyz=pyrazine), which have no net ground state dipole moment and should therefore not be significantly solvatochromic. The authors ascribed this solvent effect to differences in polarizability of the complex between its ground and excited state.

Quite recently, this explanation was rejected by Dodsworth and Lever [61], who pointed out that the observed solvent shifts are far too large to be due to dispersion forces. According to these authors any explanation of the solvatochromism should be applicable to both the mononuclear and binuclear species since both types of complexes show good correlation with Lees' E^*_{MLCT} parameter. A good correlation was also obtained when the solvent data for one of these centrosymmetric complex, $(CO)_5W(pyz)W(CO)_5$, were fitted to McRae's equation using a two-parameter fit. This correlation was not improved when the Stark effect term, which depends on the difference in polarizabilities of the ground and excited states, was included in the equation. From the good correlation with the polar part of McRae's equation, the authors concluded that dipole–dipole interactions are also the main cause of solvatochromism in the case of the centrosymmetric com-

plexes. Such interactions are of importance here since these complexes consist of two polar halves which interact separately with the surrounding solvent molecules. According to the solvatochromism, the extent of this ordering of the solvent is comparable with that in mononuclear complexes.

The influence of the electronic structure of the α-diimine ligand on the extent of solvatochromism has been studied by Kaim and coworkers for several $M(CO)_4$(N-N) complexes [62]. These authors reported that an increase in π-acceptor capability of the ligand gave rise not only to a shift of the MLCT band to lower energy but also to an increase in solvatochromism. This means that the main electronic transition has its greatest degree of charge transfer character in complexes with the best π-acceptor ligand. This result is at variance with previous observations by tom Dieck and Renk [38,53,54] and with the results from the above-mentioned RR data (Fig. 7 [43]) that an increase in the amount of mixing of the metal and α-diimine ligand by making the ligand a stronger π acceptor decreases instead of increases the charge transfer character of the electronic transition and as a result the solvatochromism. Kaim and coworkers [62] assumed, however, that their complexes had equal metal–ligand bond polarities in their ground states, which is rather unlikely.

The RR data, presented as EPs for the complexes $W(CO)_4$(N-N) (N-N=4,7-Ph_2-phen, iPr-PyCa or iPr-DAB) in Fig. 7 [43], clearly show that the MLCT character of the main electronic transition ($b_2 \rightarrow b_2^*$) decreases on going from the 4,7-Ph_2-phen to the iPr-DAB complex. This effect was reflected in a decrease in the RR effects for the ligand stretching modes and an increase in the RR effect for ν_s(W–N). In the case of the iPr-DAB complex the transition has no MLCT character any more and it has become metal–ligand bonding to antibonding (see Fig. 6 right). Since there is no charge transfer, there is also no solvatochromism. We are dealing here with a maximum of back donation in the ground state since the b_2 orbital has $d_\pi + \pi^*$ character. In the case of the iPr-PyCa and 4,7-Ph_2-phen complexes the HOMO has more metal d_π character (less π back donation). As a result the $b_2 \rightarrow b_2^*$ transition has more MLCT character and a negative solvatochromism.

The influence of the metal on the MLCT character and solvatochromism of this electronic transition is nicely reflected in the RR spectra of the complexes $Re(CO)_3$(N-N)(Cl), $Mo(CO)_4$(N-N) and $W(CO)_4$(N-N) (N-N=Mes-DAB) (Fig. 8) [42].

The solvatochromism decreases from top to bottom and becomes zero for $W(CO)_4$(Mes-DAB). At the same time the MLCT character decreases since ν_s(CN) (1400–1500 cm^{-1}) decreases in intensity, whereas the RR intensity of ν_s(M–N) (about 290 cm^{-1}) increases. It will be shown hereafter that this change of MLCT character also has important consequences for the photophysical and photochemical properties of these complexes.

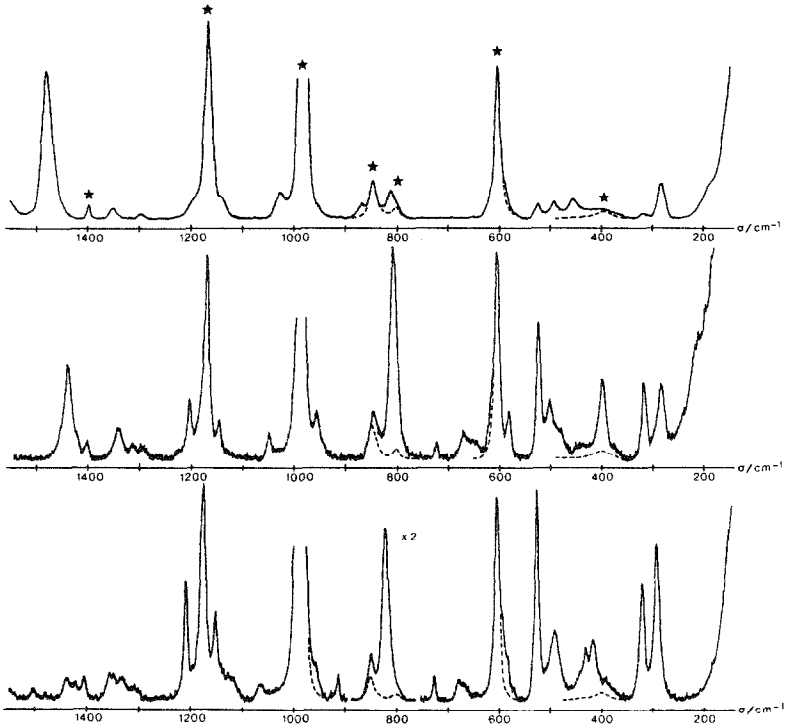

Fig. 8. Resonance Raman spectra for $ClRe(CO)_3$(Mes-DAB) (top), $Mo(CO)_4$(Mes-DAB) (middle) and $W(CO)_4$(Mes-DAB) (bottom) in C_6H_6 (*). (Reproduced with permission from ref. 42.)

(iii) Photophysical properties

Most luminescence studies of transition metal complexes have been performed at low temperature in a rigid medium such as a glass or matrix. Only a few metal carbonyls were found to luminesce at room temperature [16,68–78] and these emissions mainly originated from low energy ^{3}MLCT states. In this respect the $M(CO)_4$(N-N) complexes are particularly interesting since they may give rise to dual emission in fluid solution [43,75,76,78]. This dual emission is illustrated in Fig. 9, which presents the absorption and emission spectra of $Mo(CO)_4$(phen) in benzene at 298 K. In their first two articles on these emission spectra, Manuta and Lees [75,76] assigned both RT emissions as originating from different MLCT states. It was, however, shown by Servaas et al. [43] that the high energy (HE) emission at about 600 nm shifted position when the wavelength of the exciting laser line was varied. In the case of $W(CO)_4$(iPr-DAB), nearly two separated emissions within the HE band could be observed upon excitation with λ=458 nm. In accordance with the results for $W(CO)_4$(tmen) (tmen=*N*,*N*,*N*′,*N*′-tetra-

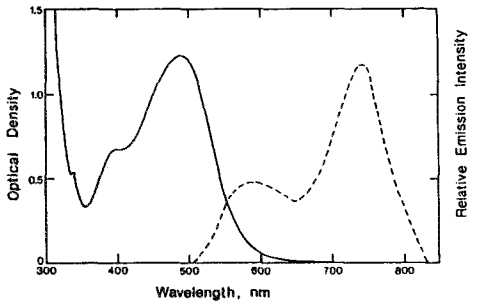

Fig. 9. Electronic absorption (——) and emission (– – –) spectra of $Mo(CO)_4(phen)$ in C_6H_6 at 298 K. (Reproduced with permission from ref. 76.)

methylethylenediamine), which complex has a weak ^{3}LF emission at about 540 nm, they assigned the HE band to emissions from a ^{3}LF and ^{3}MLCT state. This conclusion was recently verified by Rawlins and Lees [78], who measured the emission lifetimes of these HE bands in the case of several $M(CO)_4$(substituted phen) (M=Mo, W) complexes. Each 293 K HE emission decay curve could be resolved into two emission lifetimes. The short-lived component (τ=3–6 ns) was assigned to ^{3}LF emission and the longer component (τ=25–28 ns) to emission from the ^{3}MLCT state corresponding to the z-polarized $a_2 \rightarrow a_2^*$ transition to the second π^* orbital of the α-diimine ligand. The 298 K spectrum in Fig. 9 shows that the low energy (LE) emission at about 750 nm is much more intense than the HE band. Lifetime measurements [78] showed that the decay curve of this LE emission is single exponential. Moreover, the observed lifetime corresponds to the longer component of the HE emission. Apparently, at room temperature all emissive ^{3}MLCT states are in thermal equilibrium with each other but not with the short-lived ^{3}LF state.

Lowering the temperature of the solution (EPA or 2-MeTHF) caused the emission intensities to increase approximately 100-fold when the solution solidified to a glass ($T < 120$ K) [43,78]. This is illustrated for the emission of $W(CO)_4$(4,7-Ph_2-phen) in Fig. 10(a). Moreoever, the LE emissions shifted to higher energy and their lifetimes increased appreciably (τ=0.5–10 μs) [78]. The increase in emission quantum yields and lifetimes is consistent with a substantial reduction in the competing non-radiative processes in the rigid medium. At the same time the local solvent environment changes dramatically in the glass, causing both the absorption and emission bands to shift to higher energy. Rawlins and Lees [78] resolved the HE emission in the 80 K spectra of their complexes into two emission lifetimes. The characters of the LE emissions had, however, changed upon cooling since their decay curves now resolved into two different lifetimes. The two

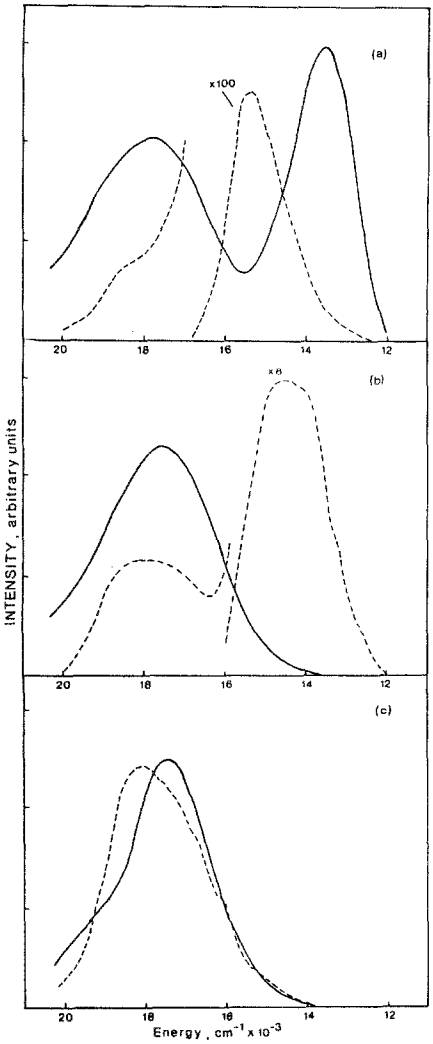

Fig. 10. Emission spectra in C_6H_6 at 293 K (——) and in 2-MeTHF at 80 K (- - -) of (a) $W(CO)_4$(4,7-Ph_2-phen), (b) $W(CO)_4$(iPr-PyCa) and (c) $W(CO)_4$(iPr-DAB), obtained by excitation with 488 nm. (Reproduced with permission from ref. 43.)

emissions were proposed to originate from different ^{3}MLCT states. The more intense emission (τ=4–10 μs) was assigned to the $b_2 \rightarrow b_2^*$ state and the other (τ=0.6–1.1 μs) to the $a_1 \rightarrow b_2^*$ state. The nature of the exponential deconvolution suggested that a third level, presumably the $a_2 \rightarrow b_2^*$ state, also contributed weakly to the LE emission at 80 K.

As mentioned above, this $a_2 \rightarrow b_2^*$ transition could be observed in the EPs derived from the RR spectra (see Fig. 7 [43]). It was also observed in the 80

K absorption spectrum of one of the complexes studied by Rawlins and Lees [78].

Excitation spectra monitored at the maximum of the LE emission [43] showed that this emission indeed arises mainly from the excited states contained in the low energy MLCT band.

A remarkable result was obtained by Servaas et al. [43], who studied the influence of the α-diimine ligand on the emission and RR spectra of the $W(CO)_4$(N-N) complexes. Their RR EPs have been discussed before (see Fig. 7) and the 293 and 80 K emission spectra of three representative complexes are presented in Fig. 10. In agreement with the results of Lees and coworkers [75,76,78] two emission bands (HE and LE) were observed for $W(CO)_4$(4,7-Ph_2-phen). The corresponding iPr-PyCa complex also showed both emissions at 80 K but only the HE band at 293 K, whereas the LE emission was completely absent in the spectra of the iPr-DAB complex.

As shown above, this LE emission mainly originates from the $b_2 \rightarrow b_2^*$ state. The character of the corresponding transition changes completely, however, upon going from the 4,7-Ph_2-phen to the iPr-PyCa and iPr-DAB complexes, as can be seen from the solvatochromism and from the RR EPs depicted in Fig. 7. The $b_2 \rightarrow b_2^*$ transition of $W(CO)_4$(4,7-Ph_2-phen) is MLCT in character as shown by its large negative solvatochromism and by strong RR effects for the symmetrical ligand stretching modes. The corresponding band of $W(CO)_4$(iPr-DAB) is not solvent dependent and the transition only shows a strong RR effect for ν_s(W–N). It has therefore no MLCT character but is instead metal–ligand bonding to antibonding.

With the following equation the RR intensities I of two vibrations k and k' can be related to the changes in equilibrium distances (Δ_k) between the ground and excited state potential energy curves [79]:

$$\frac{I_k}{I_{k'}} = \frac{\Delta_k^2 \omega_k^2}{\Delta_{k'}^2 \omega_{k'}^2} \qquad (6)$$

In this equation, ω_k represents the wavenumber of vibration k. A high RR intensity for a low frequency mode ($\omega_{W-N}=\nu_s$(W–N)=230 cm^{-1}) will therefore correspond to a large shift of the potential energy curve along the normal coordinate of that vibration. Such a large shift may cause an efficient crossing between these surfaces and increase the rate of non-radiative decay. Moreover, according to Robbins and Thomson [80], the electronic integral $J_k(m,n)$, which is part of the matrix element connecting ground and excited states, is largest when the promoting mode k belongs to metal–ligand skeletal vibrations. As a result the LE emission quantum yield will decrease upon going from the 4,7-Ph_2-phen to the iPr-PyCa and iPr-DAB complexes. Apparently, the emission behaviour of $W(CO)_4$(iPr-PyCa) is in

between that of the other two complexes since it only shows the LE emission in the 80 K spectra.

(iv) Photochemical behaviour

Wrighton and Morse [81] were the first who studied in detail the photochemistry of several of these $M(CO)_4(N\text{-}N)$ complexes. They followed the reactions of $W(CO)_4(N\text{-}N)$ (N-N=bpy, R-phen) with different nucleophiles and used Hg lines between 313 and 436 nm. The following substitution reaction was observed:

$$W(CO)_4(N\text{-}N) \xrightarrow[L]{h\nu} W(CO)_3(N\text{-}N)L + CO \qquad (7)$$

Quantum yields appeared to be wavelength dependent and varied from 10^{-4} at 436 nm to 10^{-2} upon irradiation with 313 nm. From this wavelength dependence the authors concluded that the MLCT states themselves are not reactive and that a thermally populated LF state is responsible for the CO substitution. Manuta and Lees [76] extended these investigations to complexes of chromium and molybdenum and to measurements at a longer wavelength. From their quantum yield data they also concluded that these reactions most probably occur from a close lying ^{3}LF state.

Recently, Vlček and coworkers [82] reported the quantum yields for the photosubstitution of CO by PPh_3 in $Cr(CO)_4(bpy)$ at different wavelengths of irradiation within the MLCT band. The quantum yield ϕ appeared to increase monotonically with the excitation energy, pointing to the involvement of higher electronically non-relaxed states. The authors discarded a reaction from ^{3}LF thermally populated from equilibrated ^{3}MLCT states since ϕ did not correlate with the solvent-determined LF-MLCT energy gap. It was concluded that this reaction proceeds either from the ^{1}MLCT states or from ^{3}LF after direct intersystem crossing from these ^{1}MLCT states. It is, however, questionable whether intersystem crossing to ^{3}LF can still occur at such low energies ($\lambda \approx 550$ nm) of excitation. Balk et al. [41] studied the influence of the metal and the α-diimine ligand on both the RR spectra and the photosubstitution quantum yields of the complexes $M(CO)_4(N\text{-}N)$ (M=Cr, Mo, W; N-N=bpy, phen, R-PyCa, R-DAB). The quantum yield varied from 0 to 5×10^{-2} mol einstein^{-1} and decreased on going from chromium to molybdenum and tungsten and from bpy and phen to R-PyCa and R-DAB. In the case of the tungsten complexes they observed a large influence of the electronic and steric properties of the substituting ligand on ϕ. They explained this effect by adopting an associative reaction from the ^{3}MLCT states. This mechanism was confirmed by van Dijk et al.

[83] who investigated for a series of $W(CO)_4$(N-N) complexes the influence of the concentration and of the steric and electronic properties of the substituting PR_3 ligand on the quantum yield. The value of ϕ appeared to depend strongly on these ligand properties and increased, for example, by a factor of nearly a thousand, when the PR_3 concentration was raised. The quantum yield also depended on the electronic and steric properties of the α-diimine ligand. Increasing the steric requirements of the R substituent of R-DAB caused a decrease in ϕ. Moreover, for the reaction with the strong Lewis base P(nBu)$_3$, ϕ decreased by a factor of 100 on going from $W(CO)_4$(phen) to $W(CO)_4$(cPr-DAB) (cPr=cyclopropyl). Since steric effects are not important here because of the small size of the cyclopropyl substituent, electronic effects will be responsible for this decrease in ϕ.

Such electronic effects are indeed important for these associatively proceeding reactions, since the nucleophilic attack of P(nBu)$_3$ on the metal in the MLCT excited state will depend on the charge of the metal. This positive charge will decrease when the main electronic transition ($b_2 \rightarrow b_2^*$, vide supra) loses its MLCT character upon going from $W(CO)_4$(phen) to $W(CO)_4$(cPr-DAB). The associative character of the above reactions is also supported by the recent results of Wieland and van Eldik [84] who studied the pressure dependence of the quantum yields for the reaction of $W(CO)_4$(phen) with PEt_3. The pressure was varied between 0 and 200 MPa and quantum yields were measured at two wavelengths of irradiation (366 and 546 nm). From the plots of ln (ϕ/ϕ_0) (ϕ_0, quantum yield at ambient pressure) against pressure the volumes of activation $\Delta V_\phi^\#$ were derived for both wavelengths of irradiation. MLCT excitation yielded a negative volume of activation and LF irradiation a positive one. This means that 366 nm irradiation leads to a dissociative LF reaction and 546 nm irradiation to an associative reaction from the MLCT state. The corresponding chromium and molybdenum complexes do not give rise to an associative reaction but instead to dissociative loss of CO with much higher quantum yields. Balk et al. [41] stated more explicitly than Vlček and coworkers [82] that these reactions take place from one or more MLCT states. This assumption was based on the close relationship that appeared to exist between the photosubstitution quantum yields and the RR intensities obtained by excitation into the MLCT band. These RR spectra, discussed in a previous section [41,43] showed resonance enhancement of Raman intensity not only for the symmetrical α-diimine ligand and metal–ligand stretching modes, but also for the symmetrical stretching mode of the axial carbonyls (see Fig. 2).

The corresponding vibration of the equatorial carbonyls could not even be detected in the spectra of any of these complexes. Balk et al. [41] studied this effect in detail for a series of $M(CO)_4$(N-N) complexes and they excited the RR spectra at different positions within the MLCT band. The main

results of this study will now be discussed in some detail. Figure 11 presents parts of the RR spectra of $W(CO)_4$(phen) and $W(CO)_4$(bpy), excited close to the maximum of the MLCT band. Both spectra show RR effects for ligand stretching modes, for the two symmetrical metal–C stretching vibrations and for $\nu_s(CO)_{ax}$. The intensities of the two ν_s(W–C) Raman bands are clearly interrelated but no such relationship exists with the intensities of $\nu_s(CO)_{ax}$ and $\nu_s(CO)_{eq}$. The latter vibration, expected at about 1850 cm^{-1}, could not even be detected. Apparently the RR effects of the metal–C stretching modes and of $\nu_s(CO)_{ax}$ have a different origin. The metal–C stretching modes will be enhanced in intensity because the central metal atom becomes oxidized in the MLCT excited state. The origin of the RR effect of $\nu_s(CO)_{ax}$ becomes evident when the following observations are considered [41]. An increase in the size of metal (Cr→Mo) causes a decrease in the RR intensity of $\nu_s(CO)_{ax}$ with respect to those of the ligand stretching modes (see Fig. 12). The further decrease in relative intensity on going to the tungsten complex is certainly not due to a size effect since molybdenum and tungsten hardly differ from each other in this respect. This effect is caused by a decrease in solvatochromism of the MLCT band. This influence of the solvatochromism or MLCT character of the main $b_2 \rightarrow b_2^*$ transition is further demonstrated for the complexes $M(CO)_4$(iPr-DAB) (M=Mo, W) in Fig. 13. The RR spectra presented in this figure were excited

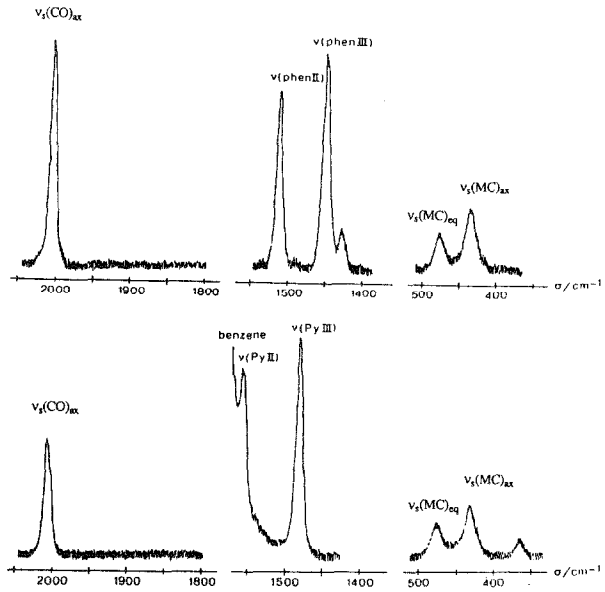

Fig. 11. Resonance Raman spectra in the metal–C, α-diimine and CO stretching region of $W(CO)_4$(phen) (top) and $W(CO)_4$(bpy) (bottom) in C_6H_6. (Reproduced with permission from ref. 41.)

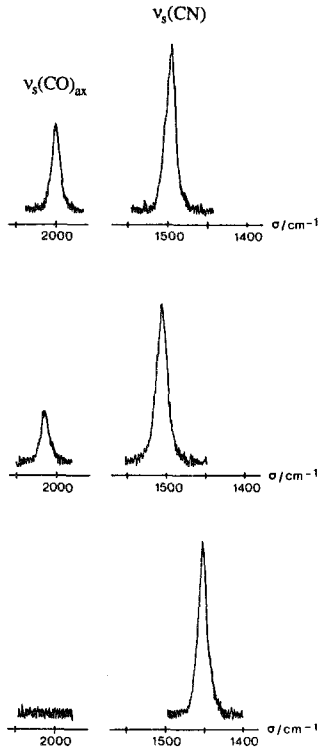

Fig. 12. Resonance-enhanced $\nu_s(CN)$ and $\nu_s(CO)_{ax}$ Raman bands of $M(CO)_4$(*p*Tol-DAB) (M=Cr (top), Mo (middle), and W (bottom)) in $CHCl_3$. (Reproduced with permission from ref. 41.)

close to the maximum of the MLCT band from solutions having the same optical density. The decrease in solvatochromism on going from the molybdenum to the tungsten complex is accompanied by a decrease in intensity for $\nu_s(CN)$ of the iPr-DAB ligand (vide supra). At the same time $\nu_s(CO)_{ax}$ decreases in intensity but this effect is even larger than for $\nu_s(CN)$.

A third factor which influences the RR intensity of $\nu_s(CO)_{ax}$ is the electron distribution in the lowest π^* orbital of the α-diimine ligand. This is evident from the RR spectra of $W(CO)_4$(phen) and $W(CO)_4$(bpy) in Fig. 11. The MLCT bands of these complexes exhibit a similar solvatochromism. However, the lowest π^* orbital of bpy has less density at the N atoms and this apparently causes a decrease in the relative RR intensity of $\nu_s(CO)_{ax}$ with respect to the phen complex.

These three effects on the RR intensity of $\nu_s(CO)_{ax}$ have been attributed by Balk et al. [41] to a through-space overlap between the α-diimine ligand π^* orbital and a π^* orbital combination of the axial carbonyls. This excited state interaction will decrease when the size of the metal increases, when the MLCT character of the $b_2 \rightarrow b_2^*$ transition decreases (decrease in solvato-

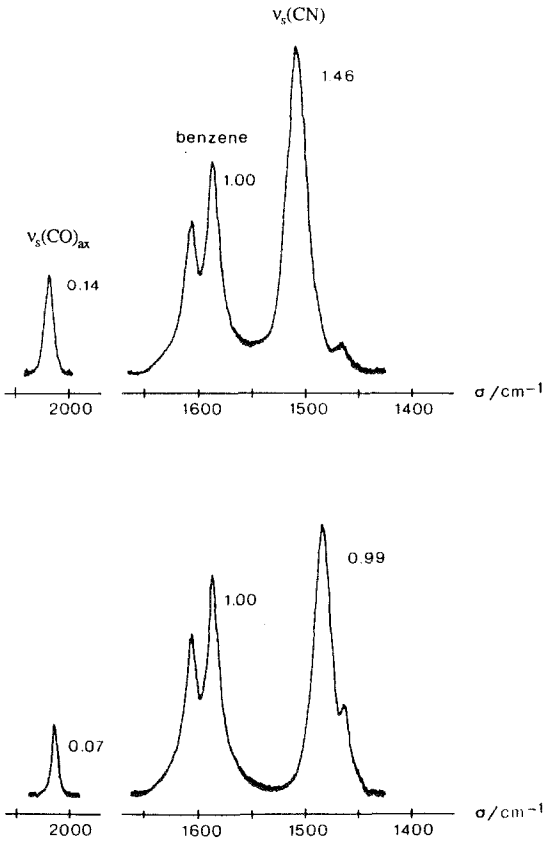

Fig. 13. Resonance-enhanced ν_s(CN) and $\nu_s(CO)_{ax}$ Raman bands of $M(CO)_4$(iPr-DAB) (M=Mo (top), W (bottom)) in C_6H_6. Spectra were obtained by excitation of solutions having the same optical density. (Reproduced with permission from ref. 41.)

chromism!) and when the electron density at the coordinating N atoms in the lowest π^* orbital of the α-diimine ligand decreases.

Quite remarkably, a qualitative relationship appeared to exist between these RR intensities of $\nu_s(CO)_{ax}$ and the photosubstitution quantum yields [41]. From this observation it was concluded that the interaction between the α-diimine and axial CO π^* orbitals is responsible for release of CO from the MLCT state(s). It has to be noted, however, that such a delocalization of the MLCT state does not result from a recent DV-$X\alpha$ molecular orbital calculation on the lowest excited state of $Cr(CO)_4$(bpy) [85].

Labilization of an axial CO ligand was also observed for the anions of these $M(CO)_4$(N-N) complexes. Miholová and Vlček [86] and Olbrich-Deussner and Kaim [87] even observed an electrocatalytic substitution of an axial CO group by a phosphine ligand.

(v) Concluding remarks

The results discussed in this section show that the character of the main MLCT transition of these $M(CO)_4(N\text{-}N)$ complexes as well as their photophysical and photochemical properties are mainly determined by the extent to which the metal $d_\pi(b_2)$ and ligand $\pi^*(b_2)$ orbitals interact in the ground and excited states. The RR data obtained for these compounds demonstrate the great importance of this technique for the characterization of electronic transitions and for the understanding of excited state properties.

C. $(CO)_5M'M(CO)_3$(α-DIIMINE) (M, M'=Mn, Re)

(i) Formation of the complexes

The metal–metal-bonded carbonyls discussed in Sections C, D and E have in common the $M(CO)_3$(α-diimine) fragment of zerovalent manganese or rhenium.

Several methods have been used to prepare these complexes [88–94]. Morse and Wrighton [90,91] synthesized $(CO)_5MnMn(CO)_3$(phen) by irradiating a solution of $Mn_2(CO)_{10}$ and phen. The resulting mixture of $Mn_2(CO)_{10}$, (phen)$(CO)_3MnMn(CO)_3$(phen) and $(CO)_5MnMn(CO)_3$(phen) was separated by chromatography. Most widely used [88,89], however, is the thermal reaction between a metal carbonyl anion and a metal carbonyl halide or cation. A representative reaction is shown in eqn. (8) (X=halide):

$$Re(CO)_5^- + XRe(CO)_3(N\text{-}N) \rightarrow (CO)_5ReRe(CO)_3(N\text{-}N) + X^- \quad (8)$$

Alternatively, use has been made of the triflate salts $M(CO)_3(N\text{-}N)^+(OTF)^-$ ($OTF=CF_3SO_3$). Kruck et al. [88,89] synthesized in this way the first representative of this series, $(CO)_4CoRe(CO)_3$(phen), by dry heating at 90°C the ionic complex $[Re(CO)_4(phen)][Co(CO)_4]$. In order to find out whether reaction (8) proceeds by simple associative nucleophilic displacement of the halide or via an electron transfer mechanism, Morse and Wrighton [90,91] studied this reaction in more detail. As the anion they used $Mn(CO)_5^-$ or $Re(CO)_5^-$, as the halide several complexes $XM(CO)_3(N\text{-}N)$ (N-N=bpy, (substituted)phen) and also *fac*-$ClRe(CO)_3(py)_2$. $Re(CO)_5^-$ reacted with all $XM(CO)_3(N\text{-}N)$ complexes but not with *fac*-$ClRe(CO)_3(py)_2$. The same result was obtained for $Mn(CO)_5^-$. Besides, this anion did not react with $ClRe(CO)_3$(phen). From these observations the authors concluded that reaction (8) proceeds via an electron transfer mechanism. This conclusion was confirmed by a comparison of the reduction potentials of the halides, $Mn_2(CO)_{10}$ and $Re_2(CO)_{10}$. These potentials appeared to be much higher for $ClRe(CO)_3(py)_2$ than for $Re_2(CO)_{10}$ and $Mn_2(CO)_{10}$. Moreover,

$Re_2(CO)_{10}$ has a higher reduction potential than the $XM(CO)_3(N\text{-}N)$ complexes, whereas $Mn_2(CO)_{10}$ has a lower $E_{1/2}$ value than $ClRe(CO)_3(phen)$.

Staal et al. [92] used this method for the preparation of a series of $(CO)_5MnMn(CO)_3(R\text{-}DAB)$ complexes and could also synthesize in this way the complexes $(CO)_5MnRe(CO)_3(R\text{-}DAB)$. This result is not at variance with the above results of Morse and Wrighton [90,91] since the R-DAB complexes are known to have lower reduction potentials than the bpy and phen complexes [96]. For the preparation of the complexes $Ph_3ERe(CO)_3(N\text{-}N)$ (E=Ge, Sn; N-N=bpy, phen), Luong et al. [93,94] used instead the electron transfer reaction (9) (X=halide):

$$Re(CO)_3(N\text{-}N)^- + Ph_3EX \rightarrow Ph_3ERe(CO)_3(N\text{-}N) + X^- \quad (9)$$

$Re(CO)_3(N\text{-}N)^-$ was prepared by chemical reduction of $ClRe(CO)_3(N\text{-}N)$. The same method has been used recently by Andréa et al. [95,109,111] for the synthesis of a series of $Ph_3EM(CO)_3(N\text{-}N)$ (E=Ge, Sn, Pb; M=Mn, Re; N-N = bpy', R-DAB, R-PyCa) complexes.

(ii) Electronic transitions

Figure 14 shows the structure of a $(CO)_5M'M(CO)_3(R\text{-}DAB)$ complex that is based on the X-ray structure determination by Kokkes et al. [97] for $(CO)_5ReMn(CO)_3(iPr\text{-}DAB)$. The α-diimine ligand is always σ-N, σ-N' bonded to the metal in an equatorial position. The CO ligands of the $M'(CO)_5$ and $M(CO)_3$ moieties are in a staggered position, just as in the case of the $(CO)_5M'M(CO)_5$ complexes [98].

Figure 15 presents the molecular orbitals of these complexes in a qualitative interaction diagram [90,99]. The metal–metal bonding orbital σ_b that connects the two metal fragments is assumed to be the HOMO. This

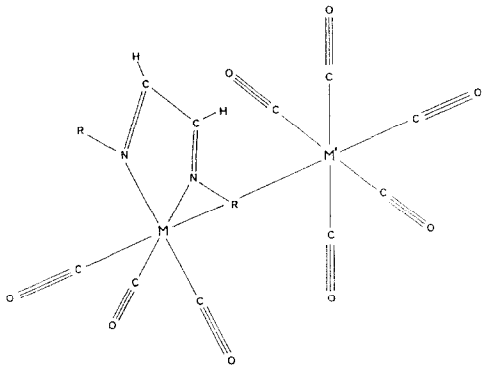

Fig. 14. Structure of $(CO)_5M'M(CO)_3(R\text{-}DAB)$ (M, M'=Mn, Re).

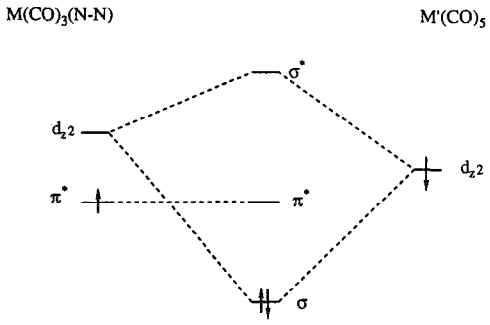

Fig. 15. Interaction of $M'(CO)_5$ and $M(CO)_3(N\text{-}N)$ molecular orbitals to give $(CO)_5M'M(CO)_3(N\text{-}N)$.

assumption agrees with the UV photoelectron spectra of these complexes [99], which show that this σ_b orbital has the lowest ionization potential (IP). $IP(\sigma_b)$ is largest for the complexes having an Re–Mn bond. This agrees with the observation that $(CO)_5ReMn(CO)_5$ has the highest M–M′ bond dissociation energy of all decacarbonyls [100]. Figure 16 shows the absorption spectrum of a representative complex. The lowest energy band has the characteristic features of an MLCT band. Its intensity is high ($\varepsilon=(8\text{–}12)\times 10^3$ M^{-1} cm^{-1}) and its position depends on the solvent and α-diimine ligand. The second band, having its maximum at about 330 nm, belongs to the intense $\sigma_b \rightarrow \sigma^*$ transition. It occurs at an energy similar to that for the parent decacarbonyl.

There has been some controversy about the correct assignment of the lowest energy band. Morse and Wrighton [90,91] observed a homolytic

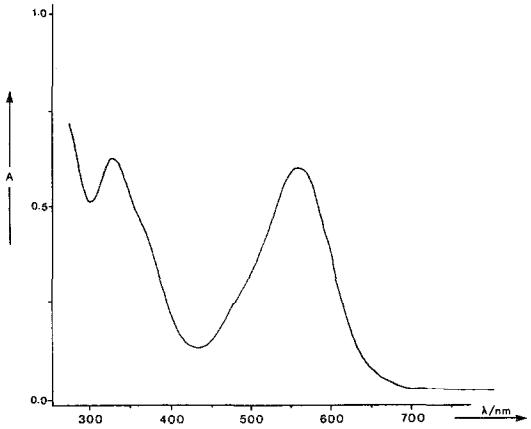

Fig. 16. Electronic absorption spectrum of $(CO)_5MnMn(CO)_3$(iPr-DAB) in *n*-pentane. (Reproduced with permission from ref. 103.)

splitting of the metal–metal bond upon irradiation into this band. On the basis of this observation they assigned this band to a $\sigma_b \rightarrow \pi^*(\alpha\text{-diimine})$ transition. The metal–metal bond will then be weakened in the excited state, which explains the photochemistry. There are, however, strong arguments against this assignment [97]. Firstly, there is a striking similarity between the energies and intensities of these bands and those of the d^6-$M(CO)_4(N\text{-}N)$ (M=Cr, Mo, W) complexes discussed in the preceding section. Upon cooling, the MLCT band even becomes structured [90,92] just as in the case of these d^6 complexes. An even more convincing argument against the $\sigma_b \rightarrow \pi^*$ assignment is presented by the RR spectra of these complexes [97], two of which are shown in Fig. 17. These spectra, recorded in an N_2 matrix in order to avoid photodecomposition, strongly differ in character. The spectrum of $(CO)_5MnRe(CO)_3$(iPr-DAB) shows a strong RR effect for ν_s(CN) and ν(CC) of the iPr-DAB ligand, which means that the electronic transition involved has a rather strong MLCT character (vide supra). Both bands have, however, nearly disappeared in the RR spectrum of $(CO)_5ReRe(CO)_3$(iPr-DAB) while two deformation modes of the iPr-DAB ligand (800–1000 cm^{-1}) and the metal–ligand stretching modes have increased in intensity. This means that the electronic transition has lost its charge transfer character and has become metal–ligand bonding to antibonding

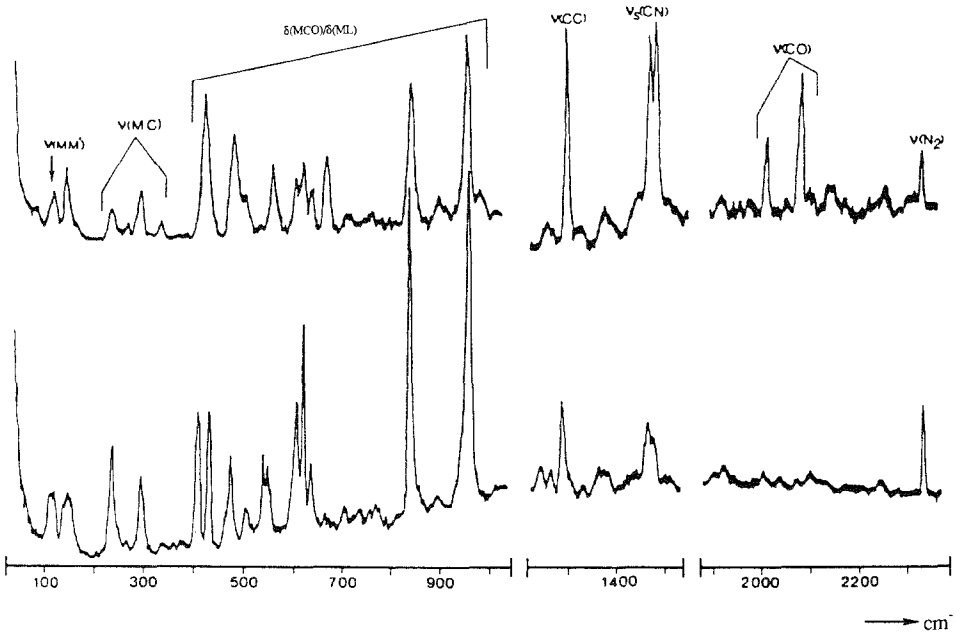

Fig. 17. Resonance Raman spectra of $(CO)_5MnRe(CO)_3$(iPr-DAB) (top) and $(CO)_5ReRe(CO)_3$(iPr-DAB) (bottom) in an N_2 matrix at 10 K. (Reproduced with permission from ref. 107.)

[43]. Such a change of MLCT character will show up when the metal *d* and α-diimine π* orbitals involved in the transition have the same symmetry and change their interaction in the ground and MLCT excited states (vide supra). Just as in the case of mononuclear $M(CO)_4(N\text{-}N)$ complexes, the main transition within the low energy band will therefore originate from that metal *d* orbital that is responsible for the metal to α-diimine π backbonding. This transition hardly influences the metal–metal bond since only weak RR effects were observed for the metal–metal stretching modes of these complexes. In the case of a $\sigma_b \rightarrow \pi^*$ transition much stronger RR effects would have been expected for these vibrations. The $\sigma_b \rightarrow \pi^*$ transition can of course underlie the MLCT band. It can, however, hardly contribute to its intensity since the RR excitation profiles only give evidence for the above metal $d_\pi \rightarrow \pi^*$ transition. The EPs of all resonance-enhanced Raman bands of $(CO)_5ReRe(CO)_3$(iPr-DAB) show a single maximum at the same position within the MLCT band [101].

(iii) Photophysical properties

Morse and Wrighton [90] measured the emission spectrum of $(CO)_5ReRe(CO)_3$(phen) in EPA at 77 K, obtained by excitation into the MLCT band. They reported a lifetime of 95 μs and a quantum yield of 10^{-2} mol einstein^{-1}. The emission spectrum was independent of the wavelength of excitation. From the long lifetime the authors concluded that the emissive state has predominant MLCT character.

Quite recently, Glezen et al. [102] extended these measurements to the complexes $(CO)_5M'Re(CO)_3(bpy')$ (M'=Mn, Re) and $(CO)_5ReRe(CO)_3$(iPr-PyCa). Only $(CO)_5ReRe(CO)_3(bpy')$ was found to emit under RT conditions. One broad solvent-dependent emission showed up in the 600 nm region. Excitation spectra recorded at the emission maximum showed that this emission was associated with one or more transitions between 350 and 400 nm and not with the low energy MLCT transitions. Emission from these low energy MLCT states was assumed to occur outside the instrumental wavelength region. This assumption was confirmed by the low temperature emission spectra. Upon cooling a solution of $(CO)_5ReRe(CO)_3(bpy')$ in 2-MeTHF, the 620 nm emission shifted to higher energy, reaching a position of 542 nm at 80 K. At the same time a new intense emission showed up at 686 nm (T=80 K). The excitation spectrum, recorded at the maximum of this band, showed that the emission is associated with the low energy MLCT transitions. A similar dual emission was recently observed for several $M(CO)_4(N\text{-}N)$ (M=Mo, W) complexes [43,78] (vide supra).

Just as for these latter complexes, the high energy emission in the 80 K spectrum of $(CO)_5ReRe(CO)_3(bpy')$ resolved into two emission lifetimes (1.5

μs and 3.5 μs respectively). It is not clear why these lifetimes are so much shorter than that reported for $(CO)_5ReRe(CO)_3$(phen) by Morse and Wrighton [90] (vide supra). The low energy emission decay curve resolved in only one lifetime of 6.8 μs.

As might be expected from the excitation spectra, the relative intensities of the two emissions appeared to depend on the wavelength of excitation. Both emissions showed up on excitation with λ=350 nm; with λ_{ex}=440 nm, only the low energy emission was observed. At the same time, variation of this wavelength of excitation caused a shift of the maximum of the high energy band. A similar effect had been observed for $W(CO)_4$(4,7-Ph_2-phen) [43]. It confirms the presence of two emissions in the high energy band and agrees with the observation of two emission lifetimes. Apparently, three distinct non-equilibrated states, one at lower and two at higher energy, are associated with these emissions at 80 K. The low energy emission was assigned to a ^{3}MLCT state. There was no indication for the presence of two such non-equilibrated low energy ^{3}MLCT states as for the $M(CO)_4$(N-N) (M=Mo, W) complexes.

Since the position of the high energy emission depended on the α-diimine ligand and the solvent, one component was associated with a ^{3}MLCT state. The second component was tentatively assigned to an emissive ^{3}LF state, just as for the $M(CO)_4$(N-N) (M=Mo, W) complexes [43,78]. The corresponding $^3\sigma_b\sigma^*$ state of the metal–metal bond is not expected to be emissive because of its large reactivity (vide infra).

The above spectroscopic and photophysical data do not point to any involvement of the metal–metal bond in the low energy transitions of these complexes. On the contrary, these transitions are completely similar in (MLCT) character as those of the mononuclear α-diimine complexes discussed in the preceding section. It is therefore not clear from these results how irradiation into such a low energy MLCT band can lead to an efficient photochemical reaction [90]. It will be shown in the next section that this high photochemical reactivity is mainly due to the repulsive character of the $^3\sigma_b\sigma^*$ state of the metal–metal bond.

(iv) Photochemical behaviour

Morse and Wrighton [90] observed the following reaction upon irradiation of $(CO)_5MM(CO)_3$(phen) (M=Mn, Re) in CH_2Cl_2/CCl_4 (1:1) into the low energy MLCT band:

$$(CO)_5MM(CO)_3(phen) \xrightarrow[CH_2Cl_2/CCl_4]{h\nu} ClM(CO)_5 + ClM(CO)_3(phen) \qquad (10)$$

Photolysis of these complexes in a degassed benzene solution afforded

$M_2(CO)_{10}$ and (phen)$(CO)_3MM(CO)_3$(phen). Both reactions point to a homolytic splitting of the metal–metal bond. The quantum yields were practically wavelength independent and as high as 0.9 mol einstein^{-1} in the case of $(CO)_5MnMn(CO)_3$(phen). From the wavelength independence of ϕ, Morse and Wrighton concluded that these reactions occur from the lowest MLCT state. In order to account for the high photoreactivity, the lowest MLCT transition was assigned as $\sigma_b \rightarrow \pi^*$(phen) instead of as a metal-$d_\pi \rightarrow \pi^*$(phen) transition as for the mononuclear analogues. Depopulation of the σ_b orbital was concluded to be sufficient to labilize the M–M bond.

As shown in a previous section this assignment does not agree with the RR data [97,101], which point to the presence of only one major transition within the MLCT band, having metal-$d_\pi \rightarrow \pi^*$(α-diimine) character. On the basis of these RR data, Kokkes et al. [103–107] proposed that these homolysis reactions occur from the $^3\sigma_b\pi^*$ state after energy transfer from a $^{1,3}d_\pi\pi^*$ state. Meyer and Caspar [11] proposed a mechanism based on the energy diagram of the parent $M_2(CO)_{10}$ complexes, which will be discussed in detail at the end of this section. In recent years the photochemical reactions of these complexes, first reported by Morse and Wrighton [90], have been extended by our group to other systems, reagents and media [103–108].

The results of these studies showed that irradiation of these complexes into the MLCT band may give rise to either homolysis of the metal–metal bond or release of CO. Besides, the radicals formed by the homolysis reaction appeared to undergo very interesting secondary reactions. Irradiation of $(CO)_5MnMn(CO)_3$(N-N) at temperatures above 200 K gave rise to the formation of $Mn_2(CO)_{10}$ and the dimer (N-N)$(CO)_3MnMn(CO)_3$(N-N) [103]. The IR and UV–visible spectral changes accompanying this reaction for $(CO)_5MnMn(CO)_3$(bpy′) are shown in Figs. 18 and 19 respectively. With respect to the parent compound the MLCT band of the dimer is shifted appreciably to lower energy. The dimers appeared to be partly split into their radicals, which were identified by ESR [103,109,110].

A similar homolysis reaction was observed for the corresponding $(CO)_5MnRe(CO)_3$(N-N) and $(CO)_5ReRe(CO)_3$(N-N) complexes. The Re$(CO)_3$(N-N) radicals, however, did not dimerize. They are also thermally more stable than the corresponding Mn radicals and Re$(CO)_3$(*t*Bu-DAB) radicals were detected even at 60°C by photolysis of $Ph_3SnRe(CO)_3$(*t*Bu-DAB) [109]. Figure 20 shows the ESR spectrum of this radical in cyclohexane with extensive hyperfine splittings (hfs) from one ^{185,187}Re nucleus, two equivalent ^{14}N nuclei and two equivalent ^{1}H nuclei. The unpaired electron mainly resides at the *t*Bu-DAB ligand which means that these radicals are best considered as 16e radical anion complexes in which Mn^+ or Re^+ (d^6) is surrounded by three carbonyl ligands and a negatively charged α-diimine

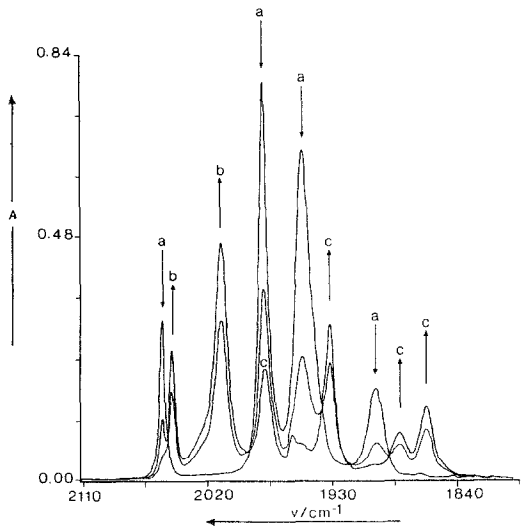

Fig. 18. IR spectral changes in the CO stretching region upon irradiation of a 2-MeTHF solution of $(CO)_5MnMn(CO)_3(bpy')$ with 500 nm: **a**, $(CO)_5MnMn(CO)_3(bpy')$; **b**, $Mn_2(CO)_{10}$; **c**, $(bpy')(CO)_3MnMn(CO)_3(bpy')$. (Reproduced with permission from ref. 105.)

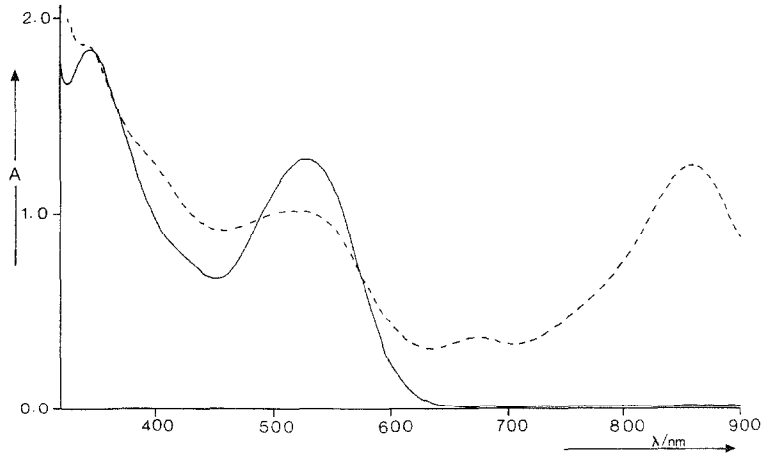

Fig. 19. Electronic absorption spectra measured before (——) and after (– – –) irradiation of $(CO)_5MnMn(CO)_3(bpy')$ in 2-MeTHF with 514.5 nm. (Reproduced with permission from ref. 105.)

ligand. Addition of $P(OPh)_3$ or $P(OMe)_3$ to a solution of this $Re(CO)_3(t$Bu-DAB) radical gave rise to the formation of a new paramagnetic species showing, apart from the hfs due to the $^{185,187}Re$, ^{14}N and ^{1}H nuclei, also hfs for one ^{31}P nucleus [109]. The phosphines apparently form the 18e adduct $Re(CO)_3(t$Bu-DAB)(PR_3). More basic phosphines reacted with the radical to give diamagnetic species. These photochemical and secondary

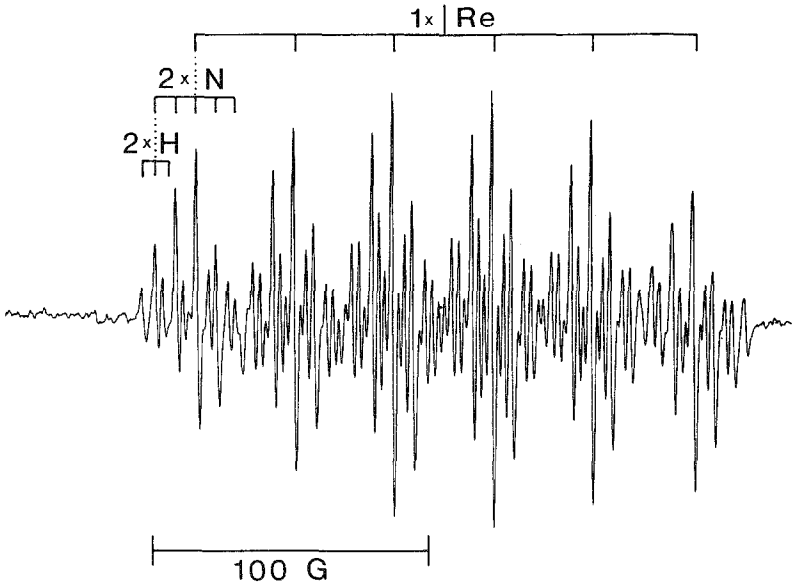

Fig. 20. ESR spectrum of $Re(CO)_3$(*t*Bu-DAB) measured in cyclohexane at 343 K (a_{Re}=35.55 G, a_N=7.34 G, a_H=5.03 G, g=2.0046). (Reproduced with permission from ref. 109.)

thermal reactions are summarized in eqns. (11)–(14) where M, M′=Mn, Re except M′=Re and M=Mn:

$$(CO)_5M'M(CO)_3(N\text{-}N) \xrightarrow{h\nu} M'(CO)_5 + M(CO)_3(N\text{-}N) \quad (11)$$

$$2M'(CO)_5 \rightarrow M'_2(CO)_{10} \quad (12)$$

$$2M(CO)_3(N\text{-}N) \rightleftarrows (N\text{-}N)(CO)_3MM(CO)_3(N\text{-}N) \quad (13)$$

$$M(CO)_3(N\text{-}N) + PR_3 \rightarrow M(CO)_3(N\text{-}N)(PR_3) \quad (14)$$

Deviating photochemical behaviour was observed for the complexes $(CO)_5ReMn(CO)_3(N\text{-}N)$ [105,108]. Irradiation in the absence of a substituting ligand gave rise to photodecomposition and to the formation of only a small amount of $Re_2(CO)_{10}$. In the presence of PR_3, $(CO)_5ReMn(CO)_2(N\text{-}N)(PR_3)$ was formed, whereas no such photosubstitution reaction was observed at RT for any of the other $(CO)_5M'M(CO)_3(N\text{-}N)$ complexes. A similar photochemistry was observed only for the complexes $Ph_3SnMn(CO)_3(N\text{-}N)$ [112] (vide infra). On the other hand, irradiation of these $(CO)_5ReMn(CO)_3(N\text{-}N)$ complexes in CH_2Cl_2 gave rise to the formation of $ClRe(CO)_5$ and $ClMn(CO)_3(N\text{-}N)$, which points to homolysis of the metal–metal bond as a primary photoprocess in addition to release of CO. Quite recently, it was, however, demonstrated that these com-

plexes $ClRe(CO)_5$ and $ClMn(CO)_3(N\text{-}N)$ are formed by a secondary photochemical reaction of CH_2Cl_2 with the primary photoproduct $(CO)_4Re(\mu\text{-}CO)Mn(CO)_2(N\text{-}N)$ [108]. The reason for the deviating behaviour of these $(CO)_5ReMn(CO)_3(N\text{-}N)$ complexes will be discussed hereafter.

The difference in character between the metal-localized $M'(CO)_5$ and (N-N)-localized $M(CO)_3(N\text{-}N)$ radicals manifests itself in the dimerization reactions (12) and (13). Reaction (12) proceeds by a direct bonding interaction between the electrons at the metal atoms. Reaction (13) proceeds according to a completely different mechanism. Irradiation of a complex $(CO)_5MnMn(CO)_3(N\text{-}N)$ (N-N=R-PyCa, R-DAB) at 170 K gave rise to the formation of intermediate **A** and $Mn_2(CO)_{10}$ [108]. **A** transformed into **B** and finally into the dimer by slowly raising the temperature of the solution in the IR cell (Scheme 1). Both **A** and **B** could be detected and identified by IR spectroscopy.

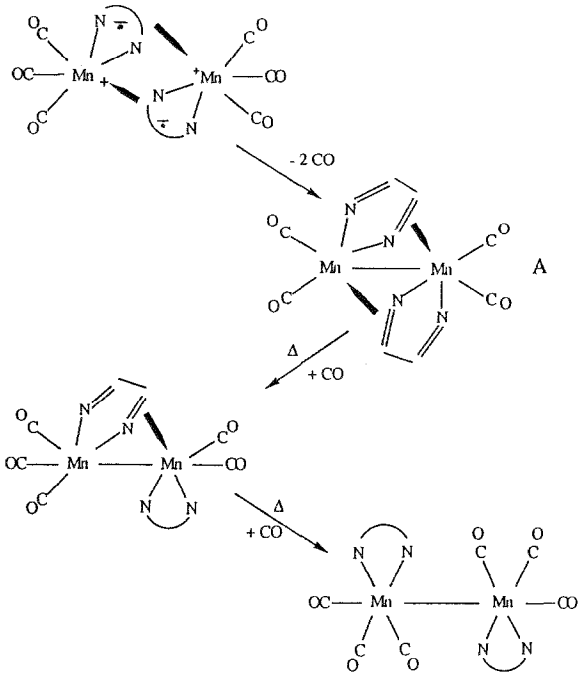

Scheme 1.

The mechanism in Scheme 1 is based on nucleophilic attack by the radical anions at the Mn centres. During this reaction, CO released by the formation of **A** did not escape from the IR cell. It was therefore available for the formation of **B** and the dimer when the temperature was raised. This reaction not only deviates from that of the $M'(CO)_5$ radicals but also from the reaction between the $RZn(t\text{Bu-DAB})$ (R=Et) radicals, which form a

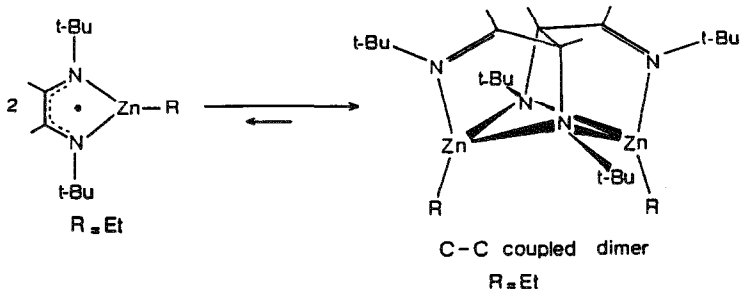

(15)

binuclear complex in which the two *t*Bu-DAB ligands are coupled via a C–C bond (see reaction (15)) [112,113]. This difference in behaviour between the $M(CO)_3$(N-N) and RZn(N-N) radicals may be due to a difference in charge at the imine carbon atoms. In the case of the RZn(*t*Bu-DAB) radicals this negative charge was calculated to be 0.2; for $Re(CO)_3$(*t*Bu-DAB) it was only 0.07 [109]. This may explain why C–C coupling reactions between the R-DAB ligands have only been observed for the Zn radicals. Of course, intermediates **A** and **B** in Scheme 1 can only be formed for the R-DAB and R-PyCA complexes and not for those of bpy and phen. Also for these latter complexes, reaction (13) will, however, most probably proceed via nucleophilic attack of the radical anion at the metal centre of a second radical.

In the case of the complexes $(CO)_5MnMn(CO)_3$(N-N) (N-N=R-DAB, R-PyCa) reactions (11)–(14) are not the only ones occurring at temperatures above 200 K. Especially when these complexes are irradiated in viscous or rigid media, at the high energy side of the MLCT band or in the presence of extra $Mn_2(CO)_{10}$, photoproducts are formed in which the α-diimine ligand bridges between the two metal centres (Scheme 2) [104,108]. The reaction is accompanied by loss of CO, yet release of CO is not the primary photoprocess of this reaction since it is completely quenched by CCl_4 as radical scavenger. According to the mechanism proposed in Scheme 2, homolysis of the Mn–Mn bond again leads to the formation of $Mn(CO)_5$ and $Mn(CO)_3$(N-N) radicals. In non-viscous media the radicals will diffuse from each other and dimerize according to reactions (12) and (13). In a viscous solvent such as paraffin, the radicals cannot diffuse. They remain close to each other and apparently react to give the products of Scheme 2. The reaction will proceed by interaction of the unpaired electrons of both radicals followed by metal–metal bond formation, coordination of one imine group to Mn and loss of CO. In this way the R-PyCa and R-DAB ligands obtain a σ,σ,η^2 coordination. In the case of the R-DAB complexes, this complex loses a second CO ligand with formation of a stable $(CO)_3Mn(\sigma,\sigma,\eta^4$-R-DAB$)Mn(CO)_3$ complex. For one of the R-PyCA photoproducts the crystal structure has recently been determined [108]. The structure of the corres-

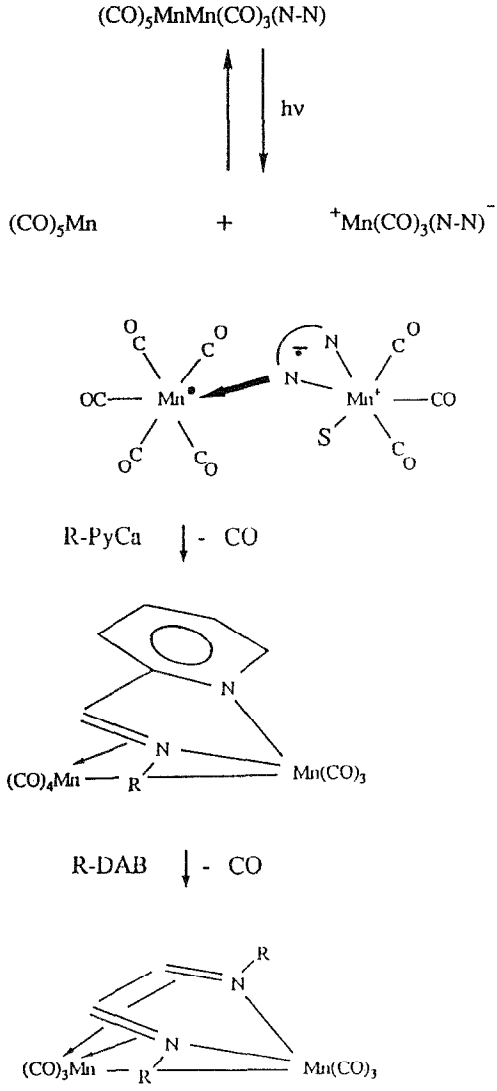

Scheme 2.

ponding R-DAB products is analogous to that of $(CO)_3Mn(\sigma,\sigma,\eta^4$-Me-DAB (MeMe))$Mn(CO)_3$ which was structurally characterized by Adams [114].

In paraffin this reaction is the only one occurring at RT whereas it competes with those of eqns. (11)–(14) in less viscous solvents. The former reaction normally predominates when irradiation takes places at the high energy side of the MLCT band and also in the presence of excess $Mn_2(CO)_{10}$. In that case more $Mn(CO)_5$ radicals are available which increase the quantum yield of product formation in Scheme 2.

In solution this reaction has been observed only for the $(CO)_5MnMn(CO)_3$(N-N) (N-N=R-PyCa, R-DAB) complexes [108]. It has, however, also been found for $(CO)_5MnRe(CO)_3$(iPr-DAB) in a CH_4 matrix and for all complexes $(CO)_5M'M(CO)_3$(iPr-DAB) (except M, M'=Re) in PVC film at 293 K [104,107].

A very interesting reaction was observed when a $(CO)_5MnMn(CO)_3$(N-N) complex was irradiated in the presence of a basic phosphine such as $P(n\text{Bu})_3$ [105]. In that case the ions $[Mn(CO)_3(N\text{-}N)(P(n\text{Bu})_3]^+$ and $[Mn(CO)_5]^-$ were formed as the only photoproducts. The reaction was clearly photocatalytic since quantum yields higher than unity and even reaching values as high as 100 mol einstein^{-1} were measured. In accordance with the mechanisms of the photodisproportionation of $Mn_2(CO)_{10}$ in N-donor solvents [115] and of $(\eta^5\text{-}CH_3C_5H_4)_2Mo_2(CO)_6$ in the presence of PR_3 [116], Kokkes et al. [105,107] proposed the following mechanism for this photodisproportionation reaction (eqns. (16)–(22) where P=PR_3):

Reaction

$$(CO)_5MnMn(CO)_3(N\text{-}N) + P \xrightarrow[\phi > 1]{h\nu} [Mn(CO)_3(N\text{-}N)P]^+ + [Mn(CO)_5]^- \quad (16)$$

Initiation

$$(CO)_5MnMn(CO)_3(N\text{-}N) \xrightarrow{h\nu} Mn(CO)_5 + Mn(CO)_3(N\text{-}N) \quad (17)$$

Propagation

$$Mn(CO)_3(N\text{-}N) + P \rightarrow Mn(CO)_3(N\text{-}N)P \quad (18)$$

$$Mn(CO)_3(N\text{-}N)P + (CO)_5MnMn(CO)_3(N\text{-}N) \rightarrow [Mn(CO)_3(N\text{-}N)P]^+ + [(CO)_5MnMn(CO)_3(N\text{-}N)]^- \quad (19)$$

$$[(CO)_5MnMn(CO)_3(N\text{-}N)]^- \rightarrow [Mn(CO)_5]^- + Mn(CO)_3(N\text{-}N) \quad (20)$$

Termination

$$Mn(CO)_3(N\text{-}N)P + Mn(CO)_5 \rightarrow [Mn(CO)_3(N\text{-}N)P]^+ + [Mn(CO)_5]^- \quad (21)$$

$$2Mn(CO)_3(N\text{-}N) \rightarrow (N\text{-}N)(CO)_3MnMn(CO)_3(N\text{-}N) \quad (22)$$

The key step in this reaction sequence is the electron transfer from the highly reducing radical $Mn(CO)_3(N\text{-}N)P$ to the parent compound (eqn. (19)). The ligand P hardly contributes to the reducing power of the $Mn(CO)_3(N\text{-}N)P$ radicals since this is mainly determined by the energy of the lowest π^* orbital of the α-diimine ligand. The primary function of P is that it binds to the radicals (eqn. (18)), thus preventing their dimerization (eqn. (22)). The ligands P also prevents the back reaction of the ions (eqn. (16)) to the parent compound. The equilibrium constant of eqn. (18) is therefore of crucial

importance for the disproportionation reaction. If it is too small as in the case of the hard bases THF and pyridine or the bulky phosphine $P(cHex)_3$, the dimerization reaction (22) competes with the electron transfer process [108].

Reaction (16) also proceeds electrocatalytically by reduction of the parent compound [108]. The reduced species decomposes according to reaction (20) and the $Mn(CO)_3L$ radicals formed start the electron transfer chain reaction.

Kochi [117,118] was the first who recognized the important role played by radicals in inorganic and organometallic chemistry. By doing so he came into conflict with the general view at that time that organometallic reactions, including catalytic ones, proceed by elementary steps involving intermediates with 16 or 18 valence electrons [119]. Nowadays it is generally accepted that radicals are the key intermediates in many organometallic reactions. Much attention has been paid recently to their physical and chemical properties [118,120–125] and especially to their application in electron transfer chain (ETC) catalysis [5,126–129]. ETC catalysis is based on the observation that catalytic amounts of an oxidizing or reducing agent can considerably increase the rate of a reaction. It was discovered that especially ligand substitution reactions proceed much more easily in the presence of an oxidizing or reducing agent or when a small cathodic or anodic current is passed through the solution [118].

Such a catalytic substitution reaction was recently observed by van der Graaf et al. [108]. To a solution of $M_3(CO)_{12}$ (M=Fe, Ru) and $P(n\text{Bu})_3$, which do not react with each other at RT, they added a small amount of a $(CO)_5MnMn(CO)_3(N\text{-}N)$ complex. When visible light was not completely excluded, a fast reaction occurred in which a CO ligand was substituted by $P(n\text{Bu})_3$. The following mechanism was proposed for this ETC reaction:

Reaction

$$M_3(CO)_{12} + P \rightarrow M_3(CO)_{11}P + CO \quad (23)$$

Initiation

$$(CO)_5MnMn(CO)_3(N\text{-}N) \xrightarrow{h\nu} Mn(CO)_5 + Mn(CO)_3(N\text{-}N) \quad (24)$$

$$Mn(CO)_3(N\text{-}N) + P \rightarrow Mn(CO)_3(N\text{-}N)P \quad (25)$$

$$Mn(CO)_3(N\text{-}N)P + M_3(CO)_{12} \rightarrow [Mn(CO)_3(N\text{-}N)P]^+ + [M_3(CO)_{12}]^- \quad (26)$$

Propagation

$$[M_3(CO)_{12}]^- + P \rightarrow [M_3(CO)_{11}P]^- + CO \quad (27)$$

$$[M_3(CO)_{11}P]^- + M_3(CO)_{12} \rightarrow M_3(CO)_{11}P + [M_3(CO)_{12}]^- \quad (28)$$

where M=Fe, Ru and P=$P(n\text{Bu})_3$.

The reaction also proceeded electrocatalytically by reduction of an $[Mn(CO)_3(N\text{-}N)P]^+$ cation. All reactions of the $(CO)_5MnMn(CO)_3(N\text{-}N)$ complexes, discussed so far, proceed by homolysis of the metal–metal bond. At temperatures below 220 K, however, a CO-loss reaction comes up at the expense of the two homolysis reactions [103,108]. At 170 K release of CO is the only reaction taking place, both in toluene and 2-MeTHF. Kokkes et al. [103] studied this reaction in 2-MeTHF at 133 K and proposed that release of CO was followed by occupation of the open site by a solvent molecule. Recently, van der Graaf et al. [108] measured, however, quite similar CO stretching frequencies for these photoproducts in toluene and 2-MeTHF. From this close correspondence they concluded that release of CO leads instead to the formation of a CO-bridged complex, $(CO)_4Mn(\mu\text{-}CO)Mn(CO)_2(N\text{-}N)$, for which the structure in Fig. 21 was proposed. The bridging CO ligand has a frequency of about 1820 cm^{-1}, which is much higher than that for the corresponding ligand in $Mn_2(CO)_9$ (ν_{CO}=1764 cm^{-1} [130,131]). Raising the temperature of the solution after the photochemical reaction caused a back reaction of the photoproduct with CO to give the parent compound [103].

Although accurate quantum yields for the above CO-loss reaction could not be determined, the efficiency of the reaction was found to be rather high and wavelength independent just as for the homolysis reaction taking place at higher temperatures. This indicates that both reactions, homolysis and release of CO, occur from the same $^3\sigma_b\sigma^*$ state. At higher temperatures the CO-loss reaction was not observed for the $(CO)_5MnMn(CO)_3(N\text{-}N)$ complexes, most probably because of a rapid re-formation of the parent compound. At lower temperatures the radicals, formed by the homolysis reaction, recombine in the viscous medium and only release of CO then leads to the formation of a stable photoproduct. The back reaction with CO occurs above 190 K. This competition between homolysis and release of CO is also evident from the photochemistry of the complexes $(CO)_5ReMn(CO)_3(N\text{-}N)$ which give rise to release of CO only with wavelength independent quantum yields [103,108] (vide supra). The complexes $(CO)_5MnRe(CO)_3(N\text{-}N)$ and $(CO)_5ReRe(CO)_3(N\text{-}N)$ gave rise only to homo-

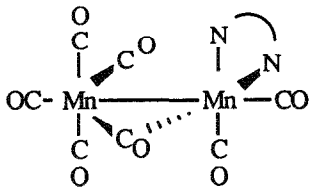

Fig. 21. Proposed structure of $(CO)_4Mn(\mu\text{-}CO)Mn(CO)_2(N\text{-}N)$.

lysis. The factors determining these reactions are discussed below for all metal–metal-bonded α-diimine complexes studied so far.

D. $Ph_3SnM(CO)_3$(α-DIIMINE) (M=Mn, Re)

Wrighton and coworkers [93,94] studied the absorption and emission spectra, photochemistry and electrochemistry of a series of complexes having the general composition $R_3EM(CO)_3$(N-N) (R=Ph or Me; E=Ge or Sn; M=Mn or Re; (N-N)=phen, bpy or 2,2′-biquinoline). These complexes, prepared according to reaction (9), all possess an intense MLCT band in the visible region. In analogy with the $(CO)_5M'M(CO)_3$(N-N) (M, M′=Mn, Re) complexes these bands were assigned to a transition from the metal–metal bonding orbital σ_b to the lowest π^* orbital of the α-diimine ligand. In a recent article, Andréa et al. [95] have questioned this assignment on the basis of RR data for several $Ph_3EM(CO)_3$(N-N) (M=Mn, E=Ge, Sn or Pb; M=Re, E=Sn) complexes. None of these complexes showed a strong RR effect for the metal–metal vibration and the RR spectra were closely analogous to those of the mononuclear $M(CO)_4$(N-N) (M=Cr, Mo, W) complexes. Just as for these latter complexes enhancement of Raman intensity was observed for the stretching mode of the axial CO ligand ($\nu(CO)_{ax}$), which is in the cis position of the α-diimine ligand (see Fig. 14) [95]. No such effect was observed for the corresponding rhenium complexes. Except for N-N=2,2′-biquinoline, all $R_3EM(CO)_3$(N-N) complexes, studied by Wrighton and coworkers [93,94] exhibited emission from the lowest excited state at 77 K. Some of the rhenium complexes were even emissive in fluid solution at RT as can be seen from Fig. 22. The manganese complexes appeared to emit at higher energy than the rhenium ones, although the rhenium complexes had their first absorption band at higher energy. The emission of the manganese complexes strongly overlapped the absorption, in contrast with the rhenium compounds. From these observations the authors concluded that the manganese complexes emit from the singlet excited state, and rhenium ones from the lowest triplet state. The excitation spectra showed that the emission efficiency was wavelength independent above 300 nm. The emissive state was therefore proposed to be the lowest $^3\sigma_b\pi^*$ MLCT state. For several $R_3ERe(CO)_3$(phen) complexes having a relatively long-lived excited state, Wrighton and coworkers [94] investigated the excited-state electron-transfer processes. A number of electron-donor and electron-acceptor quenchers were found to quench the photoexcited emission at RT with Stern–Volmer kinetics.

Wrighton and coworkers [93,94] also studied the photochemistry of several rhenium complexes in degassed CH_2Cl_2/CCl_4 and $CHCl_3$ solutions.

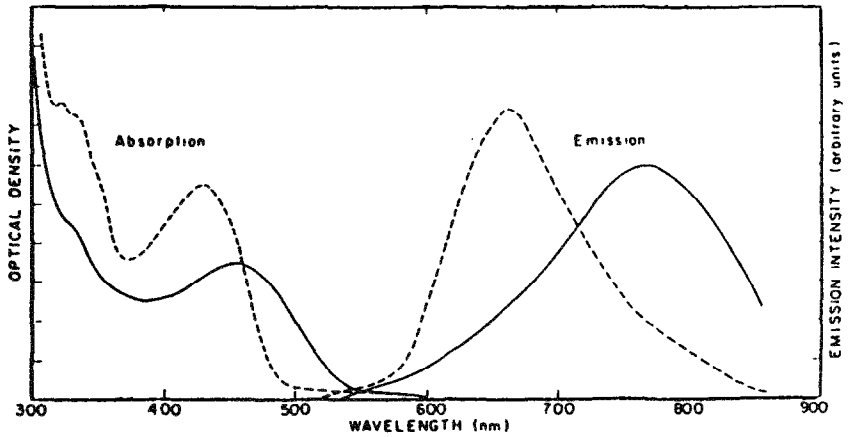

Fig. 22. Electronic absorption and emission spectra of $Ph_3GeRe(CO)_3(phen)$ in EPA at 298 K (——) and 77 K (– – –). (Reproduced with permission from ref. 93.)

Irradiation into the MLCT band gave rise to the formation of $ClRe(CO)_3(N\text{-}N)$. The quantum yields of these reactions were high ($\phi \approx 0.25$ mol einstein^{-1}) and wavelength independent just as for the $(CO)_5M'M(CO)_3(N\text{-}N)$ (M, M′=Mn, Re) complexes (vide supra). From this wavelength independence of both the emission and photochemistry, the authors concluded that both processes occur from the lowest $^3\sigma_b\pi^*$ MLCT state. It will, however, be shown below that this wavelength independence can be very well explained by another mechanism.

Recently this work of Wrighton and coworkers has been extended by our group [109,111] to the corresponding manganese compounds and to complexes of bpy, R-PyCa and R-DAB. Irradiation of $Ph_3SnRe(CO)_3(N\text{-}N)$ (N-N=bpy, R-PyCa or R-DAB) in non-chlorinated solvents [111] caused the formation of $Re(CO)_3(N\text{-}N)$ radicals, which were characterized with ESR (see Fig. 20) [109]. The Ph_3Sn radicals, formed by this reaction, most probably dimerize to give Sn_2Ph_6. The $Re(CO)_3(N\text{-}N)$ radicals were stable for hours in the dark and did not dimerize as do the corresponding $Mn(CO)_3(N\text{-}N)$ radicals (Scheme 1).

In the absence of a substituting ligand, irradiation of an RT solution of the corresponding $Ph_3SnMn(CO)_3(N\text{-}N)$ complexes in THF only gave rise to photodecomposition just as the $(CO)_5ReMn(CO)_3(N\text{-}N)$ complexes discussed in the previous section. Only in the case of $Ph_3SnMn(CO)_3(bpy')$ could a very small amount of the dimeric species $(bpy')(CO)_3MnMn(CO)_3(bpy')$ be detected in the IR spectra. Moreover, a similar photodecomposition reaction was observed for these complexes in CCl_4, whereas the rhenium complexes gave rise to the formation of $ClRe(CO)_3(N\text{-}N)$ in this solvent. Irradiation of the manganese complexes in THF at temperatures below 223

K caused the formation of $Ph_3SnMn(CO)_2(N\text{-}N)(THF)$; upon raising the temperature this product reacted back with CO to give the parent compound. In the presence of a P- or an N-donor ligand the axial CO ligand of the manganese complexes was photosubstituted at RT. The reaction was accompanied by a shift of the MLCT band towards lower energy as shown in Fig. 23 for the reaction of $Ph_3SnMn(CO)_3(t(Bu\text{-}DAB)$ with PPh_3. The photoproducts of the reactions with N-donor ligands had to be identified rapidly at RT because of their fast back reaction with CO. Even in the case of PPh_3 a slow back reaction occurred and the weakness of the Mn–P bond in the photoproducts of this ligand was evident from the small change in the ^{31}P chemical shift upon coordination [95].

A remarkable reaction was observed when $Ph_3SnMn(CO)_3(t$Bu-DAB) was irradiated in THF between 223 and 243 K or in toluene below 253 K [111]. Figure 24 shows that the axial CO ligand (ν_{CO}=1990 cm^{-1}) is released during this reaction. The frequencies of the remaining two CO bands were the same in THF and toluene and very close to those of the parent compound. The MLCT band also shifted only slightly to lower energy. From these observations it was concluded that after release of CO a *t*Bu group blocks the open axial site by an agostic Mn···H–C interaction [132]. The ^1H NMR spectrum of the photoproduct supported this conclusion since

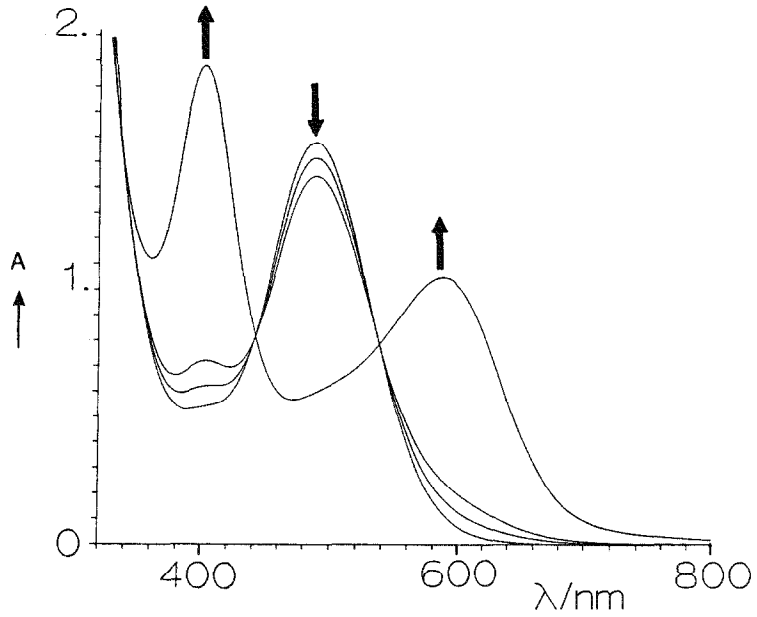

Fig. 23. Electronic absorption spectral changes during the photochemical reaction of $Ph_3SnMn(CO)_3(t$Bu-DAB) with PPh_3 in THF at 293 K. (Reproduced with permission from ref. 111.)

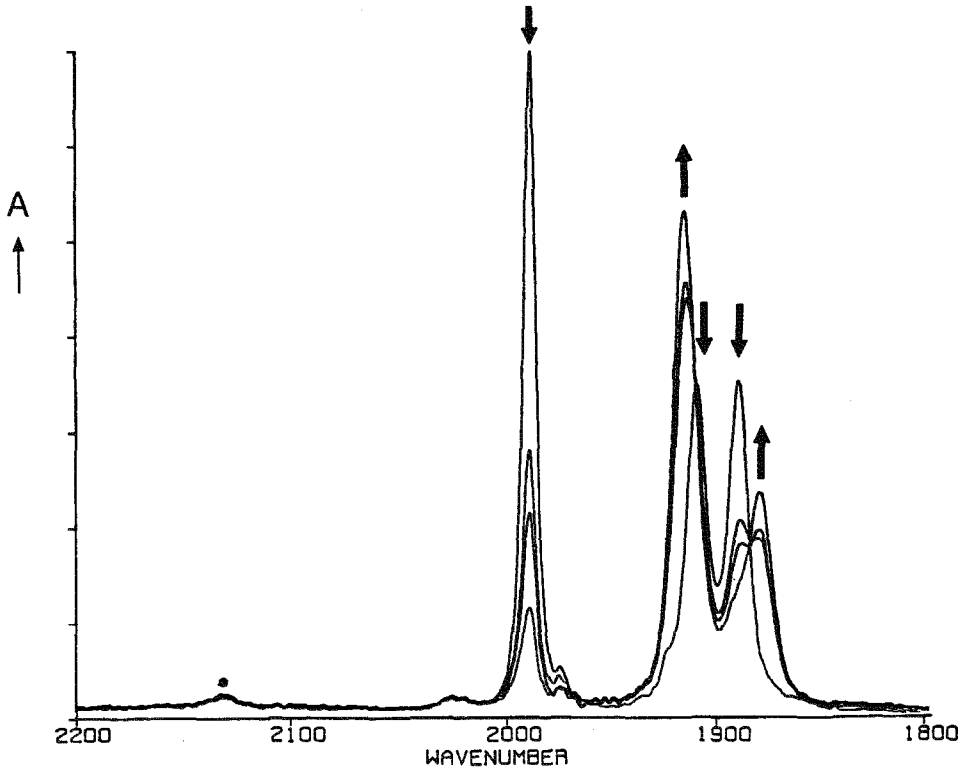

Fig. 24. IR spectral changes in the CO stretching region during the photochemical reaction of $Ph_3SnMn(CO)_3$(*t*Bu-DAB) in THF at 243 K (●, free CO). (Reproduced with permission from ref. 111.)

the *t*Bu-DAB ligand appeared to contain two inequivalent imine protons and *t*Bu groups in contrast with the parent compound and all other photosubstitution products.

According to the authors [111] the absence of reaction products of the $Mn(CO)_3$(N-N) radicals both in CCl_4 and in non-chlorinated solvents implies that release of CO is the main primary photoprocess of these Sn–Mn complexes. This conclusion was confirmed by a nanosecond flash-photolysis study in which $Ph_3SnMn(CO)_3$(iPr-PyCa) was photolysed in THF at RT. Within 20 ns of the flash the MLCT band of $Ph_3SnMn(CO)_2$(iPr-PyCa)(THF) showed up at 670 nm. Homolysis of the Sn–Mn bond did occur but only to a very small extent since the formation of $Mn(CO)_3$(N-N) radicals was only evident from the ESR spectra [109] and from the formation of a very small amount of the dimer (N-N)$(CO)_3MnMn(CO)_3$(N-N) for N-N=bpy′.

The quantum yields of the photosubstitution reactions were high (ϕ=0.2–0.8 mol einstein^{-1}) and hardly depended on the wavelength of

irradiation throughout the MLCT band (λ_{irr}=458–615 nm). A similar wavelength independence had been observed by Wrighton and coworkers [94,95] for the homolysis reaction of the Sn–Re complexes. This behaviour is in close agreement with that of the $(CO)_5M'M(CO)_3$(N-N) (M,M'=Mn, Re) complexes which also showed a wavelength-independent homolysis or CO-loss reaction.

E. $(CO)_4CoM(CO)_3$(α-DIIMINE) (M=Mn, Re)

Kruck et al. [89,133] first synthesized $(CO)_4CoRe(CO)_3$(phen) by dry heating at 90°C the ionic compound $[Re(CO)_4(phen)][Co(CO)_4]$. Van Dijk et al. [110] prepared $(CO)_4CoMn(CO)_3$(bpy) by using the general method described in reaction (8):

$$Na[Co(CO)_4] + BrMn(CO)_3(bpy) \xrightarrow{THF} (CO)_4CoMn(CO)_3(bpy) + NaBr \quad (29)$$

For the preparation of $(CO)_4CoRe(CO)_3$(bpy) the more efficient route via the orthotrifluoromethanesulphonate (OTF) salt was used.

$$Na[Co(CO)_4] + [Re(CO)_3(bpy)(THF)][OTF] \xrightarrow{THF} (CO)_4CoRe(CO)_3(bpy) + Na[OTF] \quad (30)$$

No such complexes could be prepared for R-DAB and R-PyCa since in those cases complexes $(CO)_3Co(\sigma,\sigma,\eta^2$-R-DAB)$M(CO)_3$ and $(CO)_3Co(\sigma,\sigma,\eta^2$-R-PyCa)$M(CO)_3$ (M=Mn, Re) were formed instead [134]. These latter complexes are related to the photoproduct $(CO)_4Mn(\sigma,\sigma,\eta^2$-R-PyCa)$Mn(CO)_3$ obtained by irradiation of $(CO)_5MnMn(CO)_3$(R-PyCa) in a viscous medium at RT (vide supra).

Van Dijk et al. [110] recently reported the electronic absorption and RR spectra of these $(CO)_4CoM(CO)_3$(bpy) (M=Mn, Re) complexes as well as their photochemical behaviour. The absorption spectra are characterized by an intense solvatochromic band in the visible region (450–550 nm) just as the other metal–metal-bonded systems discussed before. The assignment of these bands to metal-$d_\pi \rightarrow \pi^*$ transitions was supported by the RR spectra which showed only very weak RR effects for ν(Co–M) and large enhancements of Raman intensity for bpy stretching modes. Emission spectra were recently measured for $(CO)_4CoRe(CO)_3$(bpy′) in a 2-MeTHF glass at 80 K [102]. The spectra, obtained by excitation into the MLCT band, showed a strongly wavelength-dependent band indicative of two non-equilibrated MLCT emissions.

The photochemistry of the two bpy complexes was studied by van Dijk et al. [110] both in the absence and presence of a nucleophile. Irradiation of

the manganese complex in toluene at RT into the MLCT band caused the formation of the dimer $(bpy)(CO)_3MnMn(CO)_3(bpy)$ according to reactions (31) and (32):

$$(CO)_4CoMn(CO)_3(bpy) \xrightarrow{h\nu} Co(CO)_4 + Mn(CO)_3(bpy) \quad (31)$$

$$2Mn(CO)_3bpy \rightarrow (bpy)(CO)_3MnMn(CO)_3(bpy) \quad (32)$$

The dimer has a characteristic MLCT band at very low energy. No reaction product of the $Co(CO)_4$ radicals could be detected in the IR spectrum. The same reaction was observed in toluene at 230 K. When, however, a 133 K solution of $(CO)_4CoMn(CO)_3(bpy)$ in 2-MeTHF was irradiated, the following reaction occurred (S=2-MeTHF):

$$(CO)_4CoMn(CO)_3(bpy) \underset{\Delta}{\overset{h\nu}{\rightleftarrows}} [Mn(CO)_3(bpy)(S)]^+ + [Co(CO)_4]^- \quad (33)$$

Raising the temperature caused a complete back reaction of the ions to give the parent compound. When the reaction was performed in the presence of CBr_4, $BrMn(CO)_3(bpy)$ was formed instead of the ions. This implies that the ions were not formed by direct heterolysis of the metal–metal bond but were formed instead by a homolysis reaction. The 16e-$Mn(CO)_3(bpy)$ radicals will take up a solvent molecule and the highly reducing $Mn(CO)_3(bpy)(S)$ radicals then formed will transfer an electron to a $Co(CO)_4$ radical or to the parent compound. A similar disproportionation reaction occurred when the complex was irradiated in the presence of a PR_3 ligand. $[Mn(CO)_3(bpy)(PR_3)]^+$ and $[Co(CO)_4]^-$ were then formed with quantum yields varying from 7 (R=Ph) to 60 (R=*n*Bu) mol einstein^{-1}. These high quantum yields point to an electron transfer chain mechanism. In accordance with reactions (16)–(22), the following mechanism was proposed by van Dijk [110] (P=PR_3):

Reaction

$$(CO)_4CoMn(CO)_3(bpy) + P \xrightarrow[\phi > 1]{h\nu} [Mn(CO)_3(bpy)P]^+ + [Co(CO)_4]^- \quad (34)$$

Initiation

$$(CO)_4CoMn(CO)_3(bpy) \xrightarrow{h\nu} Co(CO)_4 + Mn(CO)_3(bpy) \quad (35)$$

Propagation

$$Mn(CO)_3(bpy) + P \rightarrow Mn(CO)_3(bpy)P \quad (36)$$

$$Mn(CO)_3(bpy)P + (CO)_4CoMn(CO)_3(bpy) \rightarrow [Mn(CO)_3(bpy)P]^+ + [(CO)_4CoMn(CO)_3(bpy)]^- \quad (37)$$

$$[(CO)_4CoMn(CO)_3(bpy)] \rightarrow Mn(CO)_3(bpy) + [Co(CO)_4]^- \quad (38)$$

Termination

$$Mn(CO)_3(bpy)P + Co(CO)_4 \rightarrow [Mn(CO)_3(bpy)P]^+ + [Co(CO)_4]^- \quad (39)$$

$$2Mn(CO)_3(bpy) \rightarrow (bpy)(CO)_3MnMn(CO)_3(bpy) \quad (40)$$

Irradiation of $(CO)_4CoRe(CO)_3(bpy)$ at RT did not given rise to the formation of any photoproduct, contrary to the corresponding $(CO)_5M'Re(CO)_3(N\text{-}N)$ (M'=Mn, Re) and $Ph_3SnRe(CO)_3(N\text{-}N)$ complexes. These latter complexes produced rather long-lived $Re(CO)_3(N\text{-}N)$ radicals which could be characterized with ESR [109] (vide supra). The photoproduction of short-lived $Re(CO)_3(bpy)$ radicals could, however, be demonstrated by van Dijk et al. [110] by adding *t*Bu-NO or CBr_4 as radical traps to the solution. From these observations the authors concluded that the $Re(CO)_3(bpy)$ radicals, formed by homolysis of the Co–Re bond, rapidly react back with the $Co(CO)_4$ radicals to give the parent compound.

In 2-MeTHF at 133 K the rhenium complex reacted according to eqn. (33), and in the presence of PR_3 a similar photodisproportionation occurred as for the manganese complex (eqn. (34)). In this case the reaction was, however, not catalytic (ϕ=0.15–0.65 mol einstein^{-1}) presumably because of the short lifetime of the $Re(CO)_3(bpy)$ radicals.

An interesting reaction was observed when $(CO)_4CoRe(CO)_3(bpy)$ was irradiated in toluene at 230 K. The complex then underwent a similar photodisproportionation reaction as in 2-MeTHF at 133 K (eqn. (33)). The reaction was quenched by CBr_4, again pointing to homolysis of the Co–Re bond as the primary photoprocess. From the low carbonyl frequencies of the $[Re(CO)_3(bpy)]^+$ cation and the splitting of the degenerate CO stretching mode of the $[Co(CO)_4]^-$ ion at 1885 cm^{-1} (see Fig. 25) it was concluded that a contact ion pair $\{Re(CO)_3(bpy)^+ \cdot Co(CO)_4^-\}$ had been formed. Apparently the $Re(CO)_3(bpy)$ radicals, formed by the homolysis reaction (eqn. (41)), transfer an electron to the $Co(CO)_4$ radical with formation of the contact ion pair (eqn. (42)):

$$(CO)_4CoRe(CO)_3(bpy) \xrightarrow[\text{Toluene, 230 K}]{h\nu} Co(CO)_4 + Re(CO)_3(bpy) \quad (41)$$

$$Re(CO)_3(bpy) + Co(CO)_4 \rightarrow \{Re(CO)_3(bpy)^+ \cdot Co(CO)_4^-\} \quad (42)$$

$$\{Re(CO)_3(bpy)^+ \cdot Co(CO)_4^-\} \xrightarrow{\Delta} (CO)_4CoRe(CO)_3(bpy) \quad (43)$$

Electron transfer to the parent complex did not occur since the quantum yield of the reaction appeared to be concentration independent [135]. This reaction clearly shows that stabilization of the ions formed in photodisproportionation reactions cannot only occur by coordinating solvents (eqn.

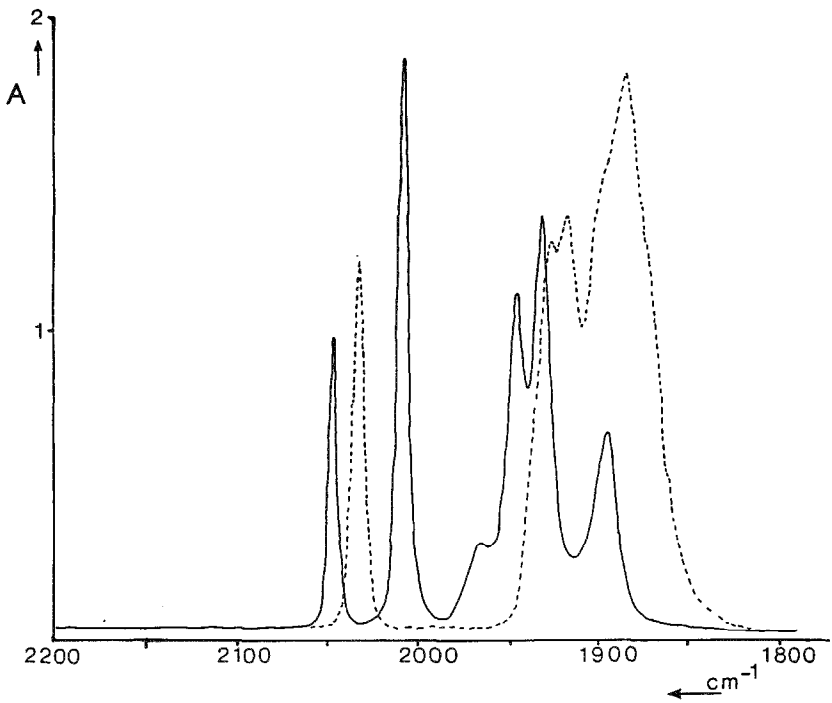

Fig. 25. IR spectra (CO stretching region) of $(CO)_4CoRe(CO)_3(bpy)$ (——) and its photoproduct (- - -) in toluene at 230 K (λ_{irr}=476.5 mn). (Reproduced with permission from ref. 110.)

(33)) or nucleophiles (eqn. (34)) but also by contact ion pair formation. The above reactions of the $(CO)_4CoM(CO)_3(bpy)$ (M=Mn, Re) complexes have in common a homolytic splitting of the metal–metal bond. Under no circumstances was a CO-loss reaction observed as in the case of the $(CO)_5M'M(CO)_3(N\text{-}N)$ (M,M'=Mn, Re) and $Ph_3SnM(CO)_3(N\text{-}N)$ (M=Mn, Re) complexes.

F. PHOTOCHEMICAL MECHANISM

All metal–metal-bonded complexes discussed in the preceding sections are characterized by intense absorption bands in the visible region, which were first assigned by Wrighton and coworkers [90,91,93,94] to a $\sigma_b(M\text{–}M')\rightarrow\pi^*(\alpha\text{-diimine})$ MLCT transition. This assignment was based on the observation that irradiation into these bands gave rise to an efficient wavelength-independent cleavage of the metal–metal bond. The reaction then occurs from the lowest $^3\sigma_b\pi^*$ state and depopulation of the σ_b orbital was proposed to be sufficient to labilize the metal–metal bond. The RR

spectra of these complexes are, however, characterized by only weak RR effects for the metal–metal stretching modes, which means that the corresponding bonds are hardly affected by this electronic transition [95,97,109].

The absorption bands are therefore better assigned to one or more MLCT transitions from (a) metal d_π orbital(s) not involved in the metal–metal bond to the lowest π^* orbital of the α-diimine ligand ($d_\pi \rightarrow \pi^*$) just as for the mononuclear $M(CO)_4(N\text{-}N)$ (M=Cr, Mo, W) complexes. The $^3d_\pi\pi^*$ MLCT states will not be reactive themselves [8] and the reactions most probably occur from a close lying reactive excited state [11,103–107,110,111]. In this respect the mechanism proposed by Meyer and Caspar [11], which is based on the energy diagram of $Mn_2(CO)_{10}$, can best account for the experimental data presented in the preceding sections. In this diagram (see Fig. 26) the relative energies of the σ_b^2 ground state and the $^1\sigma_b\sigma^*$ and $^3\sigma_b\sigma^*$ excited states are presented as a function of a normal coordinate largely M–M in character. Irradiation into the $\sigma_b \rightarrow \sigma^*$ transition will then lead to occupation

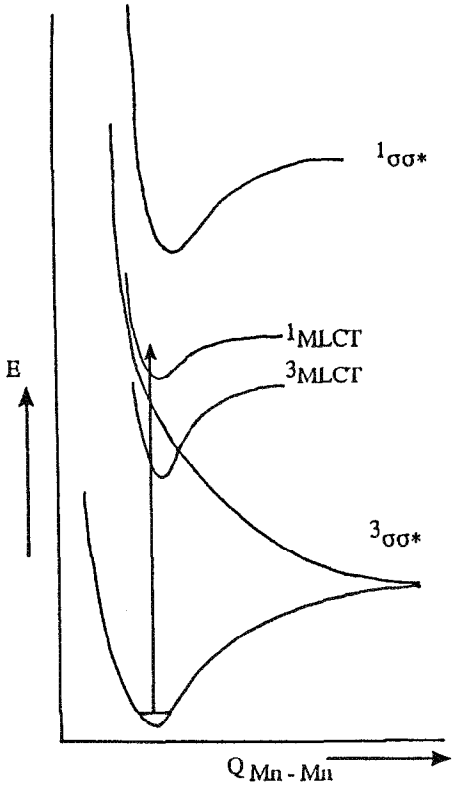

Fig. 26. Schematic potential energy vs. Mn–Mn normal coordinate diagram of $(CO)_5MnMn(CO)_3(N\text{-}N)$.

of the $^1\sigma_b\sigma^*$ state which correlates with the disproportionation products $Mn(CO)_5^+$ and $Mn(CO)_5^-$. The coulomb attraction between these ions gives rise to a minimum in the $^1\sigma_b\sigma^*$ potential energy curve. The $^3\sigma_b\sigma^*$ state, in contrast, correlates with the neutral monomers having their unpaired spins aligned. This state is dissociative because of the antibonding nature of σ^* and the absence of attractive ionic terms. Intersystem crossing to this state will therefore lead to homolysis of the M–M bond and formation of $Mn(CO)_5$ radicals. According to Meyer and Caspar the efficient homolysis reaction observed upon MLCT irradiation of the metal–metal-bonded α-diimine complexes can be explained with a similar energy diagram, which now contains, apart from $^1\sigma_b\sigma^*$ and $^3\sigma_b\sigma^*$ states, the ^{1}MLCT and ^{3}MLCT states (Fig. 26). Irradiation into the MLCT band leads to occupation of the ^{1}MLCT state followed by a surface crossing to the repulsive $^3\sigma_b\sigma^*$ state, either by direct intersystem crossing or via the ^{3}MLCT state. The repulsive character of $^3\sigma_b\sigma^*$ accounts for the high quantum yields and for their wavelength independence.

An experimental result that at first sight seems to be in conflict with this mechanism, is the observation of CO-loss reaction in competition with the homolytic splitting. The quantum yields of both reactions are high and wavelength independent throughout the MLCT band and at least for $Ph_3SnMn(CO)_3$(iPr-PyCa) release of CO was proven to be a primary photoprocess [111]. Both reactions will therefore most probably occur from the same repulsive $^3\sigma_b\sigma^*$ state. In this respect it is of importance to note the recent theoretical data obtained by Veillard and Strich [136] on the ground and excited states of $HCo(CO)_4$ and its photoproducts $Co(CO)_4$ and $HCo(CO)_3$. Their ab initio calculations showed that the repulsive $^3\sigma_b\sigma^*$ ($^3A_1$) state of $HCo(CO)_4$ will give rise to both dissociation of the Co–H bond and release of CO. From this result the authors proposed that the $^3\sigma_b\sigma^*$ state of $Mn_2(CO)_{10}$ has a similar dissociative character with respect to CO loss and metal–metal bond homolysis. $Mn(CO)_5$ and $Mn_2(CO)_9$ are then formed as primary photoproducts from the $^3\sigma_b\sigma^*$ state of $Mn_2(CO)_{10}$ [137–139]. If this assumption is correct, the same mechanism will be applicable to the photochemistry of the α-diimine complexes. The occurrence of homolysis or release of CO will then mainly be determined by the relative strengths of the metal–metal and metal–CO bonds in the $^3\sigma_b\sigma^*$ state. The experimental data confirm this conclusion at least qualitatively when the ground state bond strengths are taken into account. For the complexes $(CO)_5MnMn(CO)_3$(N-N) both bonds are weak and as a result both reactions are observed. The $(CO)_5ReMn(CO)_3$(N-N) complexes have a strong Re-Mn bond [99,100] and weak Mn–CO bonds [140]. As a result, release of CO is the only primary photoprocess. The complexes $(CO)_5ReRe(CO)_3$(N-N) have strong Re–CO bonds while the Re–Re bond strength is in between those of the Mn–Mn

and Re–Mn bonds [99,100]. As a result, only homolysis obtains for these complexes. The photochemistry of the $Ph_3SnM(CO)_3(N\text{-}N)$ (M=Mn, Re) complexes can be explained in the same way. Literature data on $Ph_3SnM(CO)_5$ (M=Mn, Re) show that the dissociation energy is highest for the manganese compound [141–144]. Moreover, Mn–CO bonds are generally much weaker than Re–CO bonds [140]. This explains why irradiation of a $Ph_3SnRe(CO)_3(N\text{-}N)$ complex leads to homolysis and irradiation of a manganese complex to release of CO. In $Mn_2(CO)_{10}$ the $^3\sigma_b\sigma^*$ state is delocalized over the whole complex [145]. If this were also the case for the corresponding $(CO)_5M'M(CO)_3(N\text{-}N)$ (M, M'=Mn, Re) complexes, irradiation of $(CO)_5MnRe(CO)_3(N\text{-}N)$ and $(CO)_5ReMn(CO)_3(N\text{-}N)$ would give rise to a similar CO-loss reaction, for the Mn–CO bonds of the $Mn(CO)_5$ moiety in the former complex will certainly not be stronger than those of the $Mn(CO)_3(N\text{-}N)$ fragment of the latter compound. However, the $(CO)_5MnRe(CO)_3(N\text{-}N)$ complexes only underwent homolysis of the Mn–Re bond. Apparently the $^3\sigma_b\sigma^*$ state of these α-diimine complexes is confined to the $M(CO)_3(N\text{-}N)$ fragment and occupation of that state will only give rise to release of CO when M=Mn. Only in the case of the $Ph_3SnMn(CO)_3(N\text{-}N)$ complexes was the influence of the α-diimine ligand on the quantum yield of the reaction studied [111]. Photosubstitution quantum yields appeared to decrease on going from the R-DAB and R-PyCa complexes to the bpy compound.

The authors argued that this effect can hardly be due to a difference in relative strengths of the metal–metal and metal–CO bonds in the $^3\sigma_b\sigma^*$ state since the decrease in ϕ was not accompanied by an increase in quantum yield for the homolysis reaction. It was proposed instead that the surface crossing between the ^{3}MLCT and $^3\sigma_b\sigma^*$ states is less effective for the bpy complex. This difference in behaviour may be caused by a weaker interaction of the lowest π^* orbital of bpy with the metal as can, for example, be seen from the differences in a_{Re} coupling constants in the ESR spectra of the $Re(CO)_3(N\text{-}N)$ radicals [109].

G. $M(CO)_3$(α-DIIMINE) (M=Fe, Ru)

(i) Formation of the complexes

The synthesis of several complexes $Fe(CO)_3$(R-DAB), having the structure shown in Fig. 27b, was described as long ago as 1967 by Otsuka and coworkers [146]. The complexes were prepared by thermal reaction of $Fe_2(CO)_9$ with the R-DAB ligand. Tom Dieck and Orlopp [147] used the same method for the preparation of a series of these complexes but also irradiated $Fe(CO)_5$ in the presence of R-DAB. In the case of R-DAB ligands

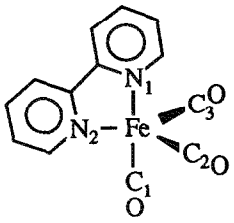

a

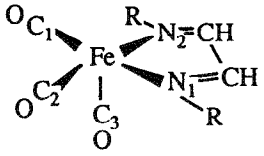

b

Fig. 27. Structures of $Fe(CO)_3(bpy)$ (a) and $Fe(CO)_3(R\text{-}DAB)$ (R=iPr_2-Ph) (b).

in which R contains a quaternary carbon atom (e.g. R=*t*Bu) they observed the formation of a complex having inequivalent imine groups according to the ^1H and ^{13}C NMR spectra. From this observation they concluded that in these complexes the R-DAB ligands are σ,π instead of σ,σ coordinated to the metal. Staal et al. [148] showed, however, that the thermal reaction of $Fe_2(CO)_9$ with such R-DAB ligands proceeds according to eqn. (44):

$$Fe_2(CO)_9 + 2R\text{-}DAB \rightarrow Fe(CO)_3(R\text{-}DAB) + R\text{-}N\text{-}CH{=}CH\text{-}N\text{-}(R)\text{-}CO + Fe(CO)_5 \quad (44)$$

The imidazolone (R–N–CH=CH–N–(R)–CO) had been found before as a side product of the reaction between $Fe_2(CO)_9$ and R-DAB [149]. Staal et al. isolated the reaction products of reaction (44) in equimolar amounts. After separation, only a single signal was observed for the imine protons and carbon atoms in the ^1H NMR and ^{13}C NMR spectra of $Fe(CO)_3(R\text{-}DAB)$ respectively. The other signals, ascribed by tom Dieck and Orlopp [147] to a π-coordinated imine group, appeared to belong to the imidazolone. This result showed that also for these $Fe(CO)_3(R\text{-}DAB)$ complexes with bulky substituents R, the R-DAB ligand is σ,σ coordinated to the metal.

The corresponding complexes of bpy and phen cannot easily be prepared by reaction of $Fe_2(CO)_9$ or $Fe(CO)_5$ with the α-diimine ligand since they react further with $Fe(CO)_4$, forming the isolable binuclear complexes $Fe_2(CO)_7(N\text{-}N)$ (N-N=bpy, phen). The $Fe(CO)_3(N\text{-}N)$ (N-N=bpy, phen) complexes were therefore prepared by Frühauf [150] either by employing an $Fe(CO)_3$ generator such as $Fe(CO)_3$(diene) or starting from $Fe_2(CO)_7(N\text{-}N)$ by eliminating $Fe(CO)_5$ under CO pressure. These reactions are shown for bpy in eqns. (45) and (46):

$$Fe(CO)_3(diene) + bpy \xrightarrow[Acetone]{20^\circ C} Fe(CO)_3(bpy) + diene \quad (45)$$

$$Fe_2(CO)_7(bpy) + CO \xrightarrow[\text{Benzene}\ 50\ \text{bar CO}]{40^\circ C} Fe(CO)_3(bpy) + Fe(CO)_5 \quad (46)$$

The corresponding ruthenium complexes are normally prepared by reaction of $Ru_3(CO)_{12}$ with the appropriate R-DAB ligand [151]. This method is, however, restricted to ligands containing substituents R which are branched in such a way that both C=N moieties are effectively screened against coordination by one or two metal atoms [19,20,151–153]. For other R groups, $Ru(CO)_3$(R-DAB) has been observed in solution. The complexes are, however, very reactive, forming $Ru_2(CO)_6$(R-DAB) with $Ru_3(CO)_{12}$ from the solution.

Recently, Mul et al. [154] have successfully prepared several $Ru(CO)_3$(R-DAB) complexes with smaller R groups by heating the C–C-coupled complex $Ru_2(CO)_5$(IAE) (IAE=bis(1-alkylimino)-2-(alkylimino)-ethane-*N*,*N'*) in toluene or *n*-heptane under CO pressure.

(ii) Bonding properties and electronic transitions

X-ray structures have been determined for $Fe(CO)_3$(bpy) [155], $Fe(CO)_3$(Ph-PyCa(Ph)) (Ph-PyCa(Ph)=C_5H_4N-Cph=NPh) [156] and $Fe(CO)_3$(iPr_2-Ph-DAB) (iPr_2-Ph=2,6-diisopropylphenyl) [157]. Going from the bpy to the iPr_2Ph-DAB complex there is an increase in π backbonding to the α-diimine ligand as is evident from a decrease in the Fe–N bond lengths and a concomitant lengthening of the Fe–C bonds. At the same time the structure of the complex changes from a trigonal bipyramid to a distorted square pyramid. The structures of the bpy and iPr_2-Ph-DAB complexes are schematically depicted in Fig. 27.

The bpy complex has an N_1–Fe–C_1 angle of nearly 180° and N_2–Fe–C_2 and N_2–Fe–C_3 angles of about 120°. The N_1–Fe–C_1 and N_2–Fe–C_2 angles of the iPr_2-Ph-DAB complex are 158° and 156° respectively. In this latter compound the Fe atom is lifted out of the N_1CCN_2 plane by 0.163 Å. In this respect the structure of the iPr_2-Ph-DAB complex deviates from that of the corresponding tetraazadiene complex $Fe(CO)_3(N_4(CH_3)_2)$ for which a planar FeN_4 conformation was established [158]. The metal to R-DAB π-backbonding is stronger for the iron complexes than for those discussed in the preceding sections. This is, for example, evident from the CN and CC bond lengths of these ligands in $(CO)_5ReMn(CO)_3$(iPr-DAB) [97], $Ph_3SnMn(CO)_3$(*t*Bu-DAB) [95] and $Fe(CO)_3$(iPr_2-Ph – DAB) [157]. In the first two complexes *r*(CN) and *r*(CC) are 1.29–1.30 Å and 1.41 Å respectively, whereas *r*(CN)=1.33 Å and *r*(CC)=1.39 Å for $Fe(CO)_3$(iPr_2-Ph-DAB). Kokkes et al. [157] performed a CNDO/S calculation on the model

compound $Fe(CO)_3$(H-DAB) and the relevant part of the resulting MO diagram is presented in Fig. 28. It shows the presence of a HOMO and LUMO, both having strongly mixed metal-d_π–ligand-π^* character. The HOMO has a lower IP than the other three occupied metal orbitals and this result agreed with the UV photoelectron (PE) data obtained for several of these $Fe(CO)_3$(R-DAB) complexes [159]. Figure 29 shows the low energy region of the He(I) and He(II) PE spectra of $Fe(CO)_3$(*t*Bu-DAB). Band A belongs to the ionization from the HOMO, bands S and B to those from the other metal *d* orbitals. Band C was assigned to the ionization from a ligand (nitrogen lone pair) orbital because of its decrease in intensity on going from He(I) to He(II) excitation. A similar PE spectrum was obtained for Ru-$(CO)_3$(iPr_2-CH-DAB) (iPr_2-CH=diisopropylmethyl). With respect to the iron complex, band A was shifted by 0.15 eV to lower ionization energy, indicative of a weaker π backbonding to the R-DAB ligand in the case of the ruthenium complexes. The lowest energy HOMO→LUMO transition will be most intense since it takes place between orbitals which strongly interact in the ground and excited states. This transition will therefore most strongly contribute to the intense absorption band in the visible region (Fig. 30). There is evidence from the RR excitation profiles and the MCD spectrum of $Fe(CO)_3$(iPr_2-Ph-DAB) that the 500 nm band consists of at least three electronic transitions, all having metal–R-DAB character [157]. This would imply that three or maybe all four allowed transitions to the LUMO fall under this low energy band. However, the RR spectra were weak and the MCD evidence was only obtained from a gaussian analysis of the spectra. It could therefore not be excluded that one or more of the metal→R-DAB transitions fall under the high energy band. Such an assignment would agree better with the UV–PE data [159] and with the assignment given by

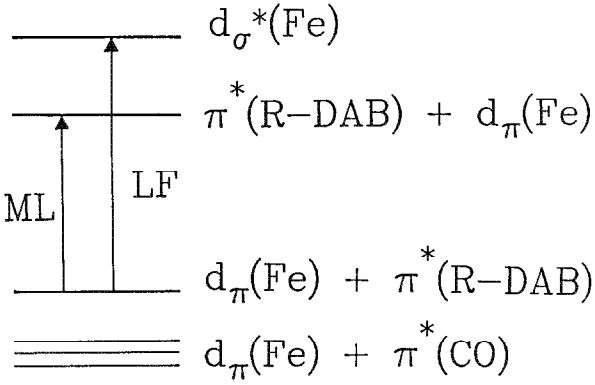

Fig. 28. Qualitative molecular orbital diagram of $Fe(CO)_3$(R-DAB). (Reproduced with permission from ref. 161.)

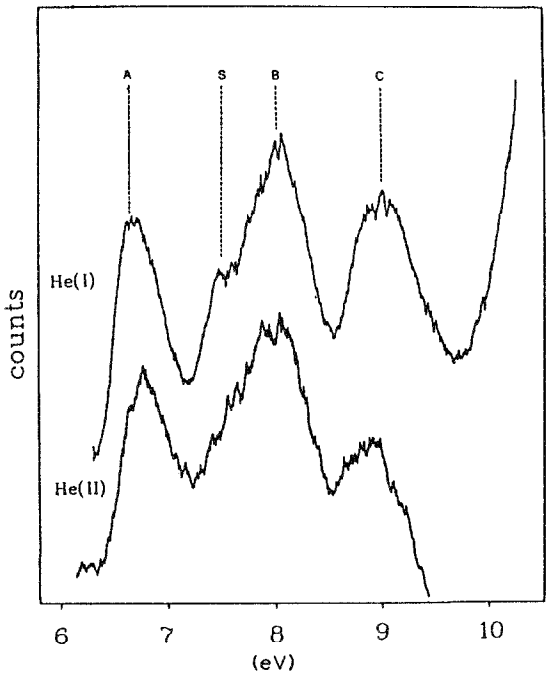

Fig. 29. Low energy region of the He(I) and He(II) PE spectra of $Fe(CO)_3$(*t*Bu-DAB). (Reproduced with permission from ref. 159.)

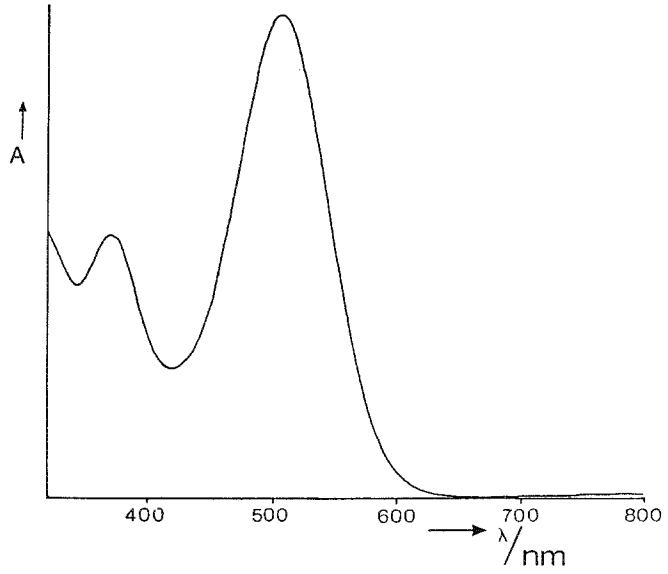

Fig. 30. Electronic absorption spectrum of $Fe(CO)_3$(cHex-DAB) in toluene at 293 K. (Reproduced with permission from ref. 161.)

Trogler et al. [160] for the absorption spectra of the complexes $Fe(CO)_3(N_4(R)_2)$ ($R=CH_3$, C_6H_5). Apart from these transitions, the 400 nm band must also contain one or more LF transitions, for the transient complex $Fe(CO)_3(\sigma\text{-N-}t\text{Bu-DAB})(CH_3CN)$, which does not contain such a metallocycle, has its lowest energy LF transition at about 420 nm (vide infra [161]).

A characteristic feature of all metal→R-DAB transitions is the lack of any MLCT character. This is evident from the absence of any solvatochromism for both absorption bands and also from the theoretical and RR data [157]. The calculations had shown that these transitions are accompanied by only minor charge shifts in the complex. This result was confirmed by the RR spectra, which were very weak and hardly showed an RR effect for ν_s(CN) of the R-DAB ligand [157]. Only Raman bands between 350 and 900 cm^{-1}, belonging to metal–C stretching vibrations and to deformation modes of the $Fe(CO)_3$ and Fe(R-DAB) moieties, appeared to be weakly resonance enhanced. This means that the HOMO→LUMO transition and possibly other transitions falling under the low energy band are not accompanied by bond order changes but only by weak distortions of the $Fe(CO)_3$ and Fe(R-DAB) moieties. It points to the presence of an Fe(R-DAB) metallocycle in which the charges are delocalized over the ring in both the ground and lowest excited states. Because of this complete lack of MLCT character for the transitions involved, the low energy band has been denoted by van Dijk et al. [161] as a metal–ligand (ML) band. The distortion of the metallocycle in the lowest excited state as evidenced by the RR spectra, will be shown hereafter to be of importance for the interpretation of the photochemical data. Similar RR spectra were obtained for the ruthenium complexes and a representative spectrum of $Ru(CO)_3$(Mes-DAB) is shown in Fig. 31. Contrary to the complexes discussed in the preceding sections, these iron and ruthenium compounds do not luminesce. Apparently the formation of the metal–R-DAB metallocycle is accompanied by an increase in the rates for the non-radiative decay processes.

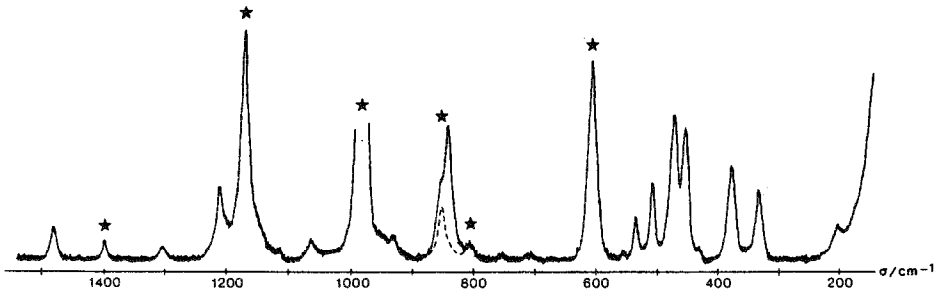

Fig. 31. Resonance Raman spectrum of $Ru(CO)_3$(Mes-DAB) in C_6H_6 obtained by excitation with 514.5 nm: bands marked with a star or a dotted curve are solvent bands. (Reproduced with permission from ref. 42.)

(iii) Photochemical behaviour

UV irradiation of $Fe(CO)_3$(R-DAB) has been used to synthesize substitution products and binuclear complexes [149,162,163]. In the presence of a diene, Fe (CO)(R-DAB)(diene) was formed in two consecutive photochemical steps (eqn. (47)) [162,163]:

$$Fe(CO)_3(\text{R-DAB}) + \text{diene} \underset{\Delta,CO}{\overset{h\nu}{\rightleftarrows}} Fe(CO)_2(\text{R-DAB})(\eta^2\text{-diene}) \underset{\Delta,CO}{\overset{h\nu}{\rightleftarrows}} Fe(CO)(\text{R-DAB})(\eta^4\text{-diene}) \quad (47)$$

Irradiation of $Fe(CO)_5$ in the presence of R-DAB led to the formation of $Fe(CO)_3$(R-DAB), which reacted further photochemically with $Fe(CO)_5$ to give $Fe_2(CO)_6$(R-DAB) [149]. Kokkes et al. [164–166] studied the photochemistry of these $Fe(CO)_3$(R-DAB) complexes in solution at RT and in inert gas matrices at 10 K. Irradiation at RT into the low energy band and in the absence of a substituting ligand did not give rise to the formation of any photoproduct. In the presence of a nucleophile L, complexes $Fe(CO)_2$(R-DAB)(L) or Fe(CO)(R-DAB)$(L)_2$ were formed. Disubstitution was only observed for small ligands L with good π-accepting properties such as $P(OMe)_3$ or aromatic isocyanides. The quantum yields varied from 0.1 to 0.3 mol einstein^{-1} and similar reactions were observed upon irradiation at higher energy.

A completely different reaction occurred, however, in an inert gas matrix at 10 K [164,165]. Irradiation into the low energy band then caused the disappearance of this absorption band. No CO was released, the CO stretching modes shifted to higher frequencies while ν_s(CN) of the R-DAB ligand was lowered in frequency. From these data Kokkes et al. concluded that the $Fe(CO)_3$ moiety was retained in the photoproduct and that the R-DAB ligand had changed its coordination from σ,σ-N,N′ into η^4-CN,C′N′ (eqn. (48)).

Such an isomerization reaction will cause a decrease in π backbonding to the CO ligands. This conclusion was confirmed by the close agreement between the CO stretching frequencies of these photoproducts and those of

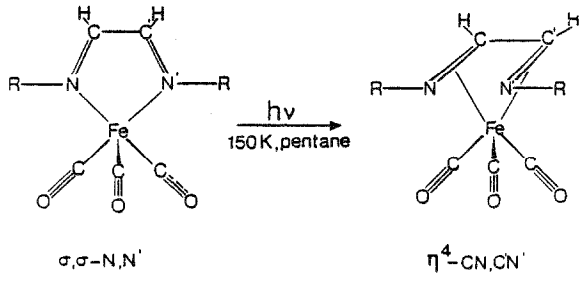

(48)

the $Fe(CO)_3$(diene) complexes. Raising the temperature caused a back reaction to the parent compound.

Van Dijk et al. [161,167] studied the mechanisms of these two photochemical reactions in more detail by using different methods for the identification of reactive intermediates. Such intermediates were characterized spectroscopically by stabilizing them in low temperature solutions or by using nanosecond flash photolysis. The latter method was used to establish the primary photoprocess of the substitution reactions, which had been the subject of some controversy. Trogler [168] had proposed that in the case of both the $Fe(CO)_3(N_4(CH_3)_2)$ and $Fe(CO)_3$(R-DAB) complexes, photosubstitution of CO proceeds via loss of CO (Scheme 3, mechanism 1), whereas Kokkes et al. [164] proposed breakage of a metal–N bond (Scheme 3, mechanism 2) as a primary photoprocess.

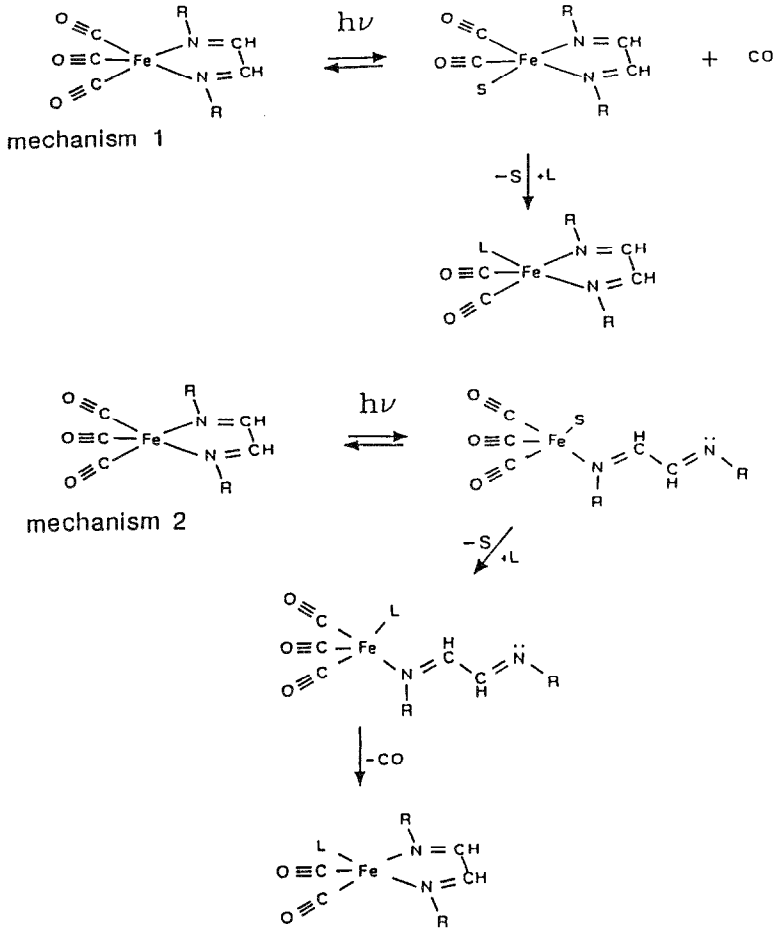

Scheme 3.

In order to establish the correct mechanism, van Dijk et al. [161] laser flash-photolysed several $Fe(CO)_3$(R-DAB) complexes and recorded the transient absorption spectra. In the case of $Fe(CO)_3$(R-DAB) (R=cHex, *p*Tol, iPr_2-Ph), these spectra, taken 10 ns after the laser flash, exhibited two new bands at lower energy, indicative of substitution of CO by a solvent molecule S (mechanism 1).

Only in the case of $Fe(CO)_3$(*t*Bu-DAB) did the transient spectrum in toluene merely show a single band at 450 nm belonging to an LF transition of the intermediate $Fe(CO)_3$(σ-N-*t*Bu-DAB)(S) (S=toluene). When the reaction was performed in CH_3CN, this LF band shifted to 420 nm. The disappearance of the ML band was taken as evidence for the breakage of a metal–N bond according to mechanism 2. The deviating behaviour of the *t*Bu-DAB complex was ascribed to a weakening effect of the bulky *t*Bu groups on the metal–N bonds. Van Dijk et al. [161] succeeded in the stabilization of the transients of mechanism 2 by performing the photochemical reactions in low temperature solutions.

Several of these $Fe(CO)_3$(R-DAB) complexes showed a wavelength-dependent photochemistry upon irradiation at 150 K in *n*-pentane in the absence of a substituting ligand. Complexes that reacted according to mechanism 1 gave rise to the formation of a binuclear complex $Fe_2(CO)_5$(R-DAB)$_2$ when R was not too bulky (R=cHex, *p*Tol) and when irradiation took place at the high energy side of the ML band ($\lambda_{irr} \leqslant 500$ nm). These binuclear complexes, for which the structure in Fig. 32 was proposed, were characterized by an intense MLCT band above 700 nm and by a bridging carbonyl ligand with a low stretching frequency of about 1750 cm^{-1}. The complexes were only formed at rather high concentrations of the parent compound by its reaction with the intermediate $Fe(CO)_2$(R-DAB)(S) (mechanism 1). When irradiation took place at the low energy side of the ML band, the same photoproducts $Fe(CO)_3$(η^4-CN,C'N'-R-DAB) were formed as in the inert gas matrices at 10 K (vide supra, eqn. (48)). In order to find out how the increase in π backbonding to R-DAB had influenced ν_s(CN) of the R-DAB

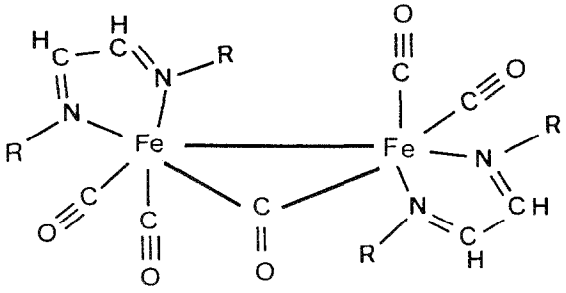

Fig. 32. Proposed structure of $Fe_2(CO)_5$(R-DAB)$_2$ (Reproduced with permission from ref. 161.)

ligand, IR spectra of the parent compound and its photoproduct were recorded from a solution in liquid xenon (LXe). This solvent does not absorb in the frequency region of ν_s(CN) (1300–1600 cm^{-1}). In fact, it is completely transparent in IR and UV–visible, so that long optical pathways can be used which makes the restricted solubility of many organometallics in this solvent less inconvenient [169]. Normally, LXe is used over the temperature range 170–240 K when kept at a pressure of 150 psi and special high pressure cryostats have been constructed for this purpose [170–175]. Irradiation of $Fe(CO)_3$(cHex-DAB) in this solvent caused a frequency decrease in ν_s(CN) from 1482 to 1362 cm^{-1} in agreement with the change in coordination of cHex-DAB during reaction (48). Raising the temperature of the solution caused a thermal back reaction of this photoproduct to the parent compound already at 180 K.

The corresponding $Fe(CO)_3$(*t*Bu-DAB) complex did not show such a wavelength-dependent photochemistry at low temperature. In fact no reaction was observed, presumably because of a fast back reaction of the photoproduct $Fe(CO)_3$(σ-N-*t*Bu-DAB)(S) (S=*n*-pentane) to give the parent compound. Besides, the *t*Bu group will be too bulky for the formation of an η^4-CN,C'N' coordinated $Fe(CO)_3$(*t*Bu-DAB) complex.

Van Dijk et al. [176] also studied the influence of substitution of CO by PR_3 on the photochemistry of two $M(CO)_3$(R-DAB) (M=Fe, Ru) complexes. Flash photolysis of $Fe(CO)_3$(iPr_2-Ph-DAB) and $Ru(CO)_3$(iPr_2-CH-DAB) (iPr_2-CH=diisopropylmethyl) established release of CO as the primary photoprocess for these complexes at RT. Irradiation of the iron complex in *n*-pentane at 150 K did not give rise to the formation of $Fe_2(CO)_5$(iPr_2-Ph-DAB)$_2$ and $Fe(CO)_3$(η^4-CN,C'N'-iPr_2-Ph-DAB) as for the corresponding cHex-DAB and *p*Tol-DAB complexes (vide supra [161]). This result was ascribed to the bulk of the iPr_2-Ph groups. Irradiation of $Ru(CO)_3$(iPr_2-CH-DAB) in *n*-pentane at 150 K produced $Ru_2(CO)_5$(iPr_2-CH-DAB)$_2$ at all wavelengths of irradiation. Again no $Ru(CO)_3$(η^4-CN,C'N'-iPr_2-CH-DAB) was formed.

The main influence of substitution of CO by PR_3 was a change of the primary photoprocess to breakage of a metal–N bond. For $Fe(CO)_2$(iPr_2-Ph-DAB)($P(OPh)_3$) this was established by flash photolysis at RT. Irradiation of this complex in *n*-pentane at 150 K caused the formation of $Fe(CO)_3$(η^4-CN,C'N'-iPr_2-Ph-DAB) at all wavelengths of irradiation.

The corresponding complexes $Ru(CO)_2$(iPr_2-CH-DAB)(PR_3) again showed a wavelength-dependent photochemistry in *n*-pentane at 150 K. Irradiation at the low energy side of the ML band caused the formation of $Ru(CO)_2$(η^4-CN,C'N'-iPr_2-Ph-DAB)(PR_3), whereas $Ru(CO)_3(PR_3)_2$ and $Ru(CO)_2(PR_3)_3$ were formed upon irradiation at higher energy.

The formation of different photoproducts at low temperature for the PR_3-

substituted complexes of iron and ruthenium was rationalized as follows. Breakage of a metal–N bond upon short-wavelength irradiation of the iron complex is apparently followed by fast rechelation of the iPr_2-Ph-DAB ligand. In the case of the ruthenium complexes the iPr_2-CH-DAB ligand is released before such a rechelation can occur. As a result $Ru(CO)_3(PR_3)_2$ and $Ru(CO)_2(PR_3)_3$ are formed. Both the iron and ruthenium complexes produced at 150 K an η^4-coordinated R-DAB complex upon low energy excitation. The iron photoproduct was, however, not stable and reacted with CO to give $Fe(CO)_3(\eta^4$-CN,C'N'-iPr_2-Ph-DAB).

An explanation for this change in photochemical behaviour upon substitution of CO by PR_3 will be given in the next section, together with a more general discussion of the mechanism underlying the temperature-dependent photochemistry.

(iv) Photochemical mechanism

The complexes discussed in this section are characterized by two absorption bands at about 500 nm and 350–400 nm respectively (see Fig. 30). The low energy band has been assigned to one or more internal transitions of the metallocycle [157,160]. The origin of the second band was less clear. Kokkes et al. [157] tentatively assigned this band to an internal transition of the R-DAB ligand. For the corresponding tetraazadiene complexes $Fe(CO)_3(N_4(CH_3)_2)$, Trogler et al. [160] assigned both bands to internal (ML) transitions of the metallocycle. Both groups of authors located the lowest LF transitions of these complexes at still higher energy ($\lambda_{max} < 350$ nm). In view of the results of the MO calculations and RR spectra, occupation of a ^{3}ML state of the metallocycle after irradiation into the lowest energy band was not expected to initiate an efficient photochemical reaction. The occurrence of photosubstitution reactions with rather high quantum yields for both the R-DAB [164] and tetraazadiene [177] complexes was therefore rather surprising, the more so as the lowest reactive (^{3}LF) states were assumed to be at much higher energy than the ^{3}ML states. For both types of complexes the quantum yields appeared to increase (about 0.1–0.5 mol einstein^{-1}) upon going from lower to higher energy irradiation. Johnson and Trogler [177] therefore explained the photochemistry of the tetraazadiene complexes with a strong coupling model according to which excited state energy is converted into vibrational motions of the complex, giving rise to the breakage of the metal–ligand bond. The amount by which the irradiation energy exceeds the threshold for Fe–L bond cleavage then accounts for the observed wavelength dependence of ϕ. The same model was adopted by Kokkes et al. [164] to explain the RT photosubstitution reactions of the $Fe(CO)_3$(R-DAB) complexes. The other reaction, a change

of coordination of the R-DAB ligand from σ,σ-N,N′ into η^4-CN,C′N′, which only occurred upon low temperature and low energy excitation, was proposed to proceed from the lowest ^{3}ML state. The quantum yield of this reaction was low as might be expected from the minor bond order changes derived for these ML transitions from the MO calculations and RR data. The change in coordination of the R-DAB ligand is then a direct consequence of the weak distortion of the metallocycle observed in the RR spectra.

Van Dijk et al. [161] observed upon flash photolysis of $Fe(CO)_3$(*t*Bu-DAB) in toluene and in CH_3CN the disappearance of both absorption bands of the parent compound and the appearance of a new band at 450 nm in toluene and at 420 nm in CH_3CN. They assigned this band to the first LF transition of $Fe(CO)_3$(σ-N-*t*Bu-DAB)(S) (S=toluene, CH_3CN) and concluded that the second band of the $Fe(CO)_3$(R-DAB) complexes at 350–400 nm should also contain such an LF transition. The lowest ^{3}LF state is then much closer in energy to the ^{3}ML states than proposed by Trogler and coworkers [160,177] and Kokkes et al. [164] so that it can be responsible for the efficient breaking of a metal–ligand bond. In fact, van Dijk et al. [161,176] explained the photochemistry of these $M(CO)_3$(R-DAB) (M=Fe, Ru) complexes with a two-level scheme as indicated in the potential energy diagram in Fig. 33. Irradiation into the low energy band causes population of a ^{1}ML state. Cross-over to the ^{3}LF state is not expected to occur directly but rather from a ^{3}ML state after intersystem crossing. The ^{3}LF state is reactive, showing loss of CO or breaking of a metal–N bond.

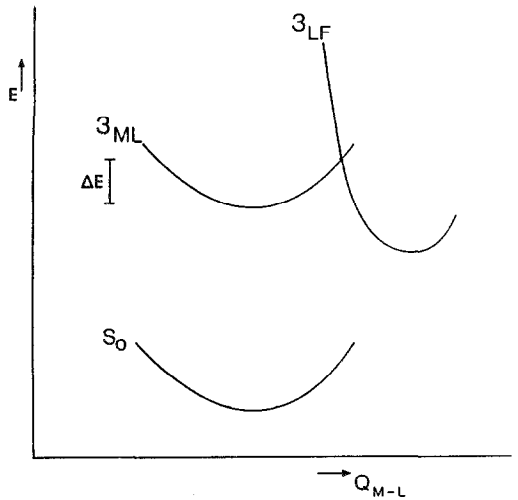

Fig. 33. Potential energy diagram of $M(CO)_3$(R-DAB) (M=Fe, Ru) showing the lowest ^{3}ML and ^{3}LF states. (Reproduced with permission from ref. 161.)

For one of the photosubstitution reactions, van Dijk et al. [161] derived an activation energy ΔE_a of 525 cm^{-1} from the temperature dependence of ϕ. They connected ΔE_a with the energy barrier ΔE between the lowest ^{3}ML and ^{3}LF states (see Fig. 33). The observed wavelength dependence of ϕ for the photosubstitution reactions ($\phi \approx 0.05$ at λ_{irr}=565 nm and $\phi \approx 0.15$ at λ_{irr}=458 nm) was ascribed to the presence of more than one ML transition within the low energy band. Differences in quantum yield can then be due to differences in quantum yield for the internal conversion between the various ^{3}ML states and ^{3}LF.

Analogous behaviour was observed for the substituted-pyridine (py-X) complexes $Ru(NH_3)_5(py\text{-}X)^{2+}$ [178], $CpRe(CO)_2(py\text{-}X)$ [179], $Fe(CN)_5(py\text{-}X)^{3-}$ [180] and $W(CO)_5(py\text{-}X)$ [72,181,182] (see also refs. 183 and 184), which have close lying non-reactive MLCT and reactive LF states. In the case where the MLCT states are lowest in energy, the photosubstitution quantum yields appeared to increase upon going to higher energy irradiation. This wavelength dependence of ϕ was then explained with an energy-dependent competition between cross-over into the manifold of LF states and internal conversion to the lowest MLCT state. In this respect the $M(CO)_3$(R-DAB) (M=Fe, Ru) complexes are exceptional since their lowest ^{3}ML states are reactive, giving rise to the change in coordination of the R-DAB ligand. This reaction is only observed upon low energy irradiation at low temperature, when the ^{3}LF state cannot be occupied. Otherwise the more efficient reaction from the latter state takes place. Whether CO is released or a metal–N bond is broken will depend on the relative strengths of these bonds in that ^{3}LF state. A bulky R group such as *t*Bu weakens the metal–N bond; replacement of CO by PR_3 strengthens the metal–CO bonds. This explains why $Fe(CO)_3$(*t*Bu-DAB) and $M(CO)_2$(R-DAB)(PR_3) (M=Fe, Ru) deviate from the other complexes in showing metal–N bond breakage.

This interesting behaviour, the occurrence of completely different reactions from close lying excited states, is unique. It has never been observed for complexes having close lying MLCT and LF states.

H. $Ni(CO)_2$(α-DIIMINE)

(i) Formation of the complexes

Nyholm and Short [185] were the first to prepare $Ni(CO)_2$(bpy) by thermal reaction of $Ni(CO)_4$ and bpy and the same method was used by Bock and tom Dieck [186] for the synthesis of $Ni(CO)_2$(N-N) in which N-N represents the R-DAB ligand diacetylbis(dimethylhydrazone) (=$(CH_3)_2$N-DAB(CH_3,CH_3)). Although this method is appropriate for these two lig-

ands, it is less suited for the synthesis of $Ni(CO)_2$(R-DAB) complexes in which the R-DAB molecules are stronger π acids. In that case the mixed-ligand complexes react further with R-DAB to give Ni(R-DAB)$_2$. The same holds for the preparative route via $Ni(COD)_2$ (eqn. (49)) in which the intermediate Ni(COD)(N-N) readily forms an Ni(N-N)$_2$ complex (eqn. (50)) [187]:

$$Ni(COD)_2 + N\text{-}N \xrightarrow[-COD]{} Ni(COD)(N\text{-}N) + 2CO \xrightarrow[-COD]{} Ni(CO)_2(N\text{-}N) \quad (49)$$

$$Ni(COD)(N\text{-}N) + (N\text{-}N) \xrightarrow[-COD]{} Ni(N\text{-}N)_2 \quad (50)$$

Bulky R groups inhibit the formation of Ni(R-DAB)$_2$ and Servaas et al. [187] could therefore prepare $Ni(CO)_2$(R-DAB) according to reaction (49) for R=tBu and 2,6-iPr_2-Ph. X-Ray structures have been determined for $Ni(CO)_2((CH_3)_2N\text{-}DAB(CH_3,CH_3))$ [188] and $Ni(CO)_2$(4,6-$(CH_3)_2$-bpy) [189]. For the substituted-bpy complex a tetrahedral conformation was established; in the former complex the tetrahedron was distorted.

(ii) Bonding properties and electronic transitions

For the complexes Ni(R-DAB)$_2$ tom Dieck and coworkers [190,191] observed a large influence of the dihedral angle on the absorption spectra of the complexes. Tetrahedral complexes such as Ni(cHex-DAB)$_2$ and Ni(tBu-DAB)$_2$ showed only one absorption band in the visible region, whereas two bands were observed for Ni($(CH_3)_3CCH_2$-DAB)$_2$ and Ni(2,6-Me_2-Ph-DAB)$_2$, for example, which have a distorted conformation (pseudoplanar).

Recently, these absorption bands were assigned and characterized by Servaas et al. [187] who performed a comparative CNDO/S study on the model complexes Ni(H-DAB)$_2$ and $Ni(CO)_2$(H-DAB) with different dihedral angles θ. In the case of Ni(H-DAB)$_2$ known bond distances and dihedral angles of the structures determined for Ni(cHex-DAB)$_2$ ($\theta \approx 90°$) [190] and Ni(2,6-Me_2-Ph-DAB)$_2$ (θ=44.5°) [191] were used. The MO diagrams thus obtained are depicted in Fig. 34, together with the symmetry-allowed MLCT transitions. From the four allowed $e(d_{xz}+d_{yz}+\psi^*) \rightarrow e(\psi^* - d_{xz} - d_{yz})$ transitions of the tetrahedral complexes, only that transition will be intense which has the direction of charge transfer parallel to the induced electric dipole (z axis of the molecule). In the case of the isostructural $[Cu(N\text{-}N)_2]ClO_4$ complexes, RR excitation profiles indeed showed the presence of a single MLCT transition with two overtones in the lowest energy absorption band [192].

A decrease in θ from 90° to 44.5° causes a destabilization of $d_{yz}(b_3)$ with respect to the tetrahedral complex. The orbital becomes also strongly mixed with a π^* orbital (b_3) of the ligands. Only two transitions,

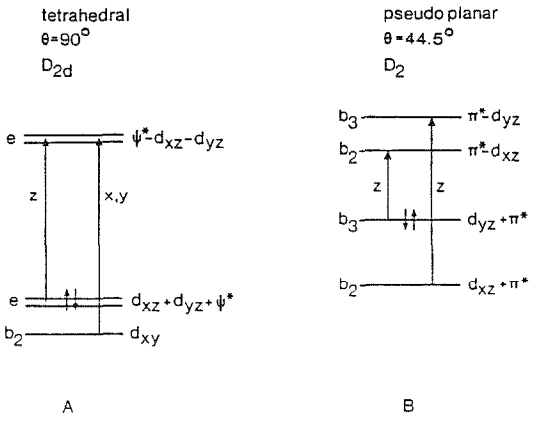

Fig. 34. Qualitative molecular orbital diagram of Ni(cHex-DAB)$_2$ (A) and Ni(2,6-Me$_2$-Ph-DAB)$_2$ (B). (Reproduced with permission from ref. 187.)

$b_3(d_{yz}+\pi^*)\rightarrow b_2(\pi^*-d_{xz})$ and $b_2(d_{xz}+\pi^*)\rightarrow b_3(\pi^*-d_{yz})$ will be intense since they are both z polarized and since the orbitals involved overlap at θ=44.5°. These transitions give rise to the two absorption bands in the visible region of, for example, Ni(2,6-Me$_2$-Ph-DAB)$_2$ [191]. In contrast with the Ni(R-DAB)$_2$ complexes, all Ni(CO)$_2$(R-DAB) compounds show only one absorption band in the visible region. Servaas et al. [187] rationalized this difference with the use of the MO diagrams of these complexes which are presented for two dihedral angles in Fig. 35. Only the z-polarized transition

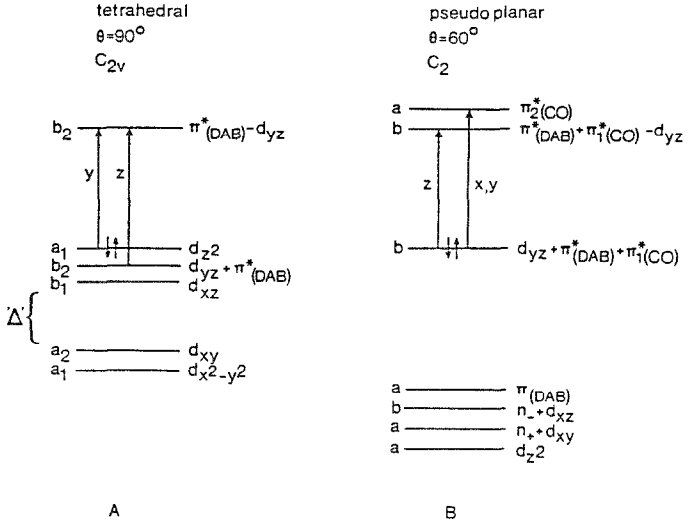

Fig. 35. Qualitative molecular orbital diagram of tetrahedral (A) and pseudoplanar (B) Ni(CO)$_2$(R-DAB). (Reproduced with permission from ref. 187.)

will be intense since it takes place between orbitals that strongly interact and since its direction of charge transfer is parallel to the induced electric dipole moment along the z axis of the molecule. Both types of complexes will therefore show only one intense absorption band in the visible region. Transitions from the lower lying d orbitals will be found in the UV region.

Bock and tom Dieck [186] first reported the absorption spectra of these complexes. Recently, Servaas et al. [187] discussed the spectra of Ni$(CO)_2$(tBu-DAB) and Ni$(CO)_2$(iPr_2-Ph-DAB), having different dihedral angles, in relationship to the MO diagrams and RR spectra. Ni$(CO)_2$(tBu-DAB) has a tetrahedral conformation since the UV–PE spectra showed the ionizations from the two groups of metal d orbitals (Fig. 35) with an intensity ratio of 3:2. According to the ^{1}H NMR spectra, Ni$(CO)_2$(iPr_2-Ph-DAB) has a distorted conformation ($\theta < 90°$). Both complexes have their first MLCT band between 500 and 550 nm. The solvatochromism is, however, much larger in the case of the tBu-DAB complex (Fig. 36), which means that the transition involved has more CT character. This agrees with the MO diagram of Fig. 35 which shows a much stronger mixing between these orbitals in the case of the distorted complex.

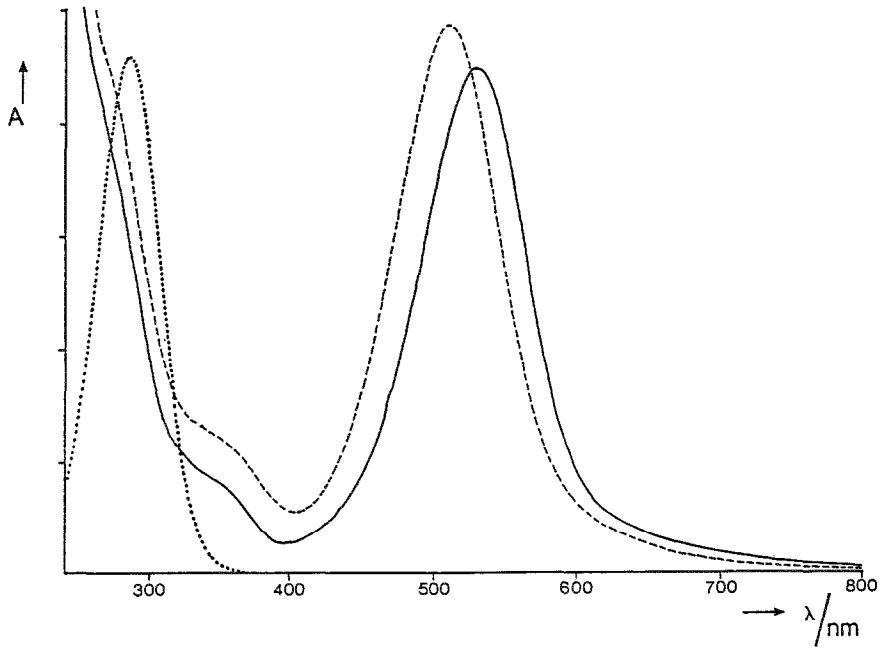

Fig. 36. Electronic absorption spectra of Ni$(CO)_2$(tBu-DAB) at 293 K in C_6H_6 (——) and CH_2Cl_2 (– – –) and of tBu-DAB in C_6H_6 (····). (Reproduced with permission from ref. 187.)

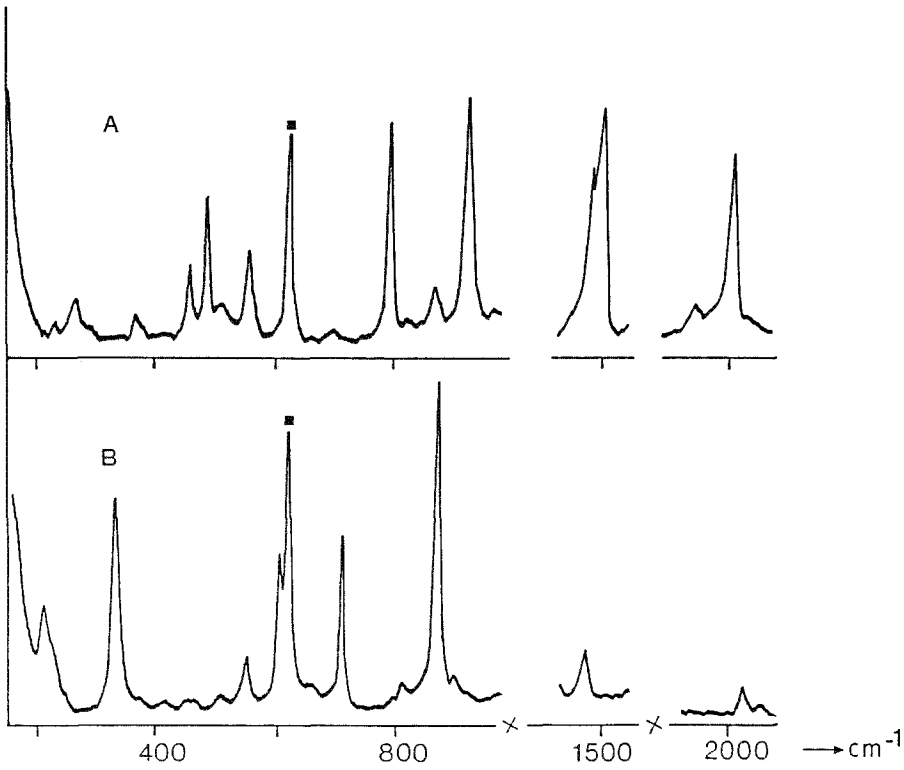

Fig. 37. Resonance Raman spectra of $Ni(CO)_2$(*t*Bu-DAB) (A) and $Ni(CO)_2$(iPr_2-Ph-DAB) (B) in C_6H_6, obtained by excitation with 514.5 nm and 540 nm respectively: ■, solvent band. (Reproduced with permission from ref. 187.)

Clear proof for this change of MLCT character was given by the RR spectra of these complexes, which are presented in Fig. 37.

The spectrum of $Ni(CO)_2$(*t*Bu-DAB) (Fig. 37A) shows resonance enhancement of Raman intensity for ν_s(CN) at 1500 cm^{-1} and ν_s(CO) at 2006 cm^{-1} in accordance with an electronic transition having considerable MLCT character. Strong RR effects are also observed for bands at 773 and 913 cm^{-1} belonging to deformation modes of the NiNCCN moiety. This means that the complex obtains a distorted configuration in the excited state. The spectrum of $Ni(CO)_2$(iPr_2-Ph-DAB) (Fig. 37B) is completely different since it shows the strongest RR effects for ν_s(Ni–N) at 209 cm^{-1}, ν_s(Ni–C) at 321 cm^{-1} and for deformation modes of the NiNCCN moiety at 698 and 853 cm^{-1}. The band belonging to ν_s(CN) is, however, very weak which means that the transition involved has hardly any MLCT character. This result agrees with the MO data and with the small solvatochromism of the absorption band. The strong RR effect observed for ν_s(Ni–C) is clear

evidence for the strong antibonding interaction between the metal d_{yz} orbital and π^*_{CO} in the excited state.

The above data clearly show that a change of dihedral angle has a dramatic influence on the character of these lowest energy transitions. A similar effect was observed by the authors for the corresponding Ni(R-DAB)$_2$ complexes. It could be proven for these compounds that such a large change of MLCT character only occurs when the dihedral angle changes. Substitution of an alkyl substituent R by an aryl group in a series of tetrahedral Ni(R-DAB)$_2$ complexes hardly influenced the MLCT character of the transition.

The above RR and MO data will be shown hereafter to be of crucial importance for the understanding of the photochemical data.

Contrary to the corresponding $[Cu(N\text{-}N)_2]^+$ cations [193], the Ni $(CO)_2(N\text{-}N)$ and Ni$(N\text{-}N)_2$ complexes do not luminesce, most probably because of a much stronger metal–ligand interaction and distortion of the complexes in the lowest excited state.

(iii) Photochemical behaviour

The first detailed photochemical study of these complexes was performed recently by Servaas et al. [194] on Ni$(CO)_2$(*t*Bu-DAB) and Ni$(CO)_2$(iPr$_2$-Ph-DAB). Their results were related to the spectroscopic and theoretical data, discussed in the preceding section. Both complexes appeared to be photostable upon irradiation at RT into the low energy MLCT band. Irradiation of these complexes at lower temperatures ($T \approx 170$ K) in *n*-pentane, however, gave rise to the formation of different photoproducts depending on the complex and the concentrations used. At low concentrations Ni$(CO)_2$(*t*Bu-DAB) formed Ni$(CO)_3$(σ-N-*t*Bu-DAB) in which the *t*Bu-DAB ligand is monodentately coordinated to the metal. At higher concentrations, $(CO)_3$Ni(μ-(σ-N,σ-N′)-*t*Bu-DAB)Ni(CO)(*t*Bu-DAB) was formed. One of the *t*Bu-DAB ligands now forms a bridge between the Ni atoms. Both photoproducts reacted back to give the parent complex upon raising the temperature. The reactions were proposed to proceed according to eqn. (51)–(53).

$$\mathrm{Ni(CO)_2(}t\mathrm{Bu\text{-}DAB)} \xrightarrow[\substack{n\text{-pentane}\\ 170\ \mathrm{K}}]{h\nu} \mathrm{Ni(CO)_2(\sigma\text{-}N\text{-}}t\mathrm{Bu\text{-}DAB)(S)} \qquad \mathbf{A} \qquad (51)$$

$$\mathbf{A} + \mathrm{CO} \rightarrow \mathrm{Ni(CO)_3(\sigma\text{-}N\text{-}}t\mathrm{Bu\text{-}DAB)} + \mathrm{S} \qquad (52)$$

$$\mathbf{A} + \mathrm{Ni(CO)_2(}t\mathrm{Bu\text{-}DAB)} \rightarrow (\mathrm{CO})_3\mathrm{Ni}(\mu\text{-}(\sigma\text{-}\mathrm{N},\sigma\text{-}\mathrm{N}')\text{-}t\mathrm{Bu\text{-}DAB})\mathrm{Ni(CO)(}t\mathrm{Bu\text{-}DAB}) \qquad (53)$$

The primary photoprocess (eqn. (51)) is the breaking of a metal–N bond. At

this low temperature rechelation of the bulky *t*Bu-DAB ligand is a slow process and the unstable solvent-coordinated photoproduct **A** will partly decompose during its back reaction to the parent compound. The CO ligands thus released will react with **A** according to eqn. (52). The complex $Ni(CO)_3(\sigma\text{-N-}t\text{Bu-DAB})$ slowly reacted back to the parent compound on standing in the dark at 170 K. At higher concentrations, **A** can also react with the parent compound according to eqn. (53). The IR spectral changes (CO stretching region) accompanying these reactions are shown in Fig. 38. When the above reaction was performed at 170 K in 2-MeTHF instead of in *n*-pentane, no reaction was observed. At this low temperature 2-MeTHF forms a rather stable solvent-coordinated photoproduct **A** which apparently does not decompose during its back reaction to the parent compound. The same photostability was observed when the complex was irradiated into its MLCT band in a CH_4 matrix at 10 K.

When $Ni(CO)_2(t\text{Bu-DAB})$ was irradiated at 170 K in the presence of

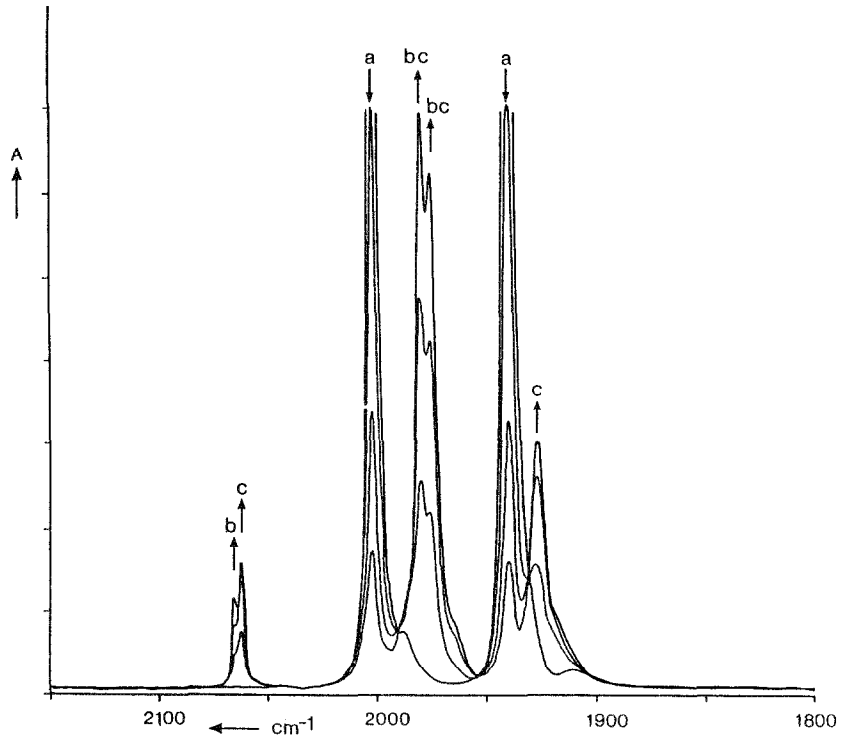

Fig. 38. IR spectral changes (CO stretching region) upon irradiation of a high starting concentration of $Ni(CO)_2(t\text{Bu-DAB})$ with 514.5 nm in *n*-pentane at 170 K: (a) $Ni(CO)_2(t\text{Bu-DAB})$; (b) $Ni(CO)_3(\sigma\text{-N-}t\text{Bu-DAB})$; (c) $(CO)_3Ni(\mu\text{-}(\sigma\text{-N},\sigma\text{-N}')\text{-}t\text{Bu-DAB})Ni(CO)(t\text{Bu-DAB})$. (Reproduced with permission from ref. 194.)

excess R-DAB, **A** reacted with this ligand according to reactions (54) and (55):

$$\mathbf{A} + \text{R-DAB} \rightarrow \text{Ni(CO)}_2(\sigma\text{-N-R-DAB})(\sigma\text{-N-}t\text{Bu-DAB}) + \text{S} \quad (54)$$

$$\text{Ni(CO)}_2(\sigma\text{-N-R-DAB})(\sigma\text{-N-}t\text{Bu-DAB}) \rightarrow \text{Ni(CO)}_2(\text{R-DAB}) + t\text{Bu-DAB} \quad (55)$$

For R=*t*Bu the product of reaction (54) not only reacted back to give the parent compound (eqn. (55)). It also formed Ni(CO)(σ-N-*t*Bu-DAB)(*t*Bu-DAB) according to eqn. (56):

$$\text{Ni(CO)}_2(\sigma\text{-N-}t\text{Bu-DAB})(\sigma\text{-N-}t\text{Bu-DAB}) \rightarrow \text{Ni(CO)}(\sigma\text{-N-}t\text{Bu-DAB})(t\text{Bu-DAB}) + \text{CO} \quad (56)$$

This reaction was not observed for R≠*t*Bu since reaction (55) then dominated completely. Irradiation in the presence of PR_3 caused the formation of a photosubstitution product according to reactions (57) and (58):

$$\mathbf{A} + \text{PR}_3 \rightarrow \text{Ni(CO)}_2(\sigma\text{-N-}t\text{Bu-DAB})(\text{PR}_3) \quad (57)$$

$$\text{Ni(CO)}_2(\sigma\text{-N-}t\text{Bu-DAB})(\text{PR}_3) \rightarrow \text{Ni(CO)}(t\text{Bu-DAB})(\text{PR}_3) + \text{CO} \quad (58)$$

In the case of P(*n*Bu)$_3$ a quantum yield of 5×10^{-3} mol einstein^{-1} was measured; this value is of the same order of magnitude as for the MLCT photochemistry of Cr(CO)$_4$(N-N) (vide supra). Reactions (54) and (57) are completely similar. Apparently, rechelation of the *t*Bu-DAB ligand with concomitant loss of CO is a more likely process than substitution of the σ-N coordinated *t*Bu-DAB ligand. When this reaction was, however, performed in the presence of P(cHex)$_3$, Ni(CO)$_3$(P(cHex)$_3$) was formed as a side product. Rechelation of *t*Bu-DAB is then partly inhibited by the steric interaction between the cHex and *t*Bu groups. *t*Bu-DAB may then be released and substituted by CO from the solution. A similar mechanism was derived for the photosubstitution of CO in Fe(CO)$_3$(*t*Bu-DAB) by PR_3 (see Scheme 3). In that case, however, complexes Fe(CO)$_3$(σ-N-*t*Bu-DAB)(PR_3) could be detected as stable intermediates at low temperature.

All these reactions have in common the breaking of a metal–N bond (reaction (51)) by irradiation into the MLCT band. Irradiation at higher energy ($\lambda < 360$ nm) caused release of CO. This was demonstrated by irradiating the complex in a CH_4 matrix at 10 K and by flash photolysis with the 308 nm line of an excimer laser.

Irradiation of Ni(CO)$_2$(iPr$_2$-Ph-DAB) in *n*-pentane at 170 K into its MLCT band only caused photodecomposition with Ni(CO)$_4$ as the main decomposition product. Just as for the *t*Bu-DAB complex no reaction was observed upon irradiation in 2-MeTHF at this temperature. In the presence of excess R-DAB, Ni(R-DAB)(iPr$_2$-Ph-DAB) was formed according to the mechanism described in reactions (59)–(61):

$$Ni(CO)_2(iPr_2\text{-Ph-DAB}) \xrightarrow{h\nu} Ni(CO)(iPr_2\text{-Ph-DAB})(S)\ (\mathbf{B}) + CO \quad (59)$$

$$\mathbf{B} + \text{R-DAB} \rightarrow Ni(CO)(\sigma\text{-N-R-DAB})(iPr_2\text{-Ph-DAB}) + S \quad (60)$$

$$Ni(CO)(\sigma\text{-N-R-DAB})(iPr_2\text{-Ph-DAB}) \rightarrow Ni(\text{R-DAB})(iPr_2\text{-Ph-DAB}) + CO \quad (61)$$

The UV–visible spectral changes accompanying the conversion of the parent complex into the photoproduct $Ni(iPr_2\text{-Ph-DAB})_2$ are shown in Fig. 39. The photoproducts Ni(R-DAB)(iPr_2-Ph-DAB) were formed in the UV–visible sample cell but not in the IR cell since the CO, released in reaction (59) and still present in the IR solution, prevented the chelation of the R-DAB ligand (eqn. (61)).

Irradiation of the complex in the presence of PR_3 gave rise to photosubstitution of CO according to reactions (59) and (62):

$$\mathbf{B} + PR_3 \rightarrow Ni(CO)(iPr_2\text{-Ph-DAB})(PR_3) + S \quad (62)$$

The authors could not give solid proof for the primary photoprocess of this complex (eqn. (59)) but indirect evidence for the mechanism was provided by the close analogy between the MLCT photochemistry of the iPr_2-Ph-DAB

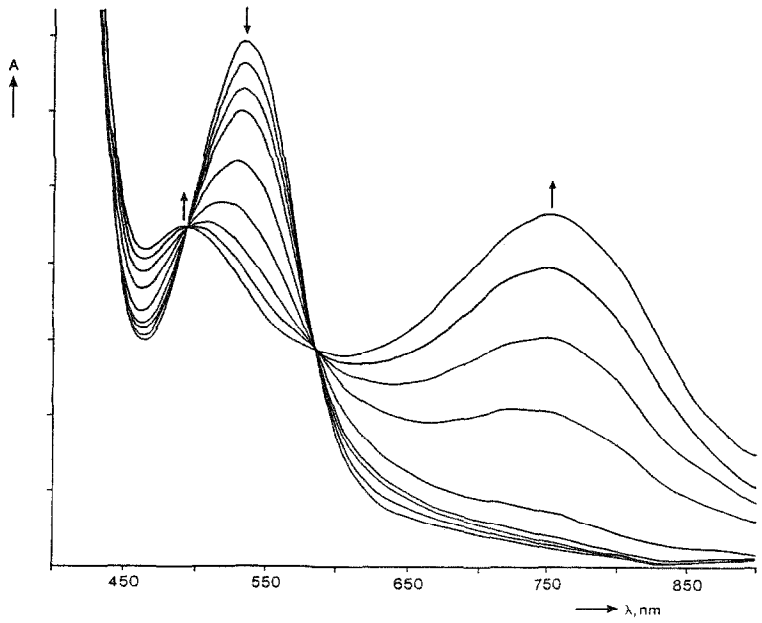

Fig. 39. Electronic absorption spectral changes during the photochemical reaction of $Ni(CO)_2(iPr_2$-Ph-DAB) with iPr_2-Ph-DAB. Irradiation with 514.5 nm in toluene at 203 K. (Reproduced with permission from ref. 194.)

complex and the UV photochemistry of $Ni(CO)_2$(*t*Bu-DAB). In both cases the reactions were proposed to proceed via the same primary photoprocess, which had been shown with flash photolysis to be release of CO for $Ni(CO)_2$(*t*Bu-DAB) (vide supra).

(iv) Photochemical mechanism

The above results show that irradiation into the MLCT band of an $Ni(CO)_2$(R-DAB) complex can cause the breaking of a metal–N bond (R=*t*Bu) or release of CO (R=iPr_2-Ph). This difference in behaviour appears to be connected with a change of structure from tetrahedral to pseudoplanar. As shown above, such structural changes influence the character of the low energy MLCT band. In the tetrahedral $Ni(CO)_2$(*t*Bu-DAB) this transition is accompanied by charge transfer from the metal to the *t*Bu-DAB ligand. According to the RR spectra, occupation of the ^{3}MLCT state will not lead to a drastic weakening of any of the metal–ligand bonds. An Ni–N bond will therefore preferably be broken from this state since it is already the weaker one in the ground state. In $Ni(CO)_2$(iPr_2-Ph-DAB) the RR spectra showed that this low energy transition is instead strongly metal–CO bonding to antibonding. This explains why release of CO is the primary photoprocess for this complex.

ACKNOWLEDGEMENTS

I gratefully acknowledge Professor Ad Oskam who closely cooperated in the research cited in the references. I also thank the coworkers Ronald Andréa, Roelof Balk, Hans van Dijk, Tim van der Graaf, Maarten Kokkes, Wim de Lange, Gerard Schoemaker, Theo Snoeck and Andries Terpstra for their skilful and enthusiastic research efforts. Professor Alistair Lees is thanked for helpful discussions and for critical reading of the manuscript.

REFERENCES

1 A.W. Adamson, J. Phys. Chem., 71 (1967) 798.
2 V. Balzani, F. Bolletta, M.T. Gandolfi and M. Maestri, Top. Curr. Chem., 1 (1978) 75.
3 V. Balzani, F. Bolletta, F. Scandola and R. Ballardini, Pure Appl. Chem., 51 (1979) 299.
4 N. Sutin and C. Creutz, Pure Appl. Chem., 52 (1980) 2717.
5 M. Julliard and M. Chanon, Chem. Rev., 83 (1983) 425.
6 K. Kalyanasundaram, Coord. Chem. Rev., 46 (1982) 159.
7 T.J. Meyer, Prog. Inorg. Chem., 30 (1983) 389.
8 T.J. Meyer, Pure Appl. Chem., 58 (1986) 1193.
9 E.A. Koerner von Gustorf, H.G. Leenders, I. Fischler and R.N. Perutz, Adv. Inorg. Chem. Radiochem., 19 (1976) 65.

10 G.L. Geoffroy and M.S. Wrighton, Organometallic Photochemistry, Academic Press, New York, 1979.
11 T.J. Meyer and J.V. Caspar, Chem. Rev., 85 (1985) 187.
12 T. Kobayashi, K. Yasufuku, J. Iwai, H. Yesaka, H. Noda and H. Ohtani, Coord. Chem. Rev., 64 (1985) 1.
13 M. Poliakoff and E. Weitz, Adv. Organomet. Chem., 25 (1986) 277.
14 D.J. Stufkens, Steric and Electronic Effects on the Photochemical Reactions of Metal–Metal Bonded Carbonyls, in I. Bernal (Ed.), Stereochemistry of Organometallic and Inorganic Compounds, Vol. 3, Elsevier, Amsterdam, 1989, pp. 226–300.
15 C.G. Kreiter, Adv. Organomet. Chem., 26 (1986) 297.
16 A.J. Lees, Chem. Rev., 87 (1987) 711.
17 G. van Koten and K. Vrieze, Recl. Trav. Chim. Pays-Bas, 100 (1981) 129.
18 G. van Koten and K. Vrieze, Adv. Organomet. Chem., 21 (1982) 151.
19 K. Vrieze and G. van Koten, Inorg. Chim. Acta, 100 (1985) 79.
20 K. Vrieze, J. Organomet. Chem., 300 (1986) 307.
21 W. Hieber and F. Mühlbauer, Z. Anorg. Allg. Chem., 221 (1935) 337.
22 E.W. Abel, M.A. Bennett and G. Wilkinson, J. Chem. Soc., (1959) 2323.
23 H. Bock and H. tom Dieck, Chem. Ber., 100 (1967) 228.
24 H. Brunner and W.A. Hermann, Chem. Ber., 105 (1972) 770.
25 L.H. Staal, D.J. Stufkens and A. Oskam, Inorg. Chim. Acta, 26 (1978) 255.
26 M.J. Schadt, N.J. Gresalfi and A.J. Lees, J. Chem. Soc., Chem. Commun., (1984) 506.
27 M.J. Schadt, N.J. Gresalfi and A.J. Lees, Inorg. Chem., 24 (1985) 2942.
28 M.J. Schadt and A.J. Lees, Inorg. Chem., 25 (1986) 672.
29 D.E. Marx and A.J. Lees, Organometallics, 5 (1986) 2072.
30 L. Chan and A.J. Lees, Inorg. Chim. Acta, 113 (1986) L3.
31 L. Chan and A.J. Lees, J. Chem. Soc., Dalton Trans., (1987) 513.
32 D.E. Marx and A.J. Lees, Inorg. Chem., 26 (1987) 620.
33 D.P. Drolet, L. Chan and A.J. Lees, Organometallics, 7 (1988) 2502.
34 R.J. Kazlauskas and M.S. Wrighton, J. Am. Chem. Soc., 104 (1982) 5784.
35 S. Oishi, Organometallics, 7 (1988) 1237.
36 K. Kalyanasundaram, J. Phys. Chem., 92 (1988) 2219.
37 R.W. Balk, D.J. Stufkens and A. Oskam, Inorg. Chim. Acta, 28 (1978) 133.
38 H. tom Dieck and I.W. Renk, Chem. Ber., 104 (1971) 110.
39 H. tom Dieck and I.W. Renk, Chem. Ber., 105 (1972) 1419.
40 R.W. Balk, D.J. Stufkens and A. Oskam, Inorg. Chim. Acta, 34 (1979) 267.
41 R.W. Balk, Th.L. Snoeck, D.J. Stufkens and A. Oskam, Inorg. Chem., 19 (1980) 3015.
42 R.W. Balk, D.J. Stufkens and A. Oskam, J. Chem. Soc., Dalton Trans., (1982) 275.
43 P.C. Servaas, H.K. van Dijk, Th.L. Snoeck, D.J. Stufkens and A. Oskam, Inorg. Chem., 24 (1985) 4494.
44 J. Friedman and R.M. Hochstrasser, Chem. Phys. Lett., 32 (1975) 414.
45 H. Saito, J. Fujita and K. Saito, Bull. Chem. Soc. Jpn., 41 (1968) 863.
46 J. Burgess, J. Organomet. Chem., 19 (1969) 218.
47 J. Burgess, J.G. Chambers and R.I. Haines, Transition Met. Chem., 6 (1981) 145.
48 H.-T. Macholdt, R. van Eldik, H. Kelm and H. Elias, Inorg. Chim. Acta, 104 (1985) 115.
49 R. bin Ali, J. Burgess, M. Kotowski and R. van Eldik, Transition Met. Chem., 12 (1987) 230.
50 M. Kotowski, R. van Eldik, R. bin Ali, J. Burgess and S. Radulovic, Inorg. Chim. Acta, 131 (1987) 225.
51 R. bin Ali, P. Banerjee, J. Burgess and A.E. Smith, Transition Met. Chem., 13 (1988) 107.
52 P. Banerjee and J. Burgess, Inorg. Chim. Acta, 146 (1988) 227.

53 H. tom Dieck and I.W. Renk, Angew. Chem., Int. Ed. Engl., 9 (1970) 793.
54 I.W. Renk and H. tom Dieck, Chem. Ber., 105 (1972) 1403.
55 D. Walther, J. Prakt. Chem., 316 (1974) 604.
56 J.A. Connor and C. Overton, Inorg. Chim. Acta, 65 (1982) L1.
57 J.A. Connor, C. Overton and N. El Murr, J. Organomet. Chem., 277 (1984) 277.
58 D.M. Manuta and A.J. Lees, Inorg. Chem., 22 (1983) 3825.
59 D.M. Manuta and A.J. Lees, Inorg. Chem., 25 (1986) 3212.
60 W. Kaim and S. Kohlmann, Inorg. Chem., 25 (1986) 3307.
61 E.S. Dodsworth and A.B.P. Lever, Inorg. Chem., in press.
62 S. Ernst, Y. Kurth and W. Kaim, J. Organomet. Chem., 302 (1986) 211.
63 C. Reichardt, Angew. Chem., Int. Ed. Engl., 4 (1965) 29; 18 (1979) 98.
64 E.M. Kosower, J. Am. Chem. Soc., 80 (1958) 3253.
65 M.J. Kamlet, J.L.M. Abbond and R.W. Taft, Prog. Phys. Org. Chem., 13 (1981) 485.
66 R.W. Taft and M.J. Kamlet, Inorg. Chem., 22 (1983) 250.
67 M.M. Zulu and A.J. Lees, Inorg. Chem., 27 (1988) 3325.
68 M.S. Wrighton and D.L. Morse, J. Am. Chem. Soc., 96 (1974) 998.
69 P.J. Giordano, S.M. Fredericks, M.S. Wrighton and D.L. Morse, J. Am. Chem. Soc., 100 (1978) 2257.
70 J.C. Luong, R.A. Faltynek and M.S. Wrighton, J. Am. Chem. Soc., 101 (1979) 1597.
71 S.M. Fredericks, J.C. Luong and M.S. Wrighton, J. Am. Chem. Soc., 101 (1979) 7415.
72 A.J. Lees and A.W. Adamson, J. Am. Chem. Soc., 104 (1982) 3804.
73 A.J. Lees, J. Am. Chem. Soc., 104 (1982) 2038.
74 S. Chun, E.E. Getty and A.J. Lees, Inorg. Chem., 23 (1984) 2155.
75 D.M. Manuta and A.J. Lees, Inorg. Chem., 22 (1983) 572.
76 D.M. Manuta and A.J. Lees, Inorg. Chem., 25 (1986) 1354.
77 M.M. Zulu and A.J. Lees, Inorg. Chem., 28 (1989) 85.
78 K.A. Rawlins and A.J. Lees, Inorg. Chem., 28 (1989) 2154.
79 J.I. Zink, L. Tutt and Y.Y. Yang, in Excited States and Reactive Intermediates, ACS Symp. Ser., 307 (1986) 39.
80 D.J. Robbins and A. Thomson, Mol. Phys., 25 (1973) 1103.
81 M.S. Wrighton and D.L. Morse, J. Organomet. Chem., 97 (1975) 405.
82 J. Víchová, F. Hartl and A. Vlček, Jr., VIIIth Int. Symp. on the Photochemistry and Photophysics of Coordination Compounds, Santa Barbara, U.S.A., 1989, C19.
83 H.K. van Dijk, P.C. Servaas, D.J. Stufkens and A. Oskam, Inorg. Chim. Acta, 104 (1985) 179.
84 S. Wieland and R. van Eldik, J. Chem. Soc., Chem. Commun., (1989) 367.
85 H. Kobayashi, Y. Kaizu, H. Kimura and H. Matsuzawa, Mol. Phys., 64 (1988) 1009.
86 D. Miholová and A.A. Vlček, J. Organomet. Chem., 279 (1985) 317.
87 B. Olbrich-Deussner and W. Kaim, J. Organomet. Chem., 340 (1988) 71.
88 Th. Kruck and M. Höfler, Angew. Chem., Int. Ed. Engl., 3 (1964) 701.
89 Th. Kruck, M. Höfler and M. Noack, Chem. Ber., 99 (1966) 1153.
90 D.L. Morse and M.S. Wrighton, J. Am. Chem. Soc., 98 (1976) 3931.
91 D.L. Morse and M.S. Wrighton, J. Organomet. Chem., 125 (1977) 71.
92 L.H. Staal, G. van Koten and K. Vrieze, J. Organomet. Chem., 175 (1979) 73.
93 J.C. Luong, R.A. Faltynek and M.S. Wrighton, J. Am. Chem. Soc., 101 (1979) 1597.
94 J.C. Luong, R.A. Faltynek and M.S. Wrighton, J. Am. Chem. Soc., 102 (1980) 7892.
95 R.R. Andréa, W.G.J. de Lange, D.J. Stufkens and A. Oskam, Inorg. Chim. Acta, 149 (1988) 77.
96 J. Reinhold, R. Benedix, P. Birner and H. Hennig, Inorg. Chim. Acta, 33 (1979) 209.
97 M.W. Kokkes, Th.L. Snoeck, D.J. Stufkens, A. Oskam, M. Cristophersen and C.H. Stam, J. Mol. Struct., 131 (1985) 11.

98 M.R. Churchill, K.N. Amoh and H.J. Wasserman, Inorg. Chem., 20 (1981) 1609.
99 R.R. Andréa, D.J. Stufkens and A. Oskam, J. Organomet. Chem., 290 (1985) 63.
100 W.K. Meckstroth and D.P. Ridge, J. Am. Chem. Soc., 107 (1985) 2281.
101 D.J. Stufkens and Th.L. Snoeck, to be published.
102 M.M. Glezen, A.J. Lees and D.J. Stufkens, to be published.
103 M.W. Kokkes, D.J. Stufkens and A. Oskam, Inorg. Chem., 24 (1985) 2934.
104 M.W. Kokkes, D.J. Stufkens and A. Oskam, Inorg. Chem., 24 (1985) 4411.
105 M.W. Kokkes, W.G.J. de Lange, D.J. Stufkens and A. Oskam, J. Organomet. Chem., 294 (1985) 59.
106 D.J. Stufkens, A. Oskam, M.W. Kokkes and R.R. Andréa, J. Mol. Struct., 141 (1986) 465.
107 D.J. Stufkens, A. Oskam and M.W. Kokkes, Metal–Ligand Charge Transfer Photochemistry, in Excited States and Reactive Intermediates, ACS Symp. Ser., 307 (1986) 66.
108 T. van der Graaf, D.J. Stufkens and A. Oskam, XIIth IUPAC Symp. Photochemistry, Bologna, Italy, 1988, ST-4; VIIIth Int. Symp. on the Photochemistry and Photophysics of Coordination Compounds, Santa Barbara, U.S.A., 1989, K-4, P-56.
109 R.R. Andréa, W.G.J. de Lange, T. van der Graaf, M. Rijkhoff, D.J. Stufkens and A. Oskam, Organometallics, 7 (1988) 1100.
110 H.K. van Dijk, J. van der Haar, D.J. Stufkens and A. Oskam, Inorg. Chem., 28 (1989) 75.
111 R.R. Andréa, W.G.J. de Lange, D.J. Stufkens and A. Oskam, Inorg. Chem., 28 (1989) 318.
112 J.T.B.H. Jastrzebski, J.M. Klerks, G. van Koten and K. Vrieze, J. Organomet. Chem., 210 (1981) C49.
113 G. van Koten, J.T.B.H. Jastrzebski and K. Vrieze, J. Organomet. Chem., 250 (1983) 49.
114 R.D. Adams, J. Am. Chem. Soc., 102 (1980) 7476.
115 A.E. Stiegman and D.R. Tyler, Inorg. Chem., 23 (1984) 527.
116 A.E. Stiegman, M. Stieglitz and D.R. Tyler, J. Am. Chem. Soc., 105 (1983) 6032.
117 J.K. Kochi, Organometallic Mechanisms and Catalysis, Academic Press, New York, 1978.
118 J.K. Kochi, J. Organomet. Chem., 300 (1986) 139.
119 C.A. Tolman, Chem. Soc. Rev., 1 (1972) 337.
120 A.E. Stiegman and D.R. Tyler, Comments Inorg. Chem., 5 (1986) 215.
121 W. Kaim, Coord. Chem. Rev., 76 (1987) 187.
122 M.C. Baird, Chem. Rev., 88 (1988) 1217.
123 D. Astruc, Chem. Rev., 88 (1988) 1189.
124 D.R. Tyler, Prog. Inorg. Chem., 36 (1988) 125.
125 M. Chanon, M. Julliard and J.C. Poite (Eds.), Paramagnetic Organometallic Species in Activation/Selectivity, Catalysis, NATO ASI Ser. C, Vol. 257, Kluwer Academic, Dordrecht, 1988.
126 D. Astruc, Angew. Chem., Int. Ed. Engl., 27 (1988) 643.
127 W. Kaim, Acc. Chem. Res., 18 (1985) 160.
128 M. Chanon and M.L. Tobe, Angew. Chem., Int. Ed. Engl., 21 (1982) 1.
129 J.K. Kochi, Angew. Chem., Int. Ed. Engl., 27 (1988) 1227.
130 A.F. Hepp and M.S. Wrighton, J. Am. Chem. Soc., 105 (1983) 5934.
131 I.R. Dunkin, P. Härter and C.J. Shields, J. Am. Chem. Soc., 106 (1984) 7248.
132 M. Brookhart and M.L.H. Green, J. Organomet. Chem., 250 (1983) 395.
133 T. Kruck and M. Höfler, Chem. Ber., 97 (1964) 2289.
134 L.H. Staal, J. Keijsper, G. van Koten, K. Vrieze, J.A. Cras and W.P. Bosman, Inorg. Chem., 20 (1981) 555.
135 R.H. Knoll, W.G.J. de Lange and D.J. Stufkens, to be published.
136 A. Veillard and A. Strich, J. Am. Chem. Soc., 110 (1988) 3793.
137 J.L. Hughey IV, C.P. Anderson and T.J. Meyer, J. Organomet. Chem., 125 (1977) C49.
138 H. Yesaka, T. Kobayashi, K. Yasufuku and S. Nagakura, J. Am. Chem. Soc., 105 (1983) 6249.
139 L.J. Rothberg, N.J. Cooper, K.S. Peters and V. Vaida, J. Am. Chem. Soc., 104 (1982) 3536.

140 J.A. Connor, Top. Curr. Chem., 71 (1977) 71.
141 A. Terzis, T.C. Strekas and T.G. Spiro, Inorg. Chem., 13 (1974) 1346.
142 R.A. Burnham and S.R. Stobart, J. Chem. Soc., Dalton Trans., (1973) 1269.
143 S. Onaka, Bull. Chem. Soc. Jpn., 46 (1973) 2444.
144 H.M. Gager, J. Lewis and M.J. Ware, J. Chem. Soc., Chem. Commun., (1966) 616.
145 W. Heijser, E.J. Baerends and P. Ros, Faraday Symp. Chem. Soc., 14 (1980) 211.
146 S. Otsuka, T. Yoshida and A. Nakamura, Inorg. Chem., 6 (1967) 20.
147 H. tom Dieck and A. Orlopp, Angew. Chem., Int. Ed. Engl., 14 (1975) 251.
148 L.H. Staal, L.H. Polm and K. Vrieze, Inorg. Chim. Acta, 40 (1980) 165.
149 H.-W. Frühauf, A. Landers, R. Goddard and C. Krüger, Angew. Chem., Int. Ed. Engl., 17 (1978) 64.
150 H.-W. Frühauf, J. Chem. Res. (M), (1983) 2035; (S), (1983) 218.
151 L.H. Staal, L.H. Polm, K. Vrieze and C.H. Stam, Inorg. Chem. 20 (1981) 3590.
152 J.J. Keijsper, L.H. Polm, G. van Koten, K. Vrieze, G. Abbel and C.H. Stam, Inorg. Chem., 23 (1984) 2142.
153 J.J. Keijsper, L.H. Polm, G. van Koten, K. Vrieze, P.F.A.B. Seignette and C.H. Stam, Inorg. Chem., 24 (1985) 518.
154 W.P. Mul, C.J. Elsevier, H.-W. Frühauf, K. Vrieze, I. Pein, M.C. Zoutberg and C.H. Stam, Inorg. Chem., in press.
155 H.-W. Frühauf, personal communication, 1989.
156 H.-W. Frühauf, Habilitationsschrift, University of Duisburg, F.R.G., 1980, p. 41.
157 M.W. Kokkes, D.J. Stufkens and A. Oskam, J. Chem. Soc., Dalton Trans., (1983) 439.
158 R.J. Doedens, J. Chem. Soc., Chem. Commun., (1968) 1271.
159 R.R. Andréa, J.N. Louwen, M.W. Kokkes, D.J. Stufkens and A. Oskam, J. Organomet. Chem., 281 (1985) 273.
160 W.C. Trogler, C.E. Johnson and D.E. Ellis, Inorg. Chem., 20 (1981) 980.
161 H.K. van Dijk, D.J. Stufkens and A. Oskam, J. Am. Chem. Soc., 111 (1989) 541.
162 H.-W. Frühauf, F.-W. Grevels and A. Landers, J. Organomet. Chem., 178 (1979) 349.
163 H.-W. Frühauf and G. Wolmershäuser, Chem. Ber., 115 (1982) 1070.
164 M.W. Kokkes, D.J. Stufkens and A. Oskam, J. Chem. Soc., Dalton Trans., (1984) 1005.
165 M.W. Kokkes, D.J. Stufkens and A. Oskam, J. Chem. Soc., Chem. Commun., (1983) 369.
166 D.J. Stufkens, M.W. Kokkes and A. Oskam, J. Mol. Struct., 114 (1984) 61.
167 D.J. Stufkens, H.K. van Dijk and A. Oskam, in H. Yersin and A. Volger (Eds.), Photochemistry and Photophysics of Coordination Compounds, Springer-Verlag, Berlin, 1987, p. 253.
168 W.C. Trogler, Photochemical Production of Reactive Organometallics for Synthesis and Catalysis, in Excited States and Reactive Intermediates, ACS Symp. Ser., 307 (1986) 177.
169 J.J. Turner, M. Poliakoff and M.B. Simpson, J. Mol. Struct., 113 (1984) 359.
170 R. Rebiai, A.J. Rest and R.G. Schrlock, Nature, 105 (1983) 412.
171 M.O. Bulanin, J. Mol. Struct., 19 (1973) 59.
172 W.B. Maier II and R.F. Holland, J. Chem. Phys., 72 (1980) 6661.
173 W.H. Beattie, W.F. Maier II, R.F. Holland, S.M. Freund and B. Stewart, SPIE Laser Spectrosc., 158 (1978) 113.
174 M.B. Simpson, M. Poliakoff, J.J. Turner, W.B. Maier II and J.G. McLaughlin, J. Chem. Soc., Chem. Commun., (1983) 1355.
175 R.R. Andréa, H. Luyten, M.A. Vuurman, D.J. Stufkens and A. Oskam, Appl. Spectrosc., 40 (1986) 1184.
176 H.K. van Dijk, J.J. Kok, D.J. Stufkens and A. Oskam, J. Organomet. Chem., 362 (1989) 163.
177 C.E. Johnson and W.C. Trogler, J. Am. Chem. Soc., 103 (1981) 6352.
178 G. Malouf and P.C. Ford, J. Am. Chem. Soc., 96 (1974) 601; 99 (1977) 7213.

179 P.J. Giordano and M.S. Wrighton, Inorg. Chem., 16 (1977) 160.
180 J.E. Figard and J.D. Petersen, Inorg. Chem., 17 (1978) 1059.
181 A.J. Lees and A.W. Adamson, J. Am. Chem. Soc., 102 (1980) 6874.
182 M.S. Wrighton, H.B. Abrahamson and D.L. Morse, J. Am. Chem. Soc., 98 (1976) 4105.
183 P.C. Ford, Rev. Chem. Intermed., 2 (1979) 267.
184 P.C. Ford, D. Wink and J. DiBenedetto, Prog. Inorg. Chem., 30 (1983) 213.
185 R. Nyholm and L.N. Short, J. Chem. Soc. A, (1953) 2670.
186 H. Bock and H. tom Dieck, Angew. Chem., Int. Ed. Engl., 5 (1966) 520.
187 P.C. Servaas, D.J. Stufkens and A. Oskam, Inorg. Chem., 28 (1989) 1774.
188 H.D. Hausen and K. Krogmann, Z. Anorg. Allg. Chem., 389 (1972) 247.
189 J. Sieler, N.-N. Than, R. Benedix, E. Dinjus and D. Walther, Z. Anorg. Allg. Chem., 522 (1985) 131.
190 M. Svoboda, H. tom Dieck, C. Krüger and Y.-H. Tsay, Z. Naturforsch., Teil B, 36 (1981) 814.
191 H. tom Dieck, M. Svoboda and T. Greiser, Z. Naturforsch., Teil B, 36 (1981) 823.
192 P. Leupin and C.W. Schläpfer, J. Chem. Soc., Dalton Trans., (1983) 1635.
193 J.R. Kirchhoff, R.E. Gamache, Jr., M.W. Blaskie, A.A. Del Paggio, R.K. Lengel and D.R. McMillin, Inorg. Chem., 22 (1983) 2380.
194 P.C. Servaas, D.J. Stufkens and A. Oskam, Inorg. Chem., 28 (1989) 1780.